INFORMATION TO USERS

This material was produced from a microfilm copy of the original document. While the most advanced technological means to photograph and reproduce this document have been used, the quality is heavily dependent upon the quality of the original submitted.

The following explanation of techniques is provided to help you understand markings or patterns which may appear on this reproduction.

1. The sign or "target" for pages apparently lacking from the document photographed is "Missing Page(s)". If it was possible to obtain the missing page(s) or section, they are spliced into the film along with adjacent pages. This may have necessitated cutting thru an image and duplicating adjacent pages to insure you complete continuity.

2. When an image on the film is obliterated with a large round black mark, it is an indication that the photographer suspected that the copy may have moved during exposure and thus cause a blurred image. You will find a good image of the page in the adjacent frame.

3. When a map, drawing or chart, etc., was part of the material being photographed the photographer followed a definite method in "sectioning" the material. It is customary to begin photoing at the upper left hand corner of a large sheet and to continue photoing from left to right in equal sections with a small overlap. If necessary, sectioning is continued again — beginning below the first row and continuing on until complete.

4. The majority of users indicate that the textual content is of greatest value, however, a somewhat higher quality reproduction could be made from "photographs" if essential to the understanding of the dissertation. Silver prints of "photographs" may be ordered at additional charge by writing the Order Department, giving the catalog number, title, author and specific pages you wish reproduced.

5. PLEASE NOTE: Some pages may have indistinct print. Filmed as received.

University Microfilms International
300 North Zeeb Road
Ann Arbor, Michigan 48106 USA
St. John's Road, Tyler's Green
High Wycombe, Bucks, England HP10 8HR

Reproduced with permission of the copyright owner. Further reproduction prohibited without permission.

77-18,303

SNOW, Arthur William, 1949-
POLY(CARBON SUBOXIDE)-A PARAMAGNETIC, PHOTO-SENSITIVE OLIGOMER.

City University of New York, Ph.D., 1977
Chemistry, polymer

Xerox University Microfilms, Ann Arbor, Michigan 48106

© COPYRIGHT BY

ARTHUR WILLIAM SNOW

1977

Reproduced with permission of the copyright owner. Further reproduction prohibited without permission.

POLY(CARBON SUBOXIDE)-A PARAMAGNETIC,PHOTOSENSITIVE OLIGOMER

by

ARTHUR WILLIAM SNOW

A dissertation submitted to the Graduate Faculty in Chemistry in partial fulfillment of the requirements for the degree of Doctor of Philosophy, The City University of New York

1977

Reproduced with permission of the copyright owner. Further reproduction prohibited without permission.

This manuscript has been read and accepted for the Graduate Faculty in Chemistry in satisfaction of the dissertation requirement for the degree of Doctor of Philosophy.

April 19, 1977
date

Chairman of Examining Committee

April 19, 1977
date

Executive Officer

Supervisory Committee

The City University of New York

Reproduced with permission of the copyright owner. Further reproduction prohibited without permission.

Abstract

POLY(CARBON SUBOXIDE)-A PARAMAGNETIC, PHOTOSENSITIVE OLIGOMER

by

Arthur William Snow

Advisers: Professors Nan-Loh Yang and Howard Haubenstock

Carbon suboxide undergoes a transformation from a colorless liquid or gas to a dark reddish-brown polymeric solid of identical elemental composition at temperatures of less than 100°C.

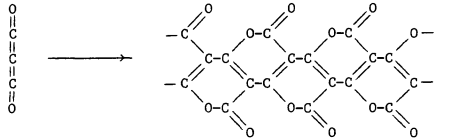

This transformation is accompanied by the growth of a narrow, intense ESR signal characterized by a g-value of 2.0050, an intensity of 2×10^{18} spin/gram and a line width of 2.3 gauss. Experiments were designed to study the structure of the polymer radical and mechanism of the polymerization.

The paramagnetism was ascribed to the polymer by finding a linear relationship between the polymer's optical density and spin density and by obtaining the same kinetic rate law of first order in both monomer and polymer from ESR measurements as had previously been obtained from optical

Reproduced with permission of the copyright owner. Further reproduction prohibited without permission.

density and monomer pressure measurements. When the polymer was prepared from C_3O_2 having an 18% carbon 13 enrichment at the central atom, a coupling constant of 9 gauss was measured. The ESR signal intensity was found to be enhanced by irradiating the polymer with visible light and to decay by a two electron process to its residual intensity. The signal was insensitive to oxygen either when introduced after the polymerization or present during the polymerization. Water vapor irreversibly reacted with the polymer causing a simultaneous decay of the ESR signal and a ketenyl band at 4.6 μ in the infrared as well as a bathochromic shift in the visible spectrum. Other more powerful but less polar nucleophiles, such as ammonia or methylamine, were much less effective. Molecular and equivalent weight measurements showed the polymer to have a degree of polymerization of between 5 and 6 and to have a functionality of 2 ketenyl groups per polymer molecule. From these results, the paramagnetism is proposed to result from an electron transfer between polymer molecules stabilized by a ketenyl and carbonyl terminated polyene chain contained within the polymer's ladder structure.

The presence of oxygen and nitric oxide had little effect on the polymerization rate while the presence of 3-methyl-1-butene and 1,3-butadiene markedly reduced the rate and acetaldehyde and acetone effectively inhibited polymerization. In dimethylformamide solution, the polymerization rate decreased as the solution polarity was decreased by diluting with toluene. A zwitterionic mechanism is proposed which is similar to a 1,3 dipolar addition of a keto-carbene to ketene.

Reproduced with permission of the copyright owner. Further reproduction prohibited without permission.

ACKNOWLEDGEMENT

The author wishes to express his sincere appreciation to Dr. Nan-Loh Yang and Dr. Howard Haubenstock for their generous support, assistance and patience which were so essential in an exploratory project such as this one. Acknowledgement is made to the following sources for financial support: (a) the City University of New York Faculty Research Award Program, Grant No. 1620, 11084 and 11420 and (b) the Petroleum Research Fund administered by the American Chemical Society.

Reproduced with permission of the copyright owner. Further reproduction prohibited without permission.

TABLE OF CONTENTS

Reproduced with permission of the copyright owner. Further reproduction prohibited without permission.

LIST OF TABLES

Reproduced with permission of the copyright owner. Further reproduction prohibited without permission.

LIST OF FIGURES

Reproduced with permission of the copyright owner. Further reproduction prohibited without permission.

Reproduced with permission of the copyright owner. Further reproduction prohibited without permission.

Reproduced with permission of the copyright owner. Further reproduction prohibited without permission.

Reproduced with permission of the copyright owner. Further reproduction prohibited without permission.

Reproduced with permission of the copyright owner. Further reproduction prohibited without permission.

Reproduced with permission of the copyright owner. Further reproduction prohibited without permission.

I. INTRODUCTION

One of carbon suboxide's most interesting properties is its spontaneous polymerization on heating to coat reaction vessel surfaces with a yellow film. The structure of the C_3O_2 thermopolymer has been investigated by several groups (1,2), and a poly(α-pyrone) has been proposed.

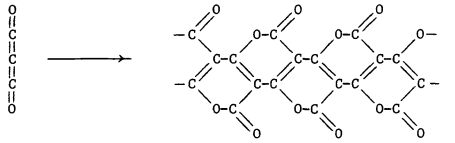

To examine the possibility that this reaction might be a free radical process, the polymerization was monitored by electron spin resonance (ESR). Following an induction period, an accelerating growth of a narrow, intense signal was observed. The signal did not reach a steady state intensity or decay but increased with monomer conversion. This paramagnetism is found to be a natural property of the polymer and to have a reversible photosensitivity to visible light.

The purpose of this work is to determine a structure for the poly(carbon suboxide) radical, to further characterize the polymer and to suggest a mechanism for the thermopolymerization. Paramagnetism is an unreported property of the C_3O_2 thermopolymer, and the polymer structure should be able to account for it. The structure of the paramagnetic center is investigated by analyzing the ESR spectrum and the spectrum's variation with temperature, with exposure to light and with exposure to chemical reagents. Polymer characterization, which has yet to include a direct molecular weight measurement, has been hampered by lack of a solvent and a sensitivity to moisture which causes the polymer to become acidic.

Reproduced with permission of the copyright owner. Further reproduction prohibited without permission.

Finding the air exposed polymer to be soluble in dimethylformamide, DMF, and dimethylsulfoxide, DMSO, enables polymer molecular weight, its relation to the equivalent weight and its variation with reaction temperature to be studied. A reaction path where only C_3O_2 units are incorporated into the accepted polymer structure has yet to be proposed. Knowledge of polymer size, identity of the end groups, polymerization kinetics and reagents that inhibit propagation provide clues for suggesting a mechanism.

Reproduced with permission of the copyright owner. Further reproduction prohibited without permission.

II. LITERATURE SURVEY

Carbon suboxide is a five atom linear molecule possessing four cumulative π bonds.

$$O=C=C=C=O$$

It was discovered in 1906 by Diels (3) who made the correct structural assignment based on a molecular weight measurement, an elemental analysis and a reaction with water from which he identified malonic acid. The two major synthetic routes are the solid state dehydration of malonic acid by phosphorus pentoxide at 140°C. (4) and the pyrolysis of diacetyltartaric anhydride at 575 to 600°C. (5). For an evaluation of these two synthetic routes and physical properties of C_3O_2 see the appendix.

Coincident with the discovery of carbon suboxide was the observation of its polymerization. In contrast to the colorless monomer, the polymer is an intensely colored solid. The polymerization is usually preceded by an induction period which increases with decreasing temperature and monomer pressure. From a gaseous monomer phase, the polymer forms as a film on the container surfaces ranging in color from yellow to dark brown depending on its thickness. From a liquid monomer phase or from most organic solvents, it precipitates as a dark brown powder. On exposure to moisture, water is irreversibly absorbed, and the polymer assumes a reddish hue which earned it the designation "red carbon" or "red coal" in the older literature (6).

Diels was the first to propose a structure for the polymer. He proposed a polyspirocyclobutanedione (7) which can be generated by a 2 + 2 cycloaddition through the C_3O_2 olefin bonds and is characteristic of substituted ketenes (8).

Reproduced with permission of the copyright owner. Further reproduction prohibited without permission.

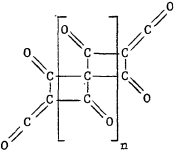

While this structure provides for a unique repeat unit based on the C_3O_2 unit and can account for a sensitivity to moisture, it was not consistent with the observations of Schmidt (9) of an x-ray diffraction spectrum similar to microcrystalline carbon and an infrared absorption attributable to a lactone functional group. They proposed an irregular clustering of C_3O_2 units into 10 Å planar graphite like sheets in which most of the carbon atoms are sp^2 bonded with oxygen occupying the edge positions in the form of lactone, ketone or ketene functional groups.

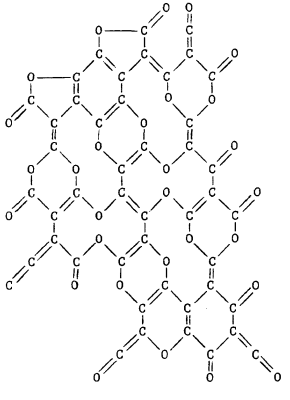

Reproduced with permission of the copyright owner. Further reproduction prohibited without permission.

An unsatisfactory feature of this structure is the lack of a unique repeat unit. Ziegler found that C_3O_2 will add stepwise to substrates having a malonyl or enol group, such as 4-hydroxycoumarin or phenol, with progressive color development (10).

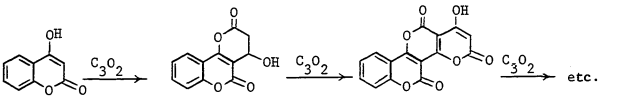

He observed infrared bands at 5.80 to 5.89μ in the C_3O_2 thermopolymer as well as with the enol initiated polypyrones. A double carbonyl absorption at this wavelength is frequently observed with unsaturated α-pyrones (11). He also observed that, when a trace of water or acetic acid was present, C_3O_2 more readily polymerized and proposed an "acetonedicarboxylic anhydride intermediate" as the polymerization initiating species (12).

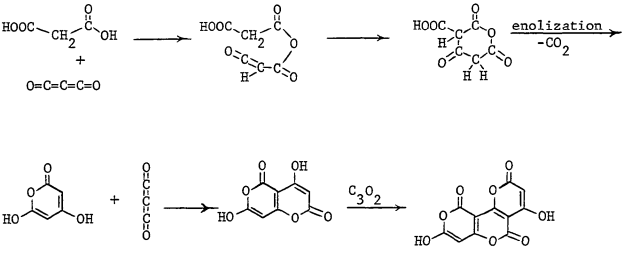

Reproduced with permission of the copyright owner. Further reproduction prohibited without permission.

While this structure accounts for the color and infrared carbonyl absorption of the thermopolymer, the initiator-polymer stoichiometry would require ladder polymers of inordinately high molecular weight or appreciable quantities of water or acetic acid to be present. It also presumes a stepwise polymerization process.

Smith studied the structure and properties of the carbon suboxide polymer prepared by gas deposition at temperatures ranging from 25 to 400°C. using infrared and visible-ultraviolet spectroscopy and thermal decomposition product analysis (1). Their infrared spectrum, in addition to exhibiting the unsaturated δ-lactone carbonyl doublet characteristic of Ziegler's α-pyrone repeat unit, also contained a 4.6μ ketenyl band but no hydroxyl band. They interpreted their results as favoring a conjugated, fused ring α-pyrone repeat unit for the polymer based on; (1) a visible light absorption characteristic of a conjugated system, (2) an evolution of carbon dioxide as the major thermal decomposition product indicating a carbon bonded to two oxygens within the polymer, (3) an unsaturated δ-lactone carbonyl infrared absorption, and (4) an equivalent weight corresponding to one C_3O_2 unit indicating complete hydrolysis of the lactone bonds. Their equivalent weight measurement appears to be more intuitive than experimental. The data is not presented and result is described as "not precise." Their result of 68 gram/equivalent is at variance with an earlier published result of 158 gram/equivalent (5) as well as with results to be presented in this work. Their rational for the total hydrolysis of the lactone bonds is based on a parallel with δ-valerolactone which is a saturated lactone. Polycyclic fused ring α-pyrones have been observed to resist total hydrolysis (13). Nevertheless their proposal of an α-pyrone repeat unit is consistent with Ziegler's work and Blake's work to be discussed below. For end groups they suggest

Reproduced with permission of the copyright owner. Further reproduction prohibited without permission.

a 1,2 or a 2,3 C_3O_2 addition to yield a five membered ring possessing a ketenyl group. However, they prefer to assign the infrared ketenyl band to absorbed monomer which can be removed by prolonged hard pumping.

Blake (2) investigated the structure and pyrolysis of carbon suboxide thermal polymers by x-ray diffraction, infrared spectroscopy and decomposition product analysis. A calculated x-ray diffraction pattern for a fused ring chain of 5 to 10 C_3O_2 units provided the best match with the observed pattern for a polymer prepared at 100°C. The variation in x-ray diffraction pattern with increasing polymerization temperature indicated a corresponding increase in chain length. Infrared results were interpreted as a structure of unsaturated, fused, 6-membered rings in a zigzag configuration, but, in contrast to Smith, the 4.6μ band was assigned to a ketenyl terminating group. Gaseous product analysis of polymer pyrolysis below 300°C. revealed only CO_2 and no CO which was interpreted to support the poly(α-pyrone) structure from which CO_2 units may thermally be eliminated.

Smith (14), by following polymer optical density at 370 nm, and Blake (15), by the fall in monomer pressure, found the polymerization to be first order with respect to monomer and to polymer. Both observed an induction period when no polymer was initially present, and that the polymer, once formed, served as the substrate for the growth of more polymer. Smith proposed C_2O, formed by the thermal decomposition of C_3O_2, is responsible for formation of the initial polymer substrate. Blake attributed the induction period to a surface poison, which he identifies as water, and the initiation to a possible surface free radical mechanism. Neither addresses themself to the structure involved in the processes of chain initiation, propagation and termination.

Reproduced with permission of the copyright owner. Further reproduction prohibited without permission.

In summary, most recent work on the carbon suboxide thermopolymer favors a poly(α-pyrone) structure of low molecular weight which increases with increasing reaction temperature although direct molecular weight measurements have yet to be reported. Five membered rings with pendant ketenyl groups have been proposed as end groups although a ketenyl functionality of two has yet to be demonstrated. A polymerization rate law of first order in both monomer and polymer has been determined, but no molecular description of initiation, propagation and termination has been proposed.

Reproduced with permission of the copyright owner. Further reproduction prohibited without permission.

III. PARAMAGNETISM

The paramagnetism was first observed as an accelerating growth of a very narrow and remarkably intense ESR signal which accompanied the thermal bulk polymerization of carbon suboxide (Figure 1). The problem is to determine the radical structure responsible for the signal, but, before doing so, it is necessary to certify that the paramagnetism is indeed a natural property of the polymer and not a paramagnetic product of a side reaction or a buried reactive radical intermediate. The radical's structure is then investigated by making a detailed analysis of the ESR spectra of polymers prepared over a temperature range of 30 to 105°C., examining the signal's temperature dependence to determine whether Curie's Law is followed, investigating the photosensitive behavior of the signal and observing the effect of exposure to water and related nucleophiles on the ESR and IR spectra.

1. PARAMAGNETISM - A NATURAL POLYMER PROPERTY

The paramagnetism was connected to the polymer by monitoring a bulk property of the polymer simultaneously with the ESR signal. The polymer, when deposited from the gas phase, forms a yellow film on the heated area of an optical cell and has an absorption maxima at 370 nm in the visible-ultraviolet spectrum (Figure 2). A cell was constructed by connecting a 100 ml pipet bulb to a flat quartz flow cell sealed at one end having a 25 mm length, a 5 mm width and a 0.5 mm path length (Figure 3). This cell was suitable for ESR, optical and IR (up to 4.8μ) measurements. The cell was filled with C_3O_2 vapor at a pressure of 190 mm Hg, and a polymer film was deposited on the flat quartz surface by heating in a small oil bath at 100°C. At various extents of conversion, the ESR signal intensity and optical absorbance at 370 nm were measured, and the spin density was found to be linearly related to the optical density (Figure 4).

Reproduced with permission of the copyright owner. Further reproduction prohibited without permission.

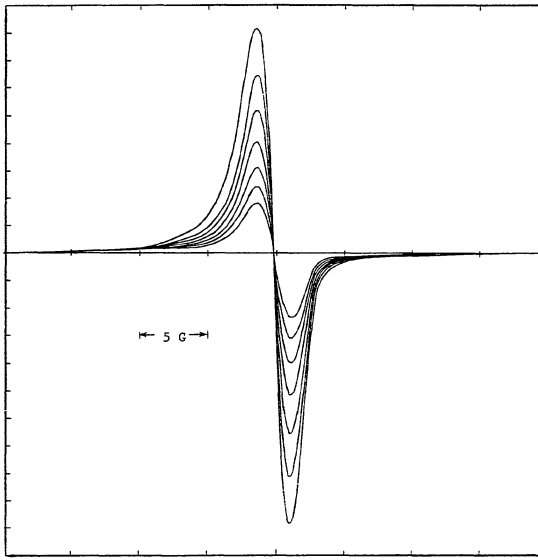

Figure 1. Repetitive scan of ESR signal during a carbon suboxide bulk polymerization.

The kinetics of the thermal bulk polymerization were followed by ESR to further connect the paramagnetism to the polymer. ESR has the advantage over optical spectroscopy that a transparent film is not required and the spin density does not become immeasurably high as the optical density does in the early stages of the reaction. Samples were prepared by transferring C_3O_2 in vacuo to a glass tube sealed at one end (ID = 2 mm, OD = 3mm) until the liquid height was about 1 cm which corresponds to approximately 35 mg. The tube was cooled with liquid

Reproduced with permission of the copyright owner. Further reproduction prohibited without permission.

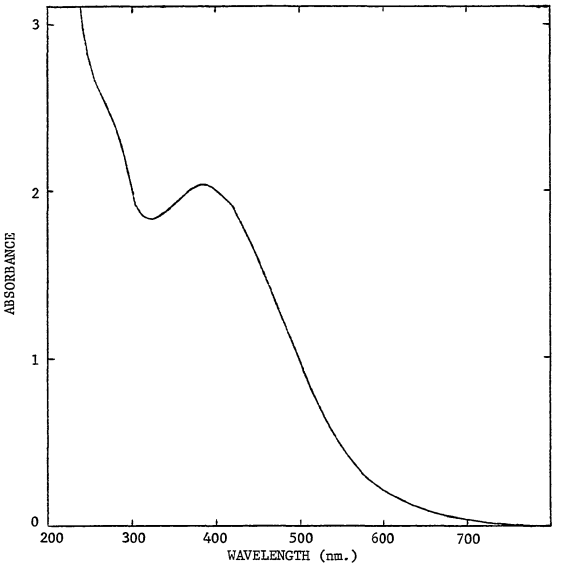

Figure 2. Visible-ultraviolet spectrum of a poly(carbon suboxide) film prepared at 75°C.

nitrogen and sealed at a total length of 2.0 to 2.5 cm. Samples prepared in this manner would easily slip into an ESR cell and were short enough for total exposure in the cavity. They also permit good monomer concentration control since a thermally induced concentration gradient between a heated surface and a monomer reservoir does not exist as would in a film deposition experiment. The polymerization rate was followed by the peak to peak intensity, D, of the ESR signal. The line width of 2.3 gauss and line shape remained constant throughout the conversion.

Reproduced with permission of the copyright owner. Further reproduction prohibited without permission.

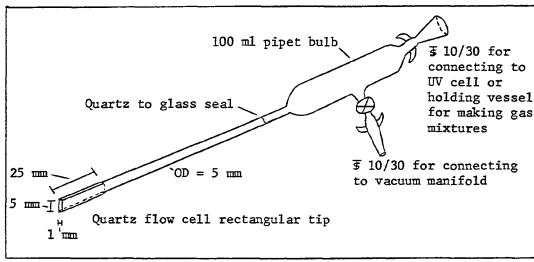

Figure 3. Carbon suboxide polymer deposition cell.

The reaction order with respect to polymer was found to be first order as the logarithmic dependence of D on time shows (Figure 5). An Arrhenius plot was found to be linear over a 0 to 50°C. temperature range yielding an activation energy of 9.9 Kcal/mole and a frequency factor of 2.4×10^3 sec^{-1}. The initial monomer concentration was then varied by adding toluene as an inert dilutent, and a plot of the natural log of the slopes of each of the ln D vs. time plots were plotted against the natural log of the initial monomer concentration (Figure 6). The slope of this plot, which corresponds to the reaction order with respect to monomer, was 0.98 indicating first order. These results correspond to the rate law:

$$\frac{d[P]}{dt} = k[M][P]$$

and to the equation:

$$M + P \longrightarrow P$$

where M is the C_3O_2 monomer and P is the C_3O_2 thermopolymer.

This is the same rate law obtained by Smith (14) based on optical density measurements at 370 nm and by Blake (15) based on monomer

Reproduced with permission of the copyright owner. Further reproduction prohibited without permission.

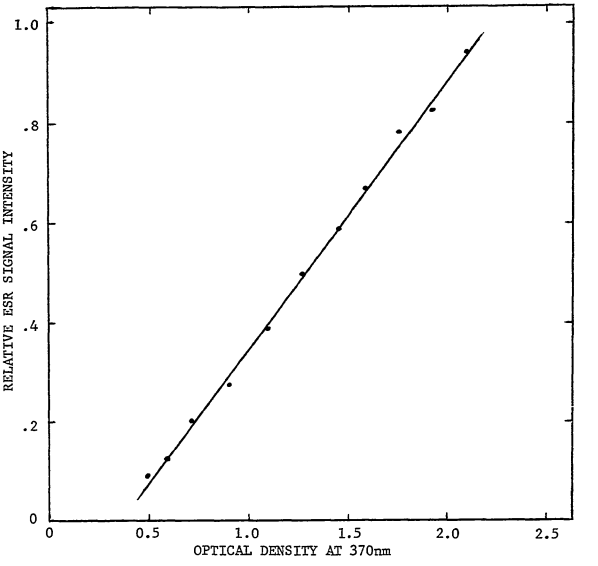

Figure 4. Spin density as a function of optical density at 370 nm.

pressure measurements. There is some discrepancy on activation energies. Smith reports 6.23 Kcal/mole for polymerization onto a silica surface, and Blake reports 8.0 Kcal/mole for a silica surface and 6.3 Kcal/mole for a pyrex surface. The polymerization is preceded by an induction period which is surface dependent (1), and a surface effect is probably reflected in these activation energies. Smith's activation energy is probably the most surface dependent since his method of measurement requires a very thin film. The ESR value is probably the least surface dependent since the surface area to monomer or polymer concentration is

Reproduced with permission of the copyright owner. Further reproduction prohibited without permission.

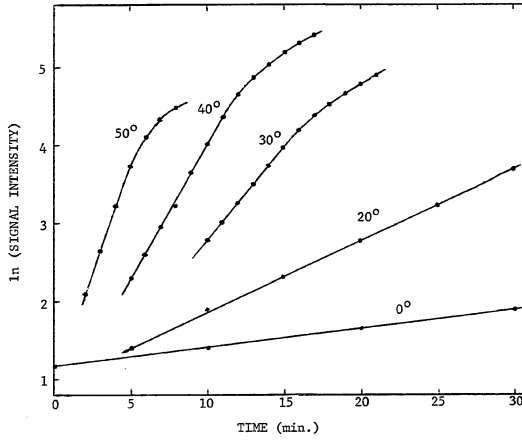

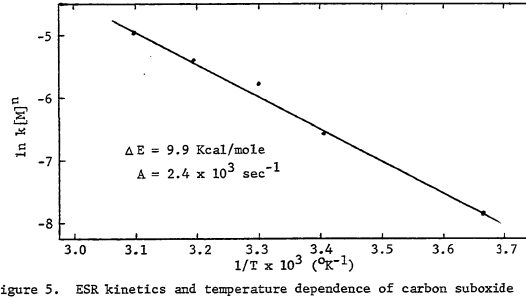

Figure 5. ESR kinetics and temperature dependence of carbon suboxide bulk thermal polymerizations.

Reproduced with permission of the copyright owner. Further reproduction prohibited without permission.

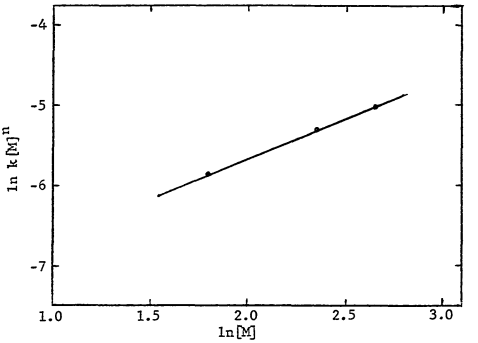

Figure 6. Polymerization rate dependence on monomer concentration.

the lowest. However, the monomer in the ESR measurement is in the liquid phase and does not possess the energy of vaporization that monomers in a gaseous deposition system would have. This could account for a positive difference in the ESR activation energy. While the activation energy agreement is fair, the agreement of rate laws based on different measurements is very good and favors ascribing the paramagnetism to the C_3O_2 polymer.

The possibility of a buried reactive radical intermediate was discounted by polymerizing C_3O_2 in the presence of an equimolar quantity of oxygen which is a free radical inhibitor. Oxygen as well as nitric oxide had no inhibiting effects on the polymerization rate (See Figure 41). This was further confirmed by running a bulk and a toluene solution C_3O_2 polymerization in the presence of a phenyl tert-butyl-nitrone spin trap. This spin trap adds to a reactive radical to produce a stable nitroxy radical (16,17).

Reproduced with permission of the copyright owner. Further reproduction prohibited without permission.

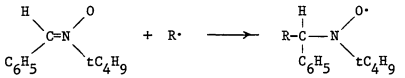

This nitroxy radical has a characteristic ESR spectrum consisting of a triplet of doublets due to the nitrogen (a_N = 15 gauss) and hydrogen (a_H = 2-3 gauss) atoms. The nitrone was verified to be active by obtaining such a spectrum on heating it to 60°C. in a toluene solution of azobisisobutyronitrile. Only the 2.3 gauss polymer signal and no nitroxy radical spectrum was observed from either the bulk or toluene solution polymerizations. The polymerization process then does not involve a reactive radical, and the polymer radical is stable enough to be unreactive toward phenyl tert-butyl nitrone. The paramagnetism is considered to be a property of the polymer structure.

2. ESR SPECTRUM ANALYSIS

This section presents an analysis of the poly(carbon suboxide) ESR signal with respect to line shape, saturation behavior, g-value, spin density and hyperfine structure over a reaction temperature range of 30 to 105°C. These results are summarized in Figure 7 and a detailed discussion of them is given below.

A. Experimental

Samples were prepared by sealing 35 mg quantities of liquid C_3O_2 in 2 cm lengths of 3 mm glass tubing and polymerized by immersion in thermostated oil baths. As a reproducibility control, two samples were prepared at each reaction temperature. At 30, 60 and 90°C., samples were characterized by progressively more rapid color development, and all displayed strong absorptions with line widths of 2.3 gauss. At 120°C. the samples exploded violently after 18 minutes immersion. The reaction temperature was reduced to 105°C. and 2 samples were immersed

Reproduced with permission of the copyright owner. Further reproduction prohibited without permission.

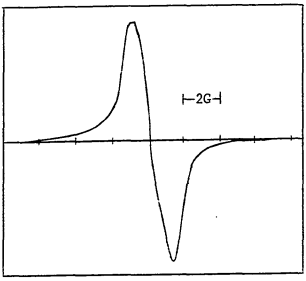

Polymerization temperature	less than 100°C.
g-value	2.0050 ± .0002
Spin density	2.5×10^{18} spin/g.
Line width	2.3 gauss
Line broadening	inhomogeneous
T_1	2.5×10^{-5} sec.
T_2	2×10^{-7} sec.

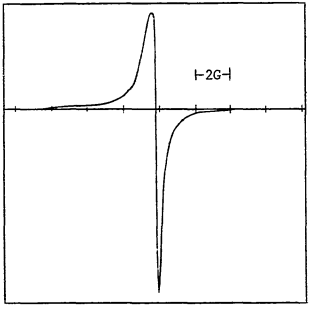

Polymerization temperature	105°C.
g-value	2.0045 ± .0002
Spin density	2×10^{19} spin/g.
Line width	0.4 gauss
Line broadening	homogeneous
T_1	2×10^{-7} sec.
T_2	1×10^{-7} sec.

Figure 7. ESR spectral characteristics of bulk C_3O_2 polymers.

in the oil bath. Neither exploded, but each had a spectrum markedly different from the other. One had a very narrow 0.4 gauss line while the other had a 2.6 gauss line. Repeating the reaction with another two samples resulted in one explosion and a sample whose spectrum appeared to be a combination of the two lines. Repeated attempts at this temperature produced either explosions or samples with spectra in

Reproduced with permission of the copyright owner. Further reproduction prohibited without permission.

which the intensities of the two lines varied. When the polymer is prepared by deposition from the gas phase, signals with a line width varying from 2 to 3.5 gauss are obtained over a temperature range of 70 to 250°C. No regular variation of line width with reaction temperature was observed nor was the transition to the narrow line at 105°C. or any other temperature observed. Bulk polymerized samples had better reproducibility and are used for the ESR spectrum analysis. The ESR spectra have not been observed to be dependent on the source of C_3O_2.

For line shape analysis and spin density measurements, a JEOL Model JES-ME-3X, X-band ESR spectrometer with a TE_{105} cylindrical dual cavity was used. The low saturation powers of the signals necessitated the use of a wave guide flap attenuator set at 17 dB.

Spectra for line shape analysis were obtained at microwave powers where the peak-to-peak signal intensity response to the square root of the power was linear and at modulation amplitudes of less than one fourth the line width. The modulation frequency was 100 KHz, although spectra obtained at 80 Hz had identical shapes.

Spin densities were measured against a known quantity of crystalline diphenylpicrylhydrazyl, DPPH, by two methods. The quantity of DPPH was determined experimentally by optical density in benzene, λ_{max} = 519 nm, log ε = 4.89. In the first method, spectra were taken with the modulation fields of the two sample positions in phase and then 180° out of phase giving the sum and difference of the poly(carbon suboxide) and DPPH signals. The sample positions were interchanged, and the relative number of spins was taken to be proportional to the root-mean-square of the absorption areas of the poly(carbon suboxide) and DPPH signals. In the second method, a manganese marker, consisting

Reproduced with permission of the copyright owner. Further reproduction prohibited without permission.

of manganous ion dispersed in magnesium oxide, was used to correct for any changes in the cavity Q, and the poly(carbon suboxide) and DPPH spectra were recorded alternately against the marker. All derivative curves were doubly integrated by the method of Wyard (18). Spin density calculations are based on the assumption of one spin per molecule DPPH.

Saturation curves and g-value measurements were obtained using a Varian model E-9, X-band ESR spectrometer with a TE_{102} rectangular cavity and a balancing arm to maintain constant detector current. Spectroscopic splitting factors were directly determined at the cross-over point by magnetic field measurements with an NMR gaussmeter and microwave frequency measurements with a frequency meter. The precision of the frequency meter was $\pm$ 1 MHz limiting that of the g-value to $\pm$ 0.0002.

B. Line Shape Analysis

Depending on the reaction temperature, two line shapes are observed. At a reaction temperature of 30, 60 or 90°C., a line with a slightly unsymmetrical shape and a width of 2.3 gauss was observed (Figure 8a). Theoretical Gaussian and Lorentzian line shapes, calculated using the experimental line width and low field derivative peak height (19), show the derivative peaks to be too narrow to closely fit either a Gaussian or Lorentzian shape. The theoretical curves also illustrate the asymmetry of the experimental line. The low field derivative peak is slightly more intense than the high field derivative peak, and the crossover does not occur midway between the derivative peaks but at a point 0.2 gauss down field. A partially resolved component is suggested by the curvature of the experimental

Reproduced with permission of the copyright owner. Further reproduction prohibited without permission.

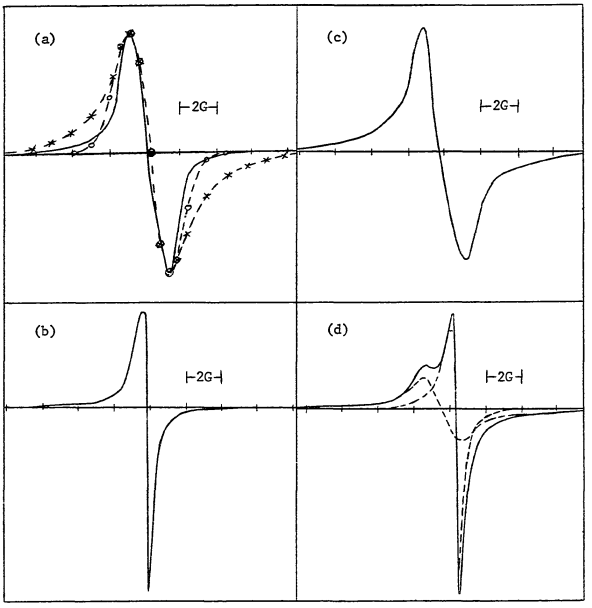

Figure 8. ESR spectra of poly(carbon suboxide) samples; (a) formed at temperatures of 30, 60 or 90°C (solid line, experimental spectrum; x, theoretical Lorentzian curve; o, theoretical Gaussian curve); (b) formed at 105°C exhibiting only the narrow signal - sample 105°#1; (c) formed at 105°C exhibiting only the broad signal - sample 105°#2; (d) formed at 105°C exhibiting both broad and narrow signals (solid line, experimental spectrum; dashed lines, shapes of individual signals).

line near the center of the spectrum where it intersects the theoretical lines. At a reaction temperature of 105°C., the first four samples produce four different results. The first, 105 #1, yielded an unsymmetrical, intense, very narrow line of width 0.4 gauss

Reproduced with permission of the copyright owner. Further reproduction prohibited without permission.

(Figure 8b). The second, 105 #2, had a broader line of width 2.6 gauss and was more similar in shape to the one produced at low reaction temperatures (Figure 8c). The third, 105 #3, and most frequently observed with subsequent samples, had a line shape that appeared to be a combination of the 2.3 and 0.4 gauss signals (Figure 8d). By normalizing the 105 #1 line to the 105 #3 peak-to-peak height and subtracting it vectorially from the 105 #3 line, a line of proper width, shape and g-value to correspond to the one produced at low reaction temperatures was obtained. The fourth was a violent explosion.

Increasing the gain by a factor of 10 allowed resolution of shoulders at approximately 6 gauss on either side of the crossover point on the 30, 60 and 90°C. signals but not the 105°C. signals. The intensities of these shoulder peaks could not be accurately measured, but the order of magnitude and symmetry are correct for them to be ^{13}C satellites.

A thorough search over a 500 to 5500 gauss scan revealed no half field ($\Delta M = 2$) transition.

C. Saturation Behavior

In addition to line shape, the broad 2.3 gauss and narrow 0.4 gauss signals show markedly different saturation behavior. The broad line passes rapidly through a maximum intensity and becomes quite unsymmetric at high degrees of saturation, while high microwave powers are necessary to reach the narrow line's saturation maxima, and its shape is preserved passed saturation. In Figure 8d, the low field shoulder disappears at powers corresponding to saturation of the broad signal. To characterize this behavior, the nature of the line broadening and the spin-spin and spin-lattice relaxation times are examined.

Reproduced with permission of the copyright owner. Further reproduction prohibited without permission.

The line width of the broad signal gradually decreased on passing through saturation from 2.3 to 2.1 gauss, and, at very high degrees of saturation, gradually returned to 2.3 gauss. Also at high degrees of saturation, half of the derivative curve flattens out, and the line has the appearance of a dispersion curve superimposed on an absorption curve. The overall shape of the saturated line is dependent on the modulation amplitude and the tuning of the spectrometer. The small variation in line width and the emergence of a dispersion curve as the signal passes through saturation indicates the 2.3 gauss signal to be inhomogeneously broadened (20). The line width of the narrow signal increases continually after the onset of saturation with increasing power, which is consistent with a homogeneously broadened line.

The applicability of the Bloch equations is tested by the linearity of a plot of the reciprocal saturation factor, 1/s, against the microwave power, P (21).

$$1/s = (H_1/D_1)^{2/3}/(1/3)^{2/3} = (S_F/7)^2$$

where H_1 is the rf magnetic field, S_F the peak-to-peak line width, and D_1 the derivative signal intensity at $H_o \pm 1/2\ S_F$. Since H_1 is proportional to $P^{1/2}$, and the total peak-to-peak intensity, D, is proportional to D_1, substitution of these quantities should also yield a linear plot for homogeneously broadened lines. The quantity 1/s is normalized to 1 where no saturation is occurring. The nonlinear curves (Figure 9) of this plot indicate the broad line to be inhomogeneously broadened, while the narrow line appears to be mostly homogeneously broadened. The deviation from linearity of the plot of the line width dependent saturation factor of 105 #1 is not understood.

Reproduced with permission of the copyright owner. Further reproduction prohibited without permission.

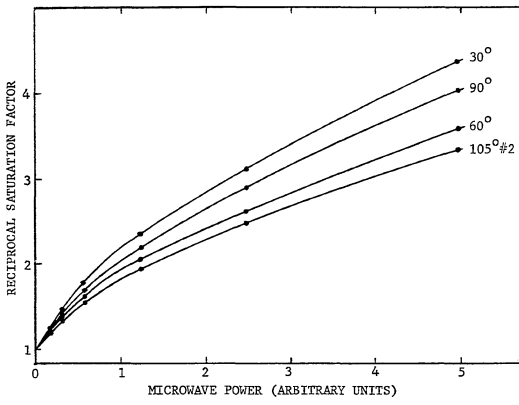

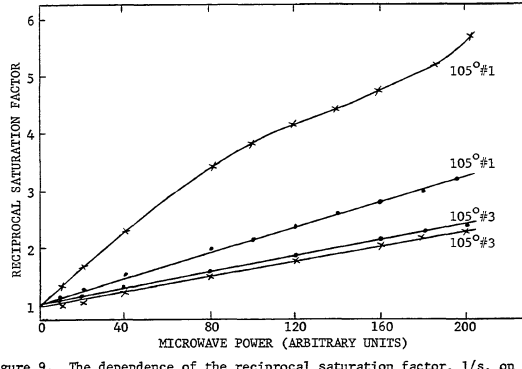

Figure 9. The dependence of the reciprocal saturation factor, $1/s$, on microwave power, P, of poly(carbon suboxide) samples. (o, $1/s = [P^{\frac{1}{2}}/I]^{\frac{1}{2}}$; x, $1/s = [S_E^{-2}]$)

Reproduced with permission of the copyright owner. Further reproduction prohibited without permission.

Spin-spin relaxation times for the signals corresponding to 105 #1 and #3 are obtained from the Bloch equations (21).

$$T_2 = \frac{1.3131 \times 10^{-7}}{g \cdot S_F}$$

T_2 for signals corresponding to the 30, 60, 90 and 105 #2 samples are calculated by Castner's method for inhomogeneously broadened lines (22).

$$T_2 = \frac{1}{a \cdot \omega_G}$$

The parameter "a" is defined as the ratio of the Lorentzian spin packet width to the inhomogeneous line width. Experimentally, it is obtained from the ratio, $P_u^{1/2}/P_L^{1/2}$. P_L is the power where D is one half its maximum value before saturation, and P_u is the power where D is one half its value after saturation (Figure 10). For the completely inhomogeneous case, a = 0, while for the completely homogeneous case a is infinite. At values of a > 1, i.e. where $P_u^{1/2}/P_L < 12$, Castner's curve for obtaining "a" becomes asymtotic. These results further indicate the homogeneous nature of the 105 #1 and #3 lines (Table I).

Spin-lattice relaxation times were obtained by plotting power curves against DPPH according to the method of Bloembergen, Purcell and Pound as applied by Singer, Spry and Smith (23) (Figure 11 and Table I).

$$T_1 = \left(\frac{P_{DPPH}}{P}\right)\left(T_{1\ DPPH}\right)^2\left(\frac{1}{T_2}\right)$$

Bloembergen and Wang (24) and Lloyd and Pake (25) have determined for DPPH single crystal $T_1 = T_2 = 6 \times 10^{-8}$ sec. The T_1 values for the broad signal may be open to question considering the experimental 100 KHz modulation frequency and the inhomogeneous broadening. This

Reproduced with permission of the copyright owner. Further reproduction prohibited without permission.

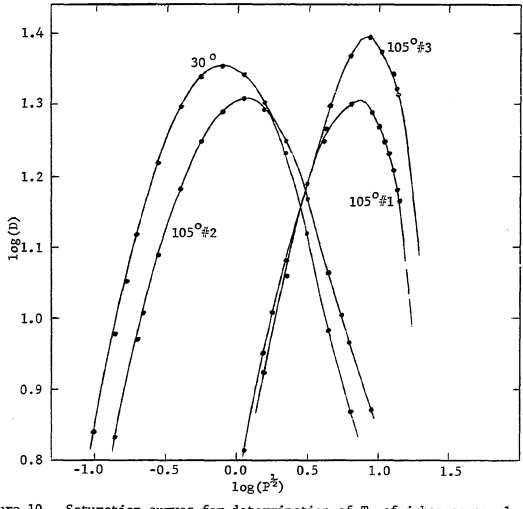

Figure 10. Saturation curves for determination of T_2 of inhomogeneously broadened lines.

TABLE I

SATURATION DATA

Sample	Line Width (gauss)	$P_U^{\frac{1}{2}}/P_L^{\frac{1}{2}}$	a	$T_2 \times 10^7$ (sec.)	$T_1 \times 10^7$ (sec.)
30°	2.3	22	0.17	1.5	320
60°	2.3	26	0.14	1.8	220
90°	2.3	23	0.17	1.5	250
105#2	2.6	29	0.14	1.6	160
105#3	0.4	9.8	____	1.7	2.2
105#1	0.6	7.3	____	1.1	1.7

Reproduced with permission of the copyright owner. Further reproduction prohibited without permission.

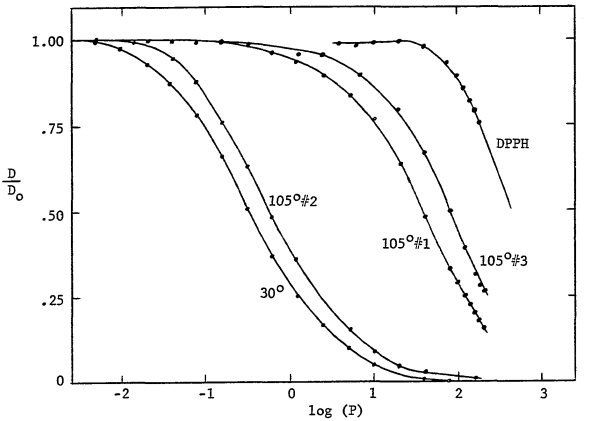

Figure 11. Saturation curves for determination of T_1.

saturation method assumes $\omega_m T_1 << 1$ and a Bloch-type absorption. However, the temperature dependence of the line width, to be discussed later, does indicate these numbers are in the right order of magnitude.

D. Spectroscopic Splitting Factor

The broad and narrow signals have significantly different g-values (Table II). The difference in g-values of 0.0005 is best illustrated in Figure 8-d, where it corresponds to a 0.8 gauss separation between the two types of signals. It is interesting to note that the "a" value yields a Lorentzian spin pack width of 0.4 gauss which corresponds closely to the narrow signal's line width. If the narrow line were a spin packet component of the broad line, a g-value shift from that of the latter to that of the former would be expected as the broad line saturated. However, the g-value was found to be the same on each side of the saturation maxima.

Reproduced with permission of the copyright owner. Further reproduction prohibited without permission.

TABLE II

SPECTROSCOPIC SPLITTING FACTORS

Sample	g ± 0.0002
30°	2.0052
60°	2.0050
90°	2.0049
105 #2	2.0052
105 #3	2.0045
105 #1	2.0045

E. Spin Densities

The 105°C reaction temperature, which, under the experimental bulk polymerization conditions, is responsible for the narrow line, also produces an increase in the spin density by one order of magnitude as Table III shows. Both methods of spin density measurement agree reasonably well although the phase modulation method requires sample and standard signals of near equal intensity.

TABLE III

SPIN DENSITIES x 10^{-18} (spin/gram)

Sample	Method A[a]	Method B[b]
30°	2.8	2.5
60°	2.5	2.3
90°	2.6	2.3
105 #2	4.8	4.6
105 #3	7.5	6.2
105 #1	43.	21.

[a] Phase modulation method.
[b] Mn^{2+} comparison method.

Reproduced with permission of the copyright owner. Further reproduction prohibited without permission.

F. Hyperfine Structure

The composition of the C_3O_2 polymer is unique in that the concentration of paramagnetic nuclei is limited to nearly that of the natural abundance of carbon 13. Carbon 13 satellite lines were suggested by barely resolvable shoulders at 6 gauss on either side of the central line. To obtain better resolution of the ^{13}C hyperfine structure, malonic acid with a carbon 13 enrichment of 18% at the central carbon atom was converted into C_3O_2 and polymerized in a 3 mm sealed glass tube at 30°C. A control of unlabelled malonic acid was converted into C_3O_2 and polymerized under identical conditions. The ESR spectrum of the carbon 13 labelled polymer showed resolution of almost one half line width of the satellite lines (Figure 12). To a first approximation a coupling constant of 10 gauss can be obtained by assuming the satellite line width equal to the central line width and the resolved maxima of the satellite lines are their true positions. Then the number of gauss separating the resolved satellite derivative peaks minus one line width gives the carbon 13 coupling constant for the position in the polymer corresponding to the monomer's central atom. A more accurate way is to obtain the absorption spectra by integrating the derivative spectra, and, after normalizing the unlabelled to the labelled spectrum at the central maxima, vectorially subtracting the unlabelled spectrum to obtain the satellite lines. The derivative spectra of the labelled and unlabelled polymers were divided into 63 intervals, and absorption spectra were obtained by a single integration using Wyard's method (18). Figure 13 shows the absorption spectra and the satellite lines obtained from the difference of the absorption spectra assuming no satellite absorption at the center of the spectrum.

Reproduced with permission of the copyright owner. Further reproduction prohibited without permission.

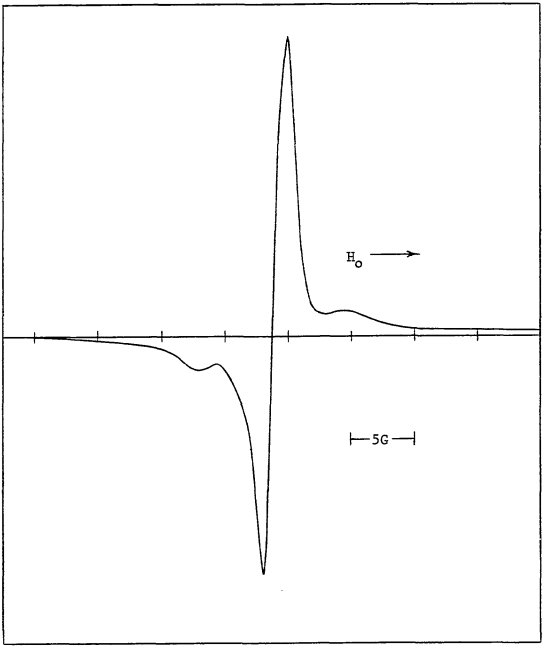

Figure 12. ESR derivative spectrum of poly(carbon suboxide) formed at 30°C from C_3O_2 having an 18% carbon 13 enrichment at the central atom.

The separation between the satellite maxima correspond to a coupling constant of 9 gauss. The area of the satellite absorptions is 24% of the total spectrum in fair agreement with the 18% carbon 13 enrichment.

G. Analysis

The two characteristics of the ESR spectrum which relate most to chemical structure are the g-value and the hyperfine structure.

Reproduced with permission of the copyright owner. Further reproduction prohibited without permission.

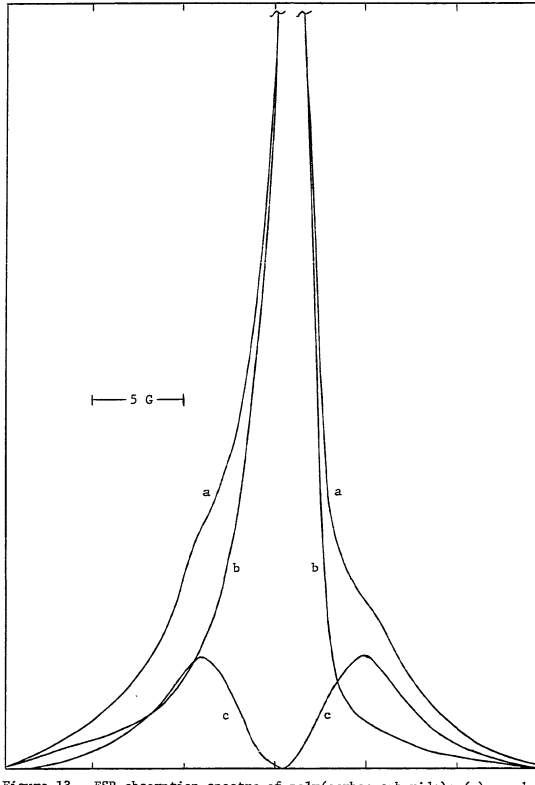

Figure 13. ESR absorption spectra of poly(carbon suboxide); (a), carbon 13 labeled; (b), unlabeled; (c), carbon 13 satellites.

Reproduced with permission of the copyright owner. Further reproduction prohibited without permission.

The magnitude of the carbon 13 hyperfine coupling constant is informative as to whether the poly(carbon suboxide) radical is sigma or pi-type in nature. More localized radicals have greater spin density at the nuclei of constituent atoms and possess higher coupling constants. For example, the methyl radical has a ^{13}C coupling constant of 38.5 gauss, while the benzene radical anion has a ^{13}C coupling constant of 2.8 gauss (26). When four oxygen atoms are placed about the benzene ring (C_3O_2 stoichiometry), a 2,5-dihydroxybenzosemiquinone radical anion can be obtained with the following coupling constants (27).

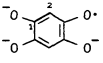

$a_H = 0.79$ G $\quad a_{^{13}C_1} = 2.8$ G $\quad a_{^{13}C_2} = 6.6$ G

The effect of the presence of a large number of oxygen atoms is to increase the spin density at certain carbon atoms and hence the ^{13}C coupling constant. While these examples are not intended to imply a semiquinone structure for the poly(carbon suboxide) radical, they do indicate it to be a delocalized π-type radical.

The g-value shift from that of 2.0023 for the free electron can be attributed to an oxygen effect. For aromatic systems, g-values are known to increase with an increase in the spin orbit coupling parameter of the constituent atoms (C, $\zeta = 28$ cm^{-1}; O, $\zeta = 152$ cm^{-1}) (28). As examples, for the benzene radical anion the g-value is 2.0028 (26), and for the o or p-benzosemiquinone the g-values are 2.0044 and 2.0047 (29). As suggested by the ^{13}C hyperfine coupling constant, the poly(carbon suboxide) g-value indicates oxygen plays an important part in the radical structure.

Considering the 2.3 gauss absorption, a g-anisotropy can best account for the line shape and broadening. Since the concentration of

Reproduced with permission of the copyright owner. Further reproduction prohibited without permission.

paramagnetic nuclei is on the order of the 1% ^{13}C natural abundance, unresolved hyperfine structure makes no significant contribution. Unresolved fine structure is precluded by the temperature dependence result of a doublet ground state (next section). To determine whether the spin concentration was responsible for any line broadening or narrowing effects, a thick wall glass capillary (ID = 0.5 mm) was sealed at one end, filled to a height of one inch with liquid C_3O_2 followed by an inch of DMF and sealed. The C_3O_2 polymerized rapidly at room temperature. One day later a strong signal of 2.3 gauss line width was observed at the C_3O_2 end, and a weak one of the same width and shape was observed at the DMF end. Two days later, the signal intensity at the DMF end had increased ten fold with no change in shape or line width. While undissolved polymer was observed in the capillary, the quantity of DMF was sufficient to plasticize the polymer. The independence of line width on spin concentration indicates dipolar broadening is not a factor in the spectrum shape. Consistent with the hyperfine structure and g-value interpretations, oxygen can be effective in increasing g-anisotropy and result in a somewhat asymmetric line shape (30). A g-anistropy is also consistent with the proposed polymer structure.

Attempts by two methods to obtain a solution spectrum of the poly(carbon suboxide) radical were unsuccessful. In the first method, a polymer sample was allowed to stand in P_2O_5 dried DMF for two weeks with no change observed in the signal. After decanting the DMF and dissolved polymer, the signal was found to reside in the undissolved polymer with no signal detectable from the solution. In the second method, the polymerization was carried out in DMF. No signal was observed unless a polymer precipitate had formed. After decanting, the

Reproduced with permission of the copyright owner. Further reproduction prohibited without permission.

signal was again found to reside in the precipitate and not in the solution. This result favors the paramagnetism being a property of the solid state although the possibility of a very low solubility of the polymer radical cannot be totally excluded.

The narrow 0.4 gauss line is easily distinguished from the 2.3 gauss absorption by saturating at substantially higher microwave powers and by possessing a significantly different g-value. The homogeneous broadening, greater spin density and lack of ^{13}C satellites are evidence for exchange narrowing. Both temperature and pressure appear to be factors in this transition to the 0.4 gauss line. The change in g-value and departure from Curie's Law in the form of an irreversible increase in spin density above 100°C. (next section) indicate a different spin center is being formed as the reaction temperature goes above 105°C. The occurrance of an explosion at 105°C. and above with the bulk samples indicate extreme pressure is being built up within the glass tube. The line narrowing and explosion are not observed at 105°C. or above when the polymer is formed by gas deposition on to a heated surface where the pressure effect would be expected to be absent. Pressure would have the effect of reducing the distance between spin centers, and, with the observed ten fold increase in spin density, a line width decrease by exchange narrowing is proposed.

The observed relaxation times are characteristic of those observed for spins distributed within a conjugated carbon atom matrix such as a polyene or pyrolytic carbon (31). The polymer's low concentration of paramagnetic nuclei and low degree of crystallinity (3) result in poor energy exchange between the spin system and the lattice yielding an easily saturable absorption. The spin-spin relaxation time measures the

Reproduced with permission of the copyright owner. Further reproduction prohibited without permission.

ability of the magnetic moment of the unpaired electron to follow the rf magnetic field in the unquantized x and y directions. Interaction with magnetic moments of other spin centers affects the precession of each unpaired electron causing a dispersity or sharpening in the quantized z spin energy levels and a broadening or narrowing of the resonance absorption depending on the identity and concentration of the spin centers. The carbon-oxygen composition of the polymer precludes the broadening effect of paramagnetic nuclei, and a relatively narrow resonance line is observed in the solid state similar to other materials of high carbon content.

3. TEMPERATURE DEPENDENCE

Most paramagnetic substances follow Curie's Law, which states that the magnetic susceptability or spin susceptability, χ, is directly proportional to the unpaired electron concentration, n, and inversely proportional to the absolute temperature, T.

$$\chi = \frac{C}{T} \cdot n$$

Interactions between unpaired electrons can cause magnetic moment alignments, and the more general Curie-Weiss Law is followed.

$$\chi = \frac{C}{T + \theta} \cdot n$$

where θ is the Weiss constant. However, if the paramagnetic state is capable of being thermally populated or depopulated, n is not constant, and the Curie-Weiss Law is not obeyed. In this case the population of the paramagnetic state has a Boltzmann thermal dependence given by

$$n = n_o e^{-\Delta E/kT}$$

where ΔE is the energy difference between the paramagnetic and diamagnetic states. The thermal dependence of the ESR signal has been

Reproduced with permission of the copyright owner. Further reproduction prohibited without permission.

very useful in determining whether the paramagnetic state was a ground state doublet or a low lying triplet state in the study of charge transfer complexes (32-36). Changes in the ESR spectrum with temperature also provide additional information about the paramagnetic state. Striking examples are the TCNQ ion radical salts where a low lying triplet state was exchanged narrow to a singlet absorption at room temperature, while at -140°C. the zero field splitting and half field transition were observed (33).

The poly(carbon suboxide) samples prepared for the ESR spectrum analysis were also used for the temperature dependence study. ESR signal intensity measurements were made using the dual cavity. Temperature was controlled in one position with a JEOL model JES-VCT-2AX variable temperature adaptor and measured by inserting an ion-constantan thermocouple into the sample position of the cavity. The other position, in which the Mn^{2+} marker was placed, was maintained at constant temperature. The signal intensity of the poly(carbon suboxide) was then measured relative to the Mn^{2+} marker at four microwave power levels of ratio 8:4:2:1 to obtain intensities where saturation was not occurring. The temperature range of the apparatus was -170 to 250°C. Spectra over a temperature range of 60 to 5°K were obtained through the courtesy of Bell Laboratories.

The line width of the ESR absorption corresponding to the 30, 60 and 90°C. samples remained constant at 2.2 to 2.3 gauss below room temperature over a range of 25 to -162°C. and of 60 to 5°K. This is consistent with a signal that has a T_2 controlled line width as the relaxation times indicate. The signal intensity's temperature dependence below room temperature is a Curie Law relationship with a Weiss constant not experimentally distinguishable from zero (Figure 14a).

Reproduced with permission of the copyright owner. Further reproduction prohibited without permission.

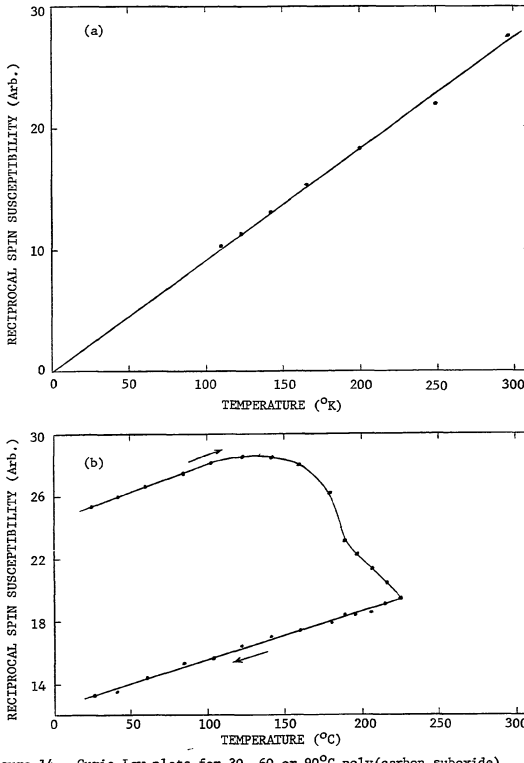

Figure 14. Curie Law plots for 30, 60 or 90°C poly(carbon suboxide) samples below (a) and above (b) room temperature.

Reproduced with permission of the copyright owner. Further reproduction prohibited without permission.

Above room temperature the Curie Law is followed up to about 100°C. where new spins are created as indicated by the negative deviation of the reciprocal spin susceptability (Figure 14b). The signal's line width also broadens to 2.7 gauss at this temperature. New spins are continually and irreversibly created with increasing temperature and follow Curie's Law as shown by measurement in the decreasing temperature direction. This suggests a thermally induced structural alteration of the polymer.

The narrow 0.4 gauss signal, resulting from C_3O_2 polymerization at 105°C., maintained a constant line width over a 25 to -162°C. temperature range, but narrowed from 0.39 to 0.30 gauss in the 60 to 19°K range and appeared to become immersureably narrow at 5°K (Figure 15a). The signal intensity, like the 2.3 gauss signal, has a Curie-Weiss law temperature dependence but a Weiss constant of 17.5 ± 2.6°K (Figure 15b). It is significant to note that the line width collapse occurs below the Weiss temperature. Below the Weiss temperature the magnetic dipole induced aligning interactions between unpaired electrons become stronger than the thermal randomizing forces. This results in very long relaxation times and can account for the line width collapse.

The spin density independence of temperature indicates the paramagnetic state is being neither thermally populated nor depopulated and is the ground state for the unpaired electron. For a paramagnetic state with a multiplicity greater than for a doublet, a zero field splitting and half field transition should be observed unless the paramagnetic centers are isolated enough to be independent of each other or concentrated enough to be exchange narrowed. Occasionally the exchange interaction can be thermally quenched at low temperatures and zero field

Reproduced with permission of the copyright owner. Further reproduction prohibited without permission.

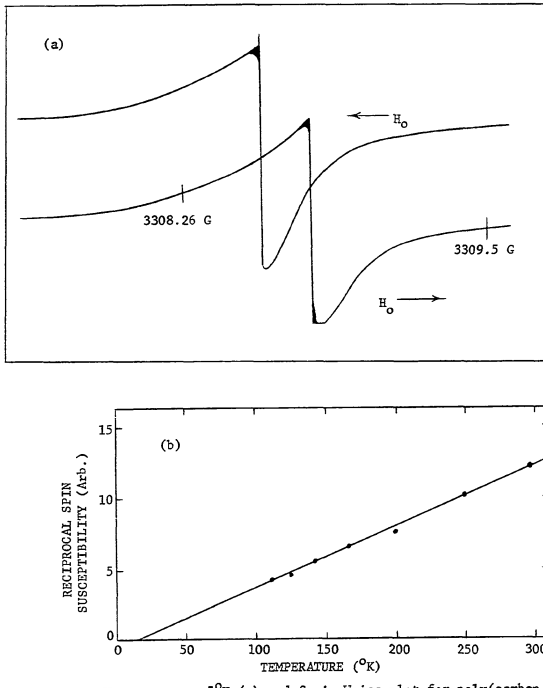

Figure 15. ESR spectra at 5°K (a) and Curie-Weiss plot for poly(carbon suboxide) sample 105°#1 (b).

splitting and $\Delta M = 2$ transition observed if the multiplicity of the state is greater than two (33). This was not observed with the poly(carbon suboxide) radical. Dilution of the paramagnetic centers will remove the

Reproduced with permission of the copyright owner. Further reproduction prohibited without permission.

effects of exchange narrowing allowing hyperfine structure as well as fine structure to be observed. The 2.3 gauss poly(carbon suboxide) absorption was observed not to be exchange narrowed and to have no half field transition. Therefore, it must correspond to a doublet ground state or the special case of a biradical.

The Curie Law behavior also indicates the unpaired electrons to be localized to a polymer molecule. Conduction electrons do not follow Curie's Law (37). Attempted resistance measurements in a nitrogen atmosphere on a compressed pellet of polymer formed at 60°C. indicated the resistance to be greater than 10^{12} ohms further confirming the unpaired electron to be localized. The result would also be expected from the X-ray diffraction result of low crystallinity (3) making band formation for electrical conduction difficult.

4. PHOTOSENSITIVITY

Electronic transitions, which are of too high energy to be brought about thermally without decomposition, can be made to occur by exposure to light. If the electronic transition involves a paramagnetic state, the possibility of monitoring it with ESR then exists. A clear, transparent sample usually in the form of a solution or film is normally required to insure good light penetration. Poly(carbon suboxide) is admirably suited for this purpose as it may be deposited from a gaseous monomer phase onto a heated surface in the form of a yellow transparent film of easily controllable thickness. The problems of solvent interference, solvent originated impurities or solvent evaporation are completely absent. A thin film is necessary since the polymer is intensely colored. The intensity of the absorbed light in the film should decline according to the Beer-Lambert Law, and the residual ESR absorption from layers within the film, displaced from the

Reproduced with permission of the copyright owner. Further reproduction prohibited without permission.

incident surface of exposure far enough not to receive significant light intensity, could mask any photoinduced effects. The cell illustrated in Figure 3 was used for photosensitivity experiments. A golden yellow film was deposited on the flat quartz surface by polymerizing C_3O_2 at a pressure of 190 mm Hg and temperature of 100°C. until an absorbance of 1.0 at 570 nm was reached. This film possessed an ESR signal with a signal to noise ratio high enough for intensity measurements to be made and a thickness thin enough not to mask photoinduced effects.

The effect of irradiating the film with the full spectrum of a 200 watt mercury-xenon lamp on the ESR spectrum is illustrated in Figure 16. There is a significant and rapid increase in the signal to a steady-state level intensity but no change in spectrum shape or line width. A scan of 500 to 5500 gauss showed no half field transition or absorptions at any other magnetic field. When the light is quickly shut off, there is an initial rapid decay followed by a gradual decay back to the original signal intensity indicating this photogeneration of unpaired electrons to be reversible. The lack of a change in spectrum shape or line width indicates the photogenerated spin centers are very similar or identical to the initially present or residual spin centers (i.e. same g-value and relaxation time). Since there is no change in line width or shape, the peak-to-peak signal intensity, D, is proportional to the signal intensity, and the residual spin density, n^R, can be used as a yardstick to measure the number of photogenerated electrons, n^P, as indicated in Figure 16. This is particularly useful in studying the temperature dependence of the photosensitivity.

To determine whether it is the ultraviolet or visible wavelengths that are responsible for the photoexcitation, a glass filter was placed

Reproduced with permission of the copyright owner. Further reproduction prohibited without permission.

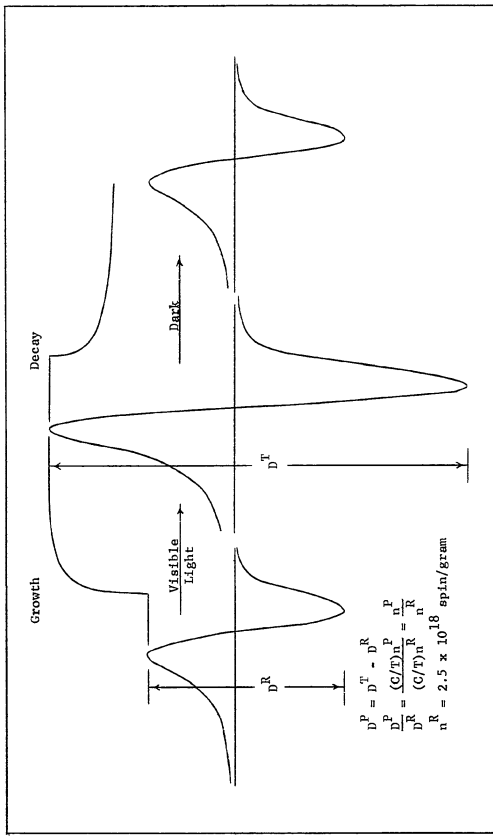

Figure 16. Effect of visible light irradiation on a poly(carbon suboxide) film's ESR spectrum.

Reproduced with permission of the copyright owner. Further reproduction prohibited without permission.

between the lamp and the film. With the ultraviolet light filtered out, the signal grew to the same intensity as when the lamp's full spectrum was used. On filtering out progressively longer wavelengths with colored glass filters, no decline in the photogenerated signal was observed until wavelengths greater than 400 nm were cut off. This indicates it is the visible and not the ultraviolet wavelengths that are responsible for the photogeneration of unpaired electrons.

The wavelength dependence of the photoexcition was examined by measuring the intensity of the ESR photosignal as the difference between the total and residual peak-to-peak intensities, D^T and D^R, as a function of wavelength. The light source was a Sylvania 750 watt, 120 volt tungsten lamp in a model 750C Standard Projector. The lamp has emission which gradually increases in intensity toward the infrared (38), and photon emission was taken to be constant between 300 and 850 nm. The light was monochromatized with a Bausch and Lomb grating monochromator (catalog #33-86-4) with 3 mm slit settings corresponding to a band pass of 20 nm. An ESR action spectrum was generated with a maxima at 570 nm and a natural band width of 135 nm (Figure 17). The maxima of the action spectrum occurs within the envelope of the absorption spectrum, although it does not correspond to an absorption maxima.

A steady-state quantum yield is obtained by measurement of the amount of light intensity absorbed at a known wavelength, the effective exposure area and the number of photogenerated spins. Light from a 1000 watt xenon lamp was monochromatized to a 20 nm band pass through the monochromator, and its intensity was measured in $erg/cm^2 sec.$ by placing the probe of a YSI-Kettering Model 65 Radiometer

Reproduced with permission of the copyright owner. Further reproduction prohibited without permission.

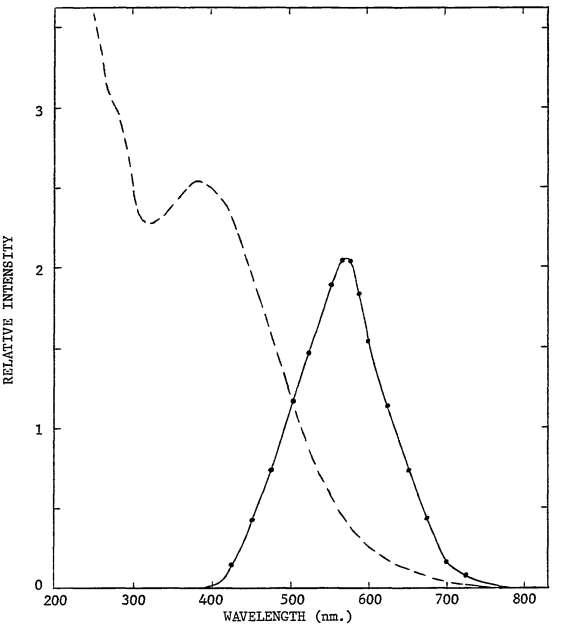

Figure 17. ESR action spectrum. Solid line - ESR photosignal intensity as a function of wavelength. Dashed line - absorption spectrum.

immediately in front of the ESR cavity window. The effective exposure area was taken from the 4 x 25 mm dimensions of the cell as 1.0 cm^2. The number of photogenerated spins was obtained by comparison of the photosignal with the signal intensity corresponding to residual spin density. The quantity of poly(carbon suboxide) composing the film was obtained by comparison of the residual signal with the signal

Reproduced with permission of the copyright owner. Further reproduction prohibited without permission.

intensity of a known quantity of poly(carbon suboxide). The energy per photon, E, in erg/quantum is given by

$$E = \frac{h \cdot c}{\lambda}$$

where h = 6.6256 x 10^{-27} erg sec/quantum, C = 2.9979 x 10^{10} cm/sec and λ is the wavelength in cm. The number of photons per unit time, N^P, is then given by the product of A, the exposure area and I, the measured light intensity divided by E.

$$N^P = \frac{A \cdot I}{E}$$

The quantity of poly(carbon suboxide) composing the film, W, was found to correspond to 0.33 mg, and the number of photogenerated unpaired electrons, N^e, is given by

$$N^e = \frac{D^T - D^R}{D^R} \cdot n^R \cdot W$$

The steady-state quantum yield, Φ_{ss}, is then given by

$$\Phi_{ss} = \frac{\text{photogenerated spins}}{\text{photons}} \approx \frac{N^e}{N^P}$$

Measurements were made at several wavelengths, and results are presented in Table IV.

TABLE IV

STEADY-STATE QUANTUM YIELDS AT 25°C.

λ(nm.)	N^e (spin)	N^P (photon/sec.)	Φ_{ss}
450	1.2 x 10^{14}	2.7 x 10^{15}	.04
500	1.3 x 10^{14}	4.2 x 10^{15}	.03
547	1.1 x 10^{14}	1.6 x 10^{15}	.07
577	1.4 x 10^{14}	2.0 x 10^{15}	.07
650	1.3 x 10^{14}	2.0 x 10^{15}	.06
700	.98 x 10^{14}	2.5 x 10^{15}	.04

Reproduced with permission of the copyright owner. Further reproduction prohibited without permission.

The steady-state quantum yield would have to be regarded as a lower limit since unpaired electrons which return to the diamagnetic state within one second's time are not counted. Also assumptions of total photon absorption and that the light intensity immediately in front of the cavity is the same as that inside the cavity are involved. However, from the order of magnitude, the photoexcitation appears to be a relatively efficient process.

The dependence of the steady-state photosignal on the light intensity was investigated with neutral density filters. The transmissions of the neutral density filters and combinations of them were calibrated with a Cary Model 118-C ultraviolet-visible spectrophotometer. The neutral density filters were placed immediately in front of the cavity window, and the photosignal intensity was measured as the difference between the peak-to-peak intensities of the light and dark signals. Measurements were made monochromatically with a band pass of 20 nm using the 547 and 577 mercury lines of the 200 watt mercury-xenon lamp as well as with the full spectrum of the 750 watt tungsten lamp. A square root dependence between the steady-state photosignal and the light intensity was observed as Figure 18 illustrates for the 547 nm mercury line. The same was true for the 577 mercury line and the full spectrum of the tungsten lamp. It was also found that by reducing the temperature, a stronger steady-state photosignal was obtained. The square root dependence indicates a two electron decay process which would be consistent with the following model

$$PP + I \xrightarrow{k_g} \dot{P}^{+} + \dot{P}^{-} = n + n$$

$$n + n \xrightarrow{k_d} PP$$

Reproduced with permission of the copyright owner. Further reproduction prohibited without permission.

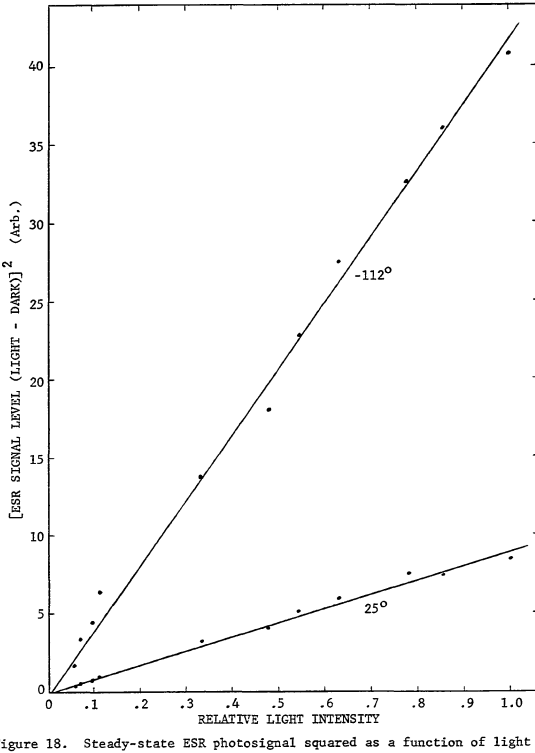

Figure 18. Steady-state ESR photosignal squared as a function of light intensity and temperature at $\lambda = 547 \pm 10$ nm.

Reproduced with permission of the copyright owner. Further reproduction prohibited without permission.

where PP is a pair of polymer molecules, I is a quantum of light, $\dot{P}^{+}$ and $\dot{P}^{-}$ are polymer radical ions, n is an unpaired electron and k_g and k_d are growth and decay rate constants. Under steady-state conditions:

$$\frac{dn}{dt} = k_g[PP]I - k_d n^2 = 0$$

$$\text{or} \quad n^2 = \frac{k_g[PP]}{k_d} \cdot I$$

A single polymer molecule transformed to a biradical could be used in place of the pair of polymer molecules. The electron transfer is favored on the basis of a light polarization experiment. When light was polarized in a perpendicular or parallel direction to the external magnetic field, photosignals of the same intensity, line shape and width were observed. Polarized light should selectively excite molecules having chromophores with a transition moment oriented in a particular direction. In a rigid matrix only those molecules with the proper molecular axis orientation will be photoexcited, and, if no electron transfer occurs, a light polarization dependent anisotropy would be expected in the ESR spectrum, especially since triplet states are observed to be highly anisotropic (39). If an unpaired electron is capable of being transferred between molecules of differing orientations, the spectrum would be independent of light polarization.

It was observed in Figure 18 that reducing the temperature had the effect of strongly increasing the photosignal intensity, in fact, much more so than the 1.85 times the Curie law would predict between those two temperatures. The temperature dependent terms in the steady-state equation are the growth and decay rate constants. Assuming an Arrhenius expression for the rate constants, a logarithmic relation between the number of photogenerated unpaired electrons and the

Reproduced with permission of the copyright owner. Further reproduction prohibited without permission.

reciprocal temperature is predicted.

$$\frac{k_g}{k_d} = \frac{n^2}{[PP]\cdot I} = \frac{A_g\, e^{-E_g/kT}}{A_d\, e^{-E_d/kT}} = \frac{A_g}{A_d}\, e^{(E_d - E_g)/kT}$$

$$\text{or} \quad \ln \frac{n^2}{[PP]^o - n} = \frac{E_d - E_g}{kT} + \ln \frac{A_g}{A_d} I$$

where $[PP] = [PP]^o - n$

The unpaired electron density, n, was obtained using the residual spin density of 2.5×10^{18} spin/gram as an internal standard, and the polymer pair density, $[PP]^o$, based on a DP of 6 (see Section IV) was calculated to be 7.4×10^{20} pairs/gram. Temperature was determined by iron-constantan thermocouple measurement.

It is not immediately apparent whether just the concentration of photogenerated spins, n^P, should be considered or whether the total spin density, n^T, should be considered for n. The ESR spectrum does not distinguish between a photogenerated unpaired electron and a residual one. The Curie law behavior indicated there is no thermal equilibrium between a diamagnetic and a paramagnetic state. However, a higher energy phototransition is possible, and, if the photogenerated spin centers are interchangeable with the residual ones, both should have to be taken into account. In Figure 19 the logarithmic expression involving n is plotted against the reciprocal temperature for both n^P and n^T. The predicted temperature dependence is reasonably well followed when the total spin density is considered, and an activation energy difference of 440 cal/mole between the decay and growth processes is obtained. When only the photogenerated unpaired electrons are considered, the plot is not linear. While this may indicate the necessity of including the residual unpaired electrons, there are other

Reproduced with permission of the copyright owner. Further reproduction prohibited without permission.

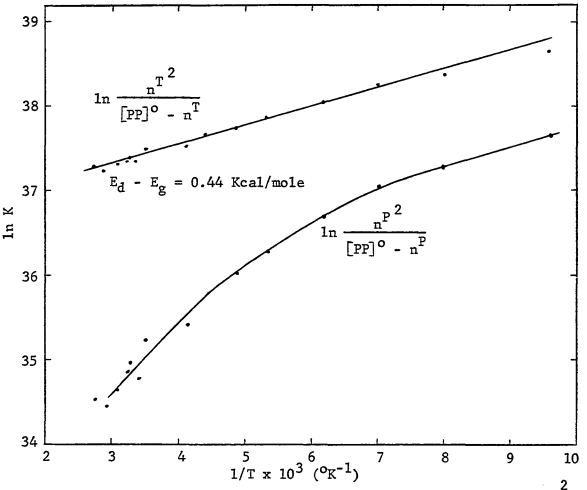

Figure 19. Temperature dependence of steady-state photosignal, $K = \frac{n^2}{[PP]^o - n}$.

possibilities. It may be that the photogenerated spins are independent from the residual spins, but only few polymer molecule pairs possess the proper orientation for electron transfer to occur, and this number is easily saturated. It is also possible that a better model exists or the Arrhenius relationship is not applicable. In a separate empirical approach, a simple plot of the photogenerated spin density against the reciprocal temperature is reasonably linear (Figure 20), but its correspondence, if any, to a physical model is unknown.

The time dependence of the growth and decay of the photosignal at several temperatures is illustrated in Figure 21. The growth and decay curves were obtained by setting the magnetic field at the derivative

Reproduced with permission of the copyright owner. Further reproduction prohibited without permission.

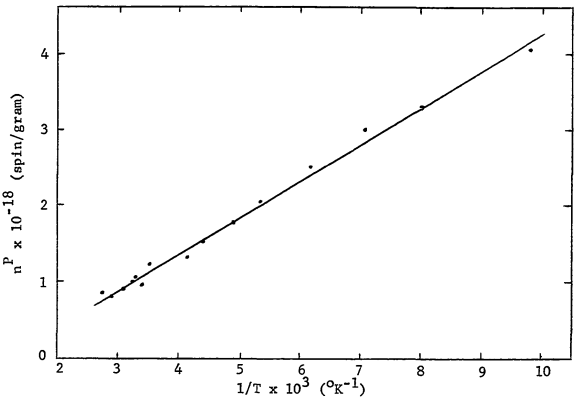

Figure 20. Photogenerated spin density vs. reciprocal temperature.

peak maxima of the residual signal and recording the signal intensity change as a linear function of time. All curves start from the same origin and approach progressively greater steady-state intensities with decreasing temperature reflecting the 440 calorie difference between the growth and decay processes. Remarkably, when the light is cut off, the photosignal rapidly decays to about half its steady-state intensity and then gradually returns back to the initial residual intensity. At low temperatures, it was necessary to remove the cell from the cavity and hold it at room temperature to restore the signal to its residual intensity in a reasonable amount of time (several minutes). The growth kinetics are difficult to follow as the initial stage may be too fast for the detector to respond accurately and, at later stages, must compete with the decay process. The decay process is slower and does not compete with growth once the light is cut off. At first consideration,

Reproduced with permission of the copyright owner. Further reproduction prohibited without permission.

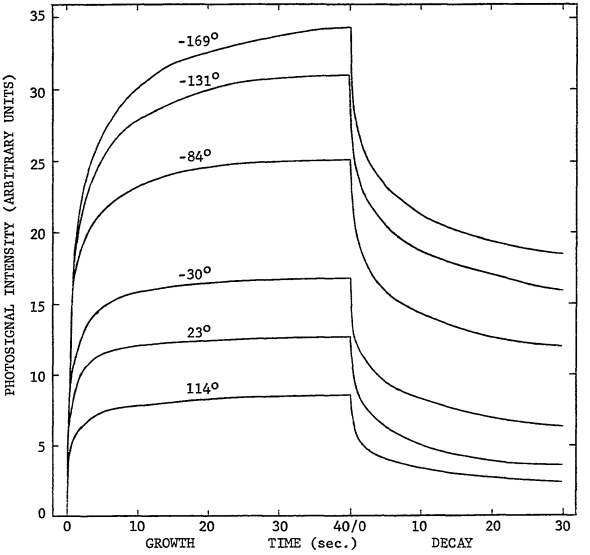

Figure 21. Photoexcitation of poly(carbon suboxide) ESR absorption over a 280°C temperature range.

it would be thought to be a simple second order process. However, that would only be applicable to a homogeneous system. It must be remembered that the light intensity declines as it penetrates the film presumably according to the Beer-Lambert Law. The result is that many photogenerated spins are produced at the incident surface of the film and very few at the exit surface since the film thickness was controlled to have a thickness corresponding to an absorbance of 1.0 at 570 nm. To deal with this spin inhomogenity, the film of thickness ℓ is divided into p intervals parallel to the surface and thin enough to

Reproduced with permission of the copyright owner. Further reproduction prohibited without permission.

have a homogeneous spin density within them. The initial or steady-state spin density within an interval is assumed to have a square root dependence on the light intensity at its position within the film, and the spin density gradient between intervals is assumed to follow the square root of the light intensity decline given by the Beer-Lambert law (i.e. the photogenerated unpaired electrons are immobile within the film matrix).

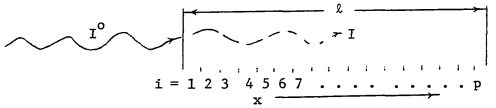

Beer-Lambert Law:

$$\frac{I_i}{I^o} = 10^{-\Sigma A_i} = 10^{-\varepsilon c \Sigma \ell_i} = 10^{-\varepsilon c \ell x_i}$$

$$x_i = \frac{\Sigma \ell_i}{\ell}$$

At time = 0, under steady-state conditions ($n_i = n_i^o$):

$$\frac{dn_i^o}{dt} = k_g[PP]I - k_d(n_i^o)^2 = 0$$

$$n_i^o = \left(\frac{k_g[PP]}{k_d}\right)^{\frac{1}{2}} \left(\frac{I_i}{I^o}\right)^{\frac{1}{2}} = \beta 10^{-\frac{1}{2}(\varepsilon c \ell x_i)} = \beta e^{-\alpha x_i}$$

$$\beta = \left(\frac{k_g}{k_d}[PP]\right)^{\frac{1}{2}} \qquad \alpha = \tfrac{1}{2}(2.3\ A)$$

After the light is cut off; time > 0, I = 0:

$$\frac{dn_i}{dt} = -k_d \cdot n_i^2$$

Reproduced with permission of the copyright owner. Further reproduction prohibited without permission.

$$\frac{1}{n_i} = k_d \cdot t + \frac{1}{n_i^o} = k_d \cdot t + \beta^{-1} \cdot e^{\alpha x_i}$$

$$n_i = \frac{\beta e^{-\alpha x_i}}{k_d \cdot t \beta e^{-\alpha x_i} + 1}$$

Summing over all the intervals for the total photoinduced spins:

$$n = \sum n_i \simeq \int_0^1 \frac{\beta \cdot e^{-\alpha x}}{k_d \cdot t \beta e^{-\alpha x} + 1} \, dx$$

$$n = \frac{1}{k_d \cdot t} - \frac{1}{k_d \cdot t \cdot \alpha} \ln \left(\frac{k_d \cdot t \cdot \beta + e^{\alpha}}{k_d \cdot t \cdot \beta + 1} \right) \qquad (1)$$

The first term in the integrated equation for n accounts for the normal second order decay within each interval. The second term allows for a slower decline to the residual signal intensity due to reduced decay rates from intervals at the low end of the spin concentration gradient profile.

The experiment to test this equation was performed using the full spectrum of the 750 watt tungsten lamp. β was obtained from the slope of a photosignal vs. square root of light intensity plot, and the absorbance for α was obtained by dividing the absorption spectrum of the film into 10 nm intervals between 400 and 750 nm and taking a weighted average based on the ESR action spectrum of the absorbance in each interval

$$A = -\log \frac{1}{n} \sum_1^n C_i \cdot 10^{-A_i}$$

where A_i is the measured absorbance at each interval, n is the total

Reproduced with permission of the copyright owner. Further reproduction prohibited without permission.

number of intervals and C_i is a weighting coefficient proportional to the intensity of the ESR action spectrum normalized to 1 at 570 nm. Experimentally, an integrated absorbance value of 1.18 was obtained, while the films absorbance at 570 nm was 0.97. The use of monochromatic light would eliminate the need for spectrum integration but would result in an unacceptable loss in photosignal intensity. The experimental decay curve with the steady-state spin density normalized to 1 and the theoretical decay curve based on equation (1) and the empirical constants α and β are presented in Figure 22. The time units of the theoretical curve are proportional to the $k_d t$ product and normalized to the experimental curve at the point where the photosignal has half its steady-state intensity. If the decay equation were valid the two curves should be coincident which is not the case. The noncoincidence cannot be ascribed to an error in the determination of α or β since, if the simple second order ($n = 1/k_d t$) homogeneous equation, which is independent of α and β, is used, a curve coincident with that corresponding to the inhomogeneous case is obtained after normalization of the time scale at half the photosignal intensity. In other words, the spin concentration gradient only alters the time scale of the decay.

A second look at the decay curves in Figure 21 suggests a leveling off or departure from a curve with an initial appearance of a second order decay. If this were to indicate a second more temperature dependent decay process, the separation of these two processes would be best at the lowest temperature where quenching of one would be the most effective. Support for such a contention is proposed by obtaining a near linear second order plot where the photosignal intensity which appears to decay by the more thermally quenched process is subtracted

Reproduced with permission of the copyright owner. Further reproduction prohibited without permission.

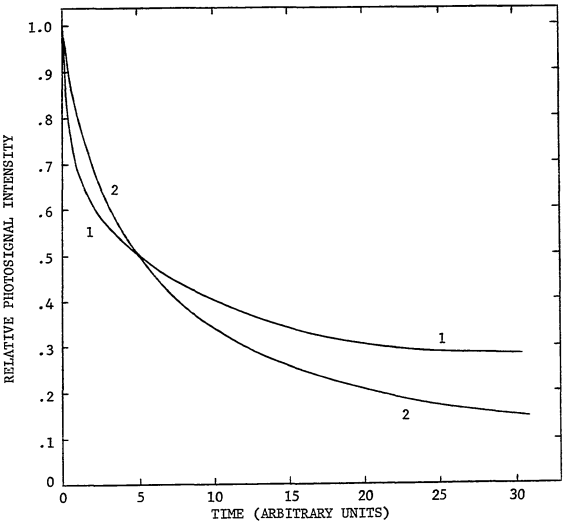

Figure 22. Experimental (1) and theoretical (2) decay curves for the poly(carbon suboxide) ESR photosignal.

as a constant, and the reciprocal of the difference instead of the reciprocal of the total photosignal is plotted against time (Figure 23). Such a dual decay process can be pictured by two possibilities involving electron transfer. One is that electron recombination need not occur between the same neighbors where the initial transfer occurred. In the recombination process some spins could become isolated and require more thermal energy to migrate through the matrix to recouple. The other possibility is that, since the polymer is disperse and of low crystallinity, metastable electron wells of varying stability may exist

Reproduced with permission of the copyright owner. Further reproduction prohibited without permission.

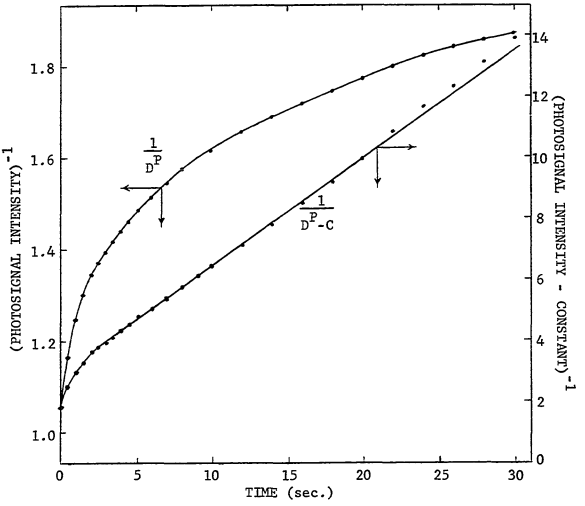

Figure 23. Second order plot of the photogenerated ESR signal decay at 169°C.

throughout the matrix and temporarily capture some of the photogenerated unpaired electrons. A model giving quantitative agreement with the decay kinetics has not been found.

The photosensitivity can be summarized as follows. Spin centers, which are very similar or identical to those residually present, can be generated photolytically with energy corresponding to 570 nm. No spin center anisotropy can be observed with polarized light on an ESR time scale. The photosignal decay is a two electron process, but the decay kinetics do not correspond to a simple homogeneous second order process.

Reproduced with permission of the copyright owner. Further reproduction prohibited without permission.

5. PARAMAGNETIC SENSITIVITY TO WATER AND RELATED NUCLEOPHILES

As pointed out in the literature survey (Section II) the polymer is irreversibly sensitive to water. Exposure of a polymer film to water vapor resulted in a slight color change from yellow or brown to orange or dark red depending on the film thickness. With films thick enough to be nontransparent, exposure resulted in a constricting and blistering from the surface on which the film was formed. The ESR signal was observed to rapidly and irreversibly disappear on exposure to water vapor. This water sensitivity can then be used to obtain information about the spin center by following parallel changes in the visible-ultraviolet and infrared spectra.

In the visible-ultraviolet spectrum of a thin film prepared at 100°C., trace exposures to water vapor resulted in the decay of the 370 nm absorption and growth of a more intense absorption at 480 nm (Figure 24). The change was irreversible and indicates that the electronic structure of the polymer is being altered.

The infrared spectrum of a polymer film was obtained by polymerizing C_3O_2 onto the NaCl windows of a 100 mm gas cell at room temperature followed by pumping the monomer from the cell once sufficient polymer had formed (Figure 25). There is some adhesion between the monomer and the polymer as the monomer's most intense band at 4.46 μ, which is well resolved from the polymer's 4.6 μ ketenyl band, required about a half hour of pumping with a mechanical pump to remove. The polymer infrared spectrum is in good agreement with those obtained by Smith (1) and Blake (2). There is general agreement on the assignments of an α-pyrone carbonyl band at 5.6 and 5.8 μ and a vinyl ether or ester band at 8.2 μ. The bands at 6.7 and 7.3 μ are assigned to conjugated cyclic olefin bonds by Blake and to a carboxylate ion on the

Reproduced with permission of the copyright owner. Further reproduction prohibited without permission.

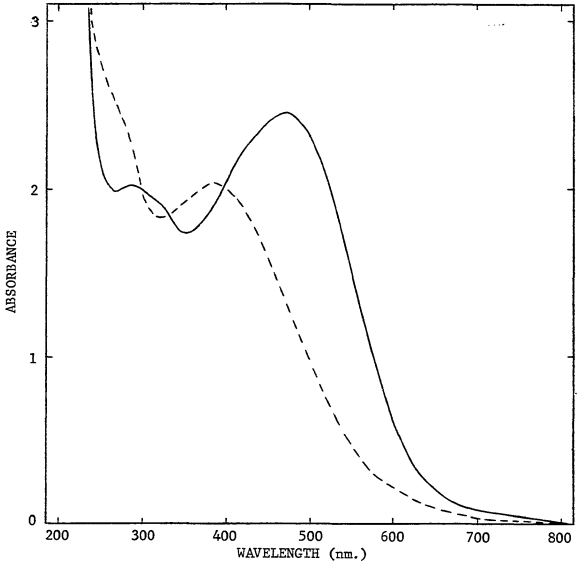

Figure 24. Effect of water vapor exposure on the visible-ultraviolet spectrum of a poly(carbon suboxide) film. Dashed line - before exposure. Solid line - after exposure.

basis of an ionic pyrilium resonance structure contribution by Smith. No assignment has been made for the band at 12.5 μ. This work favors the ketenyl functional group assignment to the 4.6 μ band. Blake contested Smith's assignment of absorbed C_3O_2 monomer to this band by pointing out that it was shifted 80 cm^{-1} to a lower frequency from the monomer's strongest absorption. The observation that the monomer is easily pumped off from the polymer film is not in agreement with Smith's 15 hours of hard pumping nor does he mention analysis of the pumped off

Reproduced with permission of the copyright owner. Further reproduction prohibited without permission.

Reproduced with permission of the copyright owner. Further reproduction prohibited without permission.

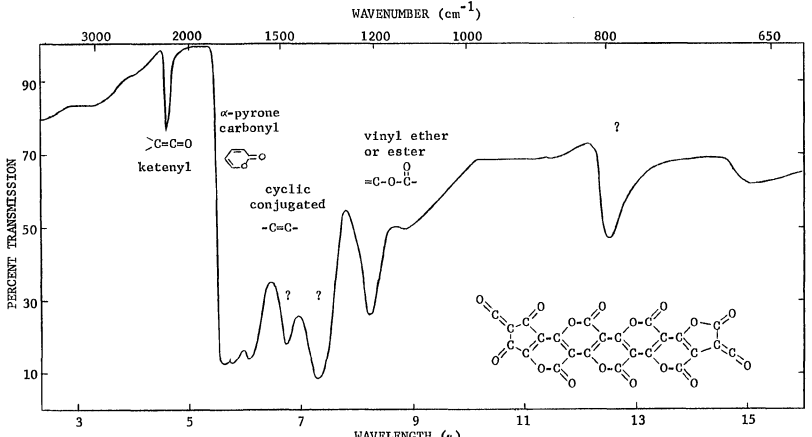

Figure 25. Infrared spectrum of poly(carbon suboxide).

product that resulted in disappearance of the ketenyl band. Attempts to obtain a mass spectrum of the polymer were hampered by difficulty in maintaining a high vacuum (10^{-7} mm Hg) with the polymer present, and, in the spectra obtained, fragments corresponding to CO^+ and CO_2^+ but not to $C_3O_2^+$ were observed. It was also observed that C_3O_2 reacts very slowly with water, while this ketenyl absorption is very sensitive to moisture. The effect of successive exposures of the film to water vapor on the infrared spectrum is presented in Figure 26. The more intense bands show a diffuse broadening with only a slight decline in the band at 8.2 μ. However, the weak ketenyl band completely disappears with a corresponding growth of a broad carboxylic acid band at 3.3 μ.

The parallel behavior of the ESR and ketenyl IR absorptions on exposure of the polymer to water vapor suggests a connection between the unpaired electron and the ketenyl functional group. To determine whether the relationship is quantitatively proportional, simultaneous ESR and ketenyl IR absorption intensity measurements were made after successive exposures to water vapor. It was found that quartz is transparent in the infrared up to 4.8 μ (see Figure 27) which is just far enough to include the 4.6 μ ketenyl band as well as monitor the growth of the 3.3 μ carboxylic acid band. The cell in Figure 3 was well suited for this experiment. The ketenyl band is a characteristically weak IR absorption so a relatively thick film was necessary to obtain an absorption strong enough to allow several exposures to water vapor. It was found that by filling the cell with 190 mm pressure C_3O_2 (vapor pressure at -23°C) and placing the quartz tip of the cell in an oil bath at 100°C. for approximately 6 hours, a dark brown barely transparent film with a ketenyl band of intensity corresponding to that in Figure 27 was obtained. Water vapor exposures were carried out

Reproduced with permission of the copyright owner. Further reproduction prohibited without permission.

Reproduced with permission of the copyright owner. Further reproduction prohibited without permission.

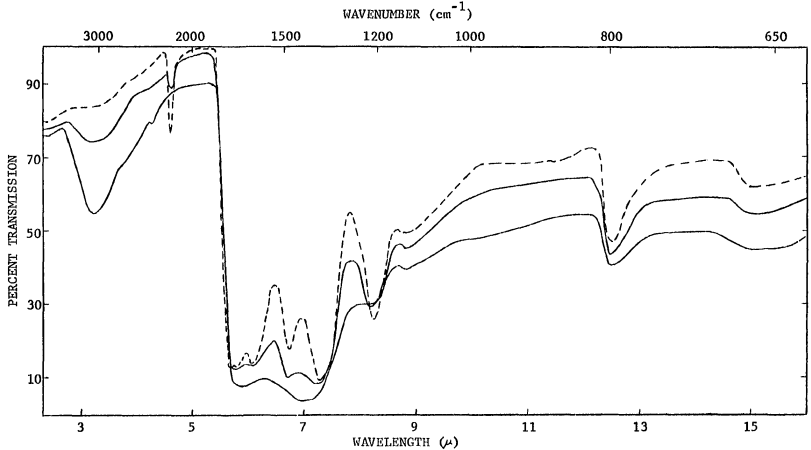

Figure 26. Effect of water vapor exposure on the infrared spectrum of a poly(carbon suboxide) film. Solid line - after successive exposures. Dashed line - before exposure.

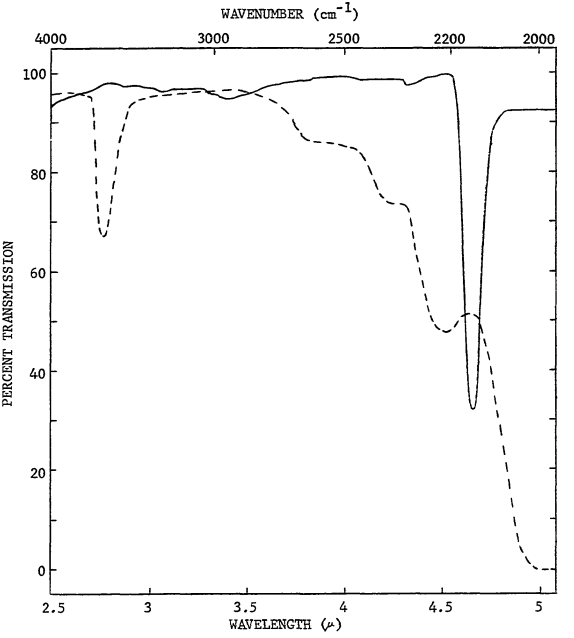

Figure 27. Infrared spectrum of a thick poly(carbon suboxide) film in a quartz cell. Dashed line - empty cell against air. Solid line - poly(carbon suboxide) against an empty cell reference.

by admitting a volume of water vapor (room temperature vapor pressure ~ 20 mm) corresponding to the volume between the cell and vacuum system stopcocks (about 3 ml) to the evacuated cell, allowing 5 to 10 minutes reaction time and reevacuating the cell. The ESR and IR spectral changes after 9 successive exposures are presented in Figure 28. Since the ESR line shape and width did not change, the peak to

Reproduced with permission of the copyright owner. Further reproduction prohibited without permission.

Reproduced with permission of the copyright owner. Further reproduction prohibited without permission.

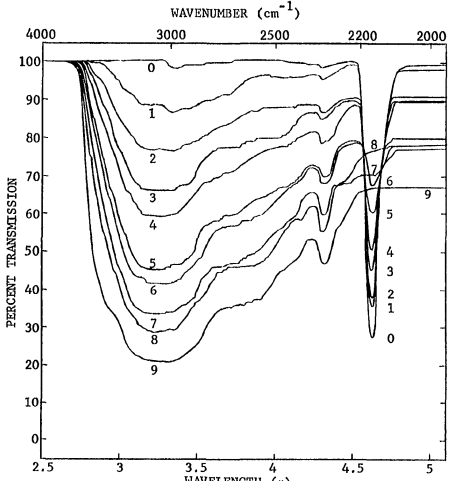

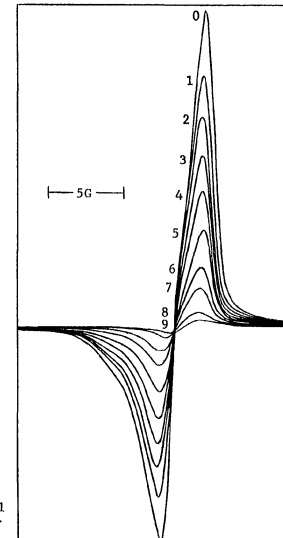

Figure 28. Simultaneous decay of poly(carbon suboxide) infrared ketenyl and ESR absorptions on successive exposures to trace quantities of water vapor.

peak signal intensities were used. In the IR spectra, the carboxylic acid peak was found to tail into the ketenyl absorption, so the base of the ketenyl band was taken to correspond to the extrapolated level of the carboxylic acid band. The ketenyl band intensity was taken as the absorbance difference between the maxima and extrapolated base of the peak. A plot of the ESR signal intensity against the ketenyl band absorbance was linear (Figure 29) indicating the existence of the unpaired electron to be dependent on the presence of the ketenyl function group.

It was of interest to compare the effectiveness of water with other nucleophiles on quenching the ESR and ketenyl IR absorptions. Since water is not usually regarded as a very reactive nucleophile, it was thought that a comparison with methanol as well as with the nitrogen and sulfur analogues of water and methanol might provide more information about the spin center and ketenyl group. All of the reagents were either gases or had substantial vapor pressures at room temperature so the nucleophile effectiveness could be semiquantitatively measured by increasing the severity of the exposure conditions. This was done by first increasing the exposure time for a few millimeters pressure of nucleophile, then increasing the reagent pressure up to one atmosphere and finally by increasing the exposure temperature up to 100°C. The results are summarized in Table V. In each case a linear relationship was observed between the ESR signal and the ketenyl band. It was initially expected that nucleophilic strength would be the most important factor and was a surprise to find that water was by far the most effective reagent. A more important factor appears to be the nucleophile polarity, which, with the exception of methylmercaptan,

Reproduced with permission of the copyright owner. Further reproduction prohibited without permission.

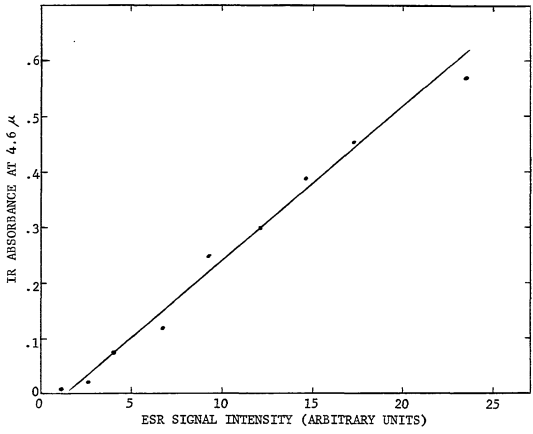

Figure 29. Relation between ketenyl IR and ESR absorptions of poly(carbon suboxide) after successive exposures to trace quantities of water vapor.

parallels the reactivity as indicated by the dipole moments. This result suggests that the poly(carbon suboxide) film has a significant ionic character which may protect the buried ketenyl groups from the less polar but more powerful nucleophiles. In fact, the attack of ammonia and methylamine is very slow but results in a bleaching of the film to a light yellow color. An elemental analysis of an ammonia exposed C_3O_2 polymer had a stoichiometry very close to $C_3O_2 \cdot NH_3$ and a shift from an ester to an amide carbonyl absorption in the IR (see Section IV) indicating that ammonia penetrates the film by slowly attacking the lactone bonds. A possible explanation for the methylmercaptan's lack of effectiveness could be a poor penetration of

Reproduced with permission of the copyright owner. Further reproduction prohibited without permission.

Reproduced with permission of the copyright owner. Further reproduction prohibited without permission.

TABLE V

ESR AND KETENYL IR ABSORPTION DECAY BY EXPOSURE TO VARIOUS REAGENTS

Exposure conditions	Trace		Vapor pressure 12 hr. exposure		1 atm. pressure 100°C heating 12 hr. exposure				Less than 20% decay	
Reagent	H_2O	$\gg$	CH_3OH	$\gg$	NH_3,	CH_3NH_2,	HCl	$>$	CH_3SH,	H_2S
Dipole moment	1.85		1.70		1.47	1.31	1.08		1.52	0.97

the polymer film. Considering the film to have an ionic character and be of high density (The polymer was found to be more dense than hexachlorobutadiene, i.e. greater than 1.6 gram/cm^3.), the mercaptan with its weak hydrogen bonding capacity and large size would be expected to be less effective than the smaller more strongly hydrogen bonding ammonia molecule.

In solution the normal reactivity of ketenes with three of the nucleophiles is in the order (40):

amine >> water > alcohol.

Hydrochloric acid is also reported to react rapidly with substituted as well as unsubstituted ketenes. The reactivity with water or alcohol of various substituted ketenes is found to increase with increasing substitution and conjugation with the substituent.

for H_2O $(C_6H_5)_2C=C=O > (C_2H_5)_2C=C=O > (CH_3)_2C=C=O > H_2C=C=O$

for CH_3OH $(C_6H_4)_2C=C=O > (C_6H_5)_2C=C=C > C_6H_5(CH_3)C=C=O > CH_3CH=C=O$

These observations would support the contention that nucleophile penetration of the polymer is responsible for the observed reactivity order and that, once penetration is accomplished, a ketenyl group pendant to an unsaturated polypyrone structure can rapidly react with water.

In the IR spectrum of the exposed polymers the weak absorption that develops at 4.3 μ (Figure 28) is of unknown origin but must be connected with hydrolysis of the polymer. When D_2O was substituted for water, its frequency remained constant while the carboxylic acid O-H band shifted to a lower frequency (Figure 30a). The band is also present when other nucleophiles are substituted for water and is particularly strong in the case of ammonia (Figure 30b). These observations indicate that this weak band does not arise from a bond formed with the nucleophile or a hydrogen transfer.

Reproduced with permission of the copyright owner. Further reproduction prohibited without permission.

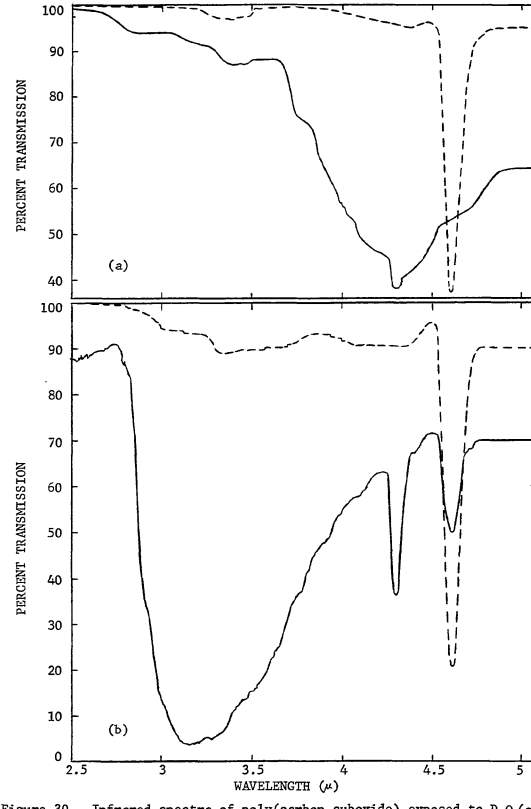

Figure 30. Infrared spectra of poly(carbon suboxide) exposed to D_2O (a) and NH_3 (b). Dashed line - before exposure. Solid line - after exposure.

Reproduced with permission of the copyright owner. Further reproduction prohibited without permission.

IV. POLYMER SIZE AND PROPERTIES

Most characterization work has involved spectroscopy of the polymer in the solid state. Wet chemistry characterization has been largely uninvestigated presumably due to lack of a solvent. The polymer is totally insoluble in nonpolar organic solvents such as carbon tetrachloride, benzene, toluene or diethyl ether and slightly soluble in moderately polar solvents such as acetone, methanol or acetonitrile. When the moderately polar solvents are freshly dried, the solubility becomes much lower. With water, an appreciable solubility was observed, but appears to be, in part, the result of an hydrolysis. However, with dipolar aprotic solvents such as DMF and DMSO, total solubility was observed when polymers were formed at low enough temperatures. DMF was selected as the primary solvent over DMSO on the basis of a lower boiling point. Experiments were conducted with polymer samples prepared over a 0 to 60°C. temperature range to examine the DMF and H_2O solubility, molecular weights, equivalent weights, elemental analyses and infrared, visible-ultraviolet and fluorescence spectra. An attempt was also made to hydrogenate the polymer.

1. POLYMER PREPARATION

Carbon suboxide was prepared by the malonic acid dehydration method and distilled to infrared purity as indicated in the appendix. Thermal bulk polymerizations were run by sealing approximately 1 ml quantities of liquid C_3O_2 in 10 x 75 mm pyrex test tubes which had been previously flamed out under vacuum. The sealed samples were placed in thermostated water baths at 0, 30 and 60°C. For an unknown reason, it was found necessary to place the sealed tubes in a horizontal position

Reproduced with permission of the copyright owner. Further reproduction prohibited without permission.

so that monomer does not fill the space between opposing walls. When they were stood up in the vertical position, the tubes frequently failed with increasing explosive force as the temperature was raised. This occurred in a latter stage of the polymerization when most of the monomer appeared to be polymerized. This was observed only very rarely with the smaller 3 mm sample tubes in this temperature range during the ESR experiments. It was thought that the polymer may be less dense than the monomer and cause excessive pressure on opposing walls of the tube at high conversion, but the polymer was found to be more dense than hexachlorobutadiene (1.6 g/ml) making it more dense than the monomer. An attempt to obtain a 90°C. sample resulted in a very powerful explosion in spite of placing the tube on its side. Samples were polymerized for two days, and no C_3O_2 odor was detected on opening indicating complete conversion. Samples were not protected from the air during transfers but were stored in desiccators and extracted in closed systems.

2. DMF AND H_2O SOLUBILITY

To insure that a property measured from solution would be representative of all fractions of the polymer, solubility was examined by extraction with DMF. Approximately 0.3 to 0.4 gram polymer was placed in a soxhlet extractor, and extraction was carried out with P_2O_5 dried DMF at a reduced pressure of 20 mm Hg until the extract was colorless. At this pressure, DMF refluxed at 50 to 60°C. which should minimize decomposition of the soluble polymer. The soluble fraction of the polymer was recovered by concentrating to about a 5 ml volume under reduced pressure followed by precipitation by adding dropwise to a 500 ml stirred volume of diethyl ether. The flocculent brown polymer

Reproduced with permission of the copyright owner. Further reproduction prohibited without permission.

precipitate was filtered from the DMF-ether mixture through a sinctered glass extractor cup, then extracted for one day with anhydrous ether and vacuum dried overnight in a desiccator. The 0 and 30°C. samples were found to be totally extractable in DMF while only 66% of the 60°C. sample was extractable.

Since the polymer is sensitive to moisture, it was of interest to observe whether an extreme exposure to water would result in a large change in polymer properties. Distilled water was substituted for DMF in the extractor and the pressure was adjusted (about 10 cm Hg) so that the water had a 50°C. reflux temperature. After two days, the extract of a 30° polymer had only a tinge of color and was stopped. The soluble fraction was concentrated to about a 5 ml volume, diluted with 100 ml DMF and reconcentrated to a 5 ml volume. The aqueous insoluble fraction was extracted with DMF and concentrated to a 5 ml volume. The two polymer fractions were worked up by precipitation and extraction with ether and vacuum drying as described above. Fifty-five percent of the 30°C. polymer was extracted with water. In appearance, it was a lighter brown than samples not extracted with water.

3. MOLECULAR WEIGHT

While no direct molecular weight has been reported for this polymer, a calculated x-ray diffraction pattern, based on 6 C_3O_2 units in the fused ring poly(α-pyrone) structure, was found to be in excellent agreement with the observed pattern (2). The x-ray diffraction data also predicted an increase in molecular weight with increasing polymerization temperature.

Molecular weight measurements were made using a Hewlett Packard Model 302B vapor pressure osmometer at 75°C. with standard and polymer DMF solution concentrations ranging from 2 to 30 g/Kg. DMF was dried

Reproduced with permission of the copyright owner. Further reproduction prohibited without permission.

and purified by stirring over P_2O_5 overnight then over KOH pellets followed by distillation at 100°C. (pressure = 14 cm Hg). The 500 ml center cut of an initial 1000 ml had no H_2O absorption in the IR at 2.85 μ which was present in the stock and had a refractive index of n_D = 1.4282 (literature n_D = 1.42817 25°C) as opposed to n_D = 1.4279 for the stock. Initially coumarin and benzil were selected as standards and were recrystallized from methanol (MP 68.5 and 94.5°C. respectively). Difficulty was encountered in obtaining stable VPO readings, and higher melting standards of recrystallized malonanilide and anthracene were substituted. The results are presented in Figure 31 and Table VI. The y axis in Figure 31 is expressed in molecular weight based on an instrument constant of K = 9030 μVKg/mole. The problem with coumarin and benzil appears to be a significant volatility of the solute. Performing the experiment with naphthalene (MP = 80°C.) which is a more volatile solid, the apparent molecular weight was twice its monomeric 128 g/mole at 75°C. and was six times higher at 101°C. The soluble extracted polymers have molecular weights ranging from 310 to 360 g/mole and increase with increasing polymerization temperature. The true number average molecular weight for the 60°C. polymer is probably higher than the 358 g/mole result since a third of it was not DMF soluble. The poorer solubility with increasing polymerization temperature is reflected in the increasing negativity of the second virial coefficients, Γ_2. The effect of extraction with water is about a 50 to 60 g/mole drop in the molecular weight with no significant difference between the H_2O soluble and H_2O insoluble fractions.

Since the polymer displays acid base behavior in solution, there was some question as to whether it is monomeric and unionized under the

Reproduced with permission of the copyright owner. Further reproduction prohibited without permission.

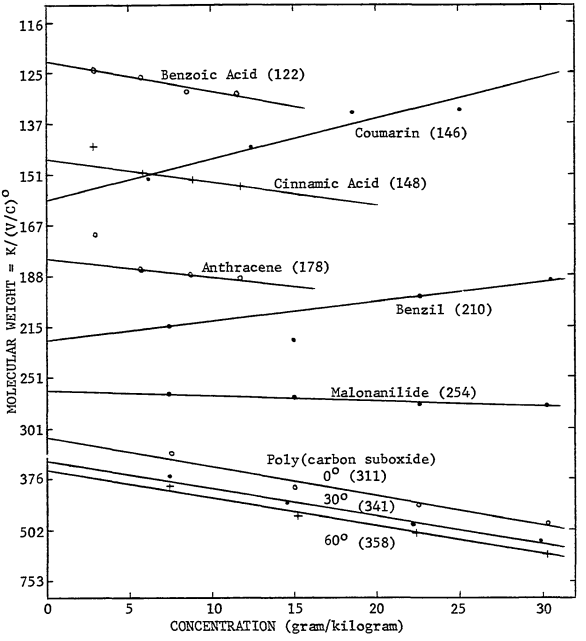

Figure 31. Vapor pressure osmometer molecular weights of carbon suboxide polymers prepared at 0, 30 and 60°C and of assorted compounds in N,N-dimethylformamide at 75°C.

molecular weight measurement conditions. Molecular weight measurements were made on benzoic and cinnamic acid to observe whether dimerization or dissociation was general behavior of unsaturated organic acids in DMF at 75°C. Experimental molecular weights were in excellent agreement with monomeric acid molecular weights (see Figure 31). This result

Reproduced with permission of the copyright owner. Further reproduction prohibited without permission.

would support the experimental molecular weights as being representative of the polymer size.

TABLE VI

SOLUBILITY, MOLECULAR AND EQUIVALENT WEIGHTS OF CARBON SUBOXIDE POLYMERS

Sample	DMF solubility	Γ_2(g/g)	Mn(g/mole)	EqWt(g/eq)	Mn/EqWt
0° polymer	100%	-12.1	311	141	2.2
30° polymer	100%	-12.8	341	154	2.2
60° polymer	66%	-13.1	358[a]	164[a]/199[b]	2.2[a]
30° polymer - H_2O soluble	100%	-13.8	281	130	2.2
30° polymer - H_2O insoluble	100%	-12.4	288	133	2.2
30° polymer - NH_3 exposed	3%	———	———	286[c]	———

[a]DMF soluble fraction.

[b]DMF insoluble fraction.

[c]Irreversible reaction observed.

To further check the validity of the polymer molecular weights, a measurement on the 0°C. polymer was made by freezing point depression of a DMSO solution. DMSO (FP = 18.54°C., K_f = 4.07 degKg/mole, ΔH_m = 3.33 Kcal/mole) was purified and dried by two slow crystallizations at 18.0°C. An evacuated, silvered cryoscopic cell similar to that described by Ross and Glasgow (47) was constructed with a linear thermistor (10°C./volt, V = 0 at 15°C.) and a helical stainless steel wire stirring rod penetrating a rubber septum fitted to the top of the cell. Cooling curves were obtained by following the thermistor output on a Hewlett Packard 7101 B strip chart recorder. An instrument

Reproduced with permission of the copyright owner. Further reproduction prohibited without permission.

constant of 5.95 degKg/mole was obtained using benzil as a standard and a molecular weight of 312 g/mole for the 0°C. polymer (Figure 32). This is in excellent agreement with the VPO result of 311 g/mole. The VPO method has the advantages of requiring a much smaller quantity of polymer (10 to 20 mg) and a higher operating temperature which favors a better polymer solubility.

4. EQUIVALENT WEIGHT

Since the infrared spectrum shows that exposure of the polymer to water results in conversion of ketenyl to carboxylic acid groups, it should be possible to titrate them and, by comparison with the molecular weight, determine the number of ketenyl groups per polymer molecule. The polymer has an appreciable acid strength giving a pH of 3.1 when placed in neutral water, but titration with aqueous hydroxide yields a potentiometric curve with a very poorly defined equivalence point. From such a curve, Hegar reported an equivalent weight of 158 g/eq (5). Hegar did not back titrate to certify that the acid-base behavior was reversible.

A titration system for the polymer was designed where approximately 40 mg of the polymer in DMF solution were titrated potentiometrically with a 0.4 N tetrabutylammonium hydroxide titrant. This was followed by a back titration with a 0.4 N perchloric acid titrant. DMF has a potential range about 2.5 times larger than water making it much better suited for sharpening the curve of a weak acid or differentiating an acid mixture (42). The basic titrant was initially prepared by diluting a 25% solution of tetrabutylammonium hydroxide in methanol (MC & B, Norwood, Ohio) to 0.4 N with DMF. This titrant was found to be unstable giving irreproducible standardizations so 2-propanol was substituted for DMF. The acidic titrant was similarly prepared by

Reproduced with permission of the copyright owner. Further reproduction prohibited without permission.

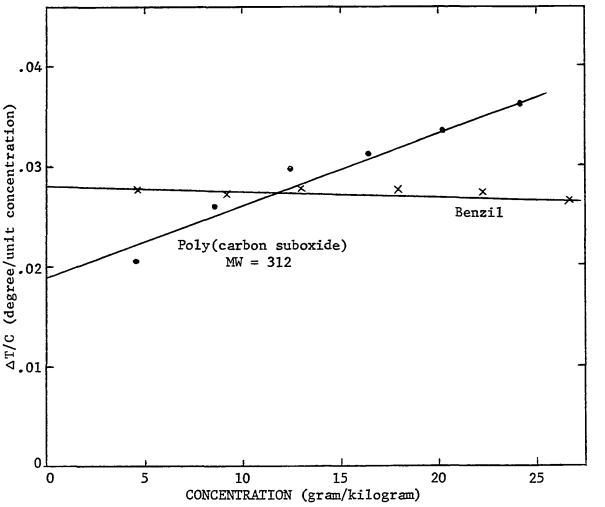

Figure 32. Freezing point depression molecular weight of poly(carbon suboxide) prepared at 0°C. Solvent - dimethylsulfoxide.

diluting concentrated perchloric acid (J.T. Baker Co., Phillipsburg, N.J.) to 0.4 N with DMF. A similar stability problem was encountered and 2-propanol was again substituted. (It should be pointed out in parallel experiments with DMSO, a violent explosion occurs when concentrated perchloric acid is diluted with DMSO with evolution of a strong sulfurous odor.) The titrants were standardized against benzoic acid (pK = 4.19), and the strength of this system in titrating weak acids was demonstrated with β-naphthol (pK = 9.51) (see Figure 33). Titration curves for the polymer (Figures 34 and 35) were sharper than in water (5) covering a potential range of 900 to 1000 mv as opposed to

Reproduced with permission of the copyright owner. Further reproduction prohibited without permission.

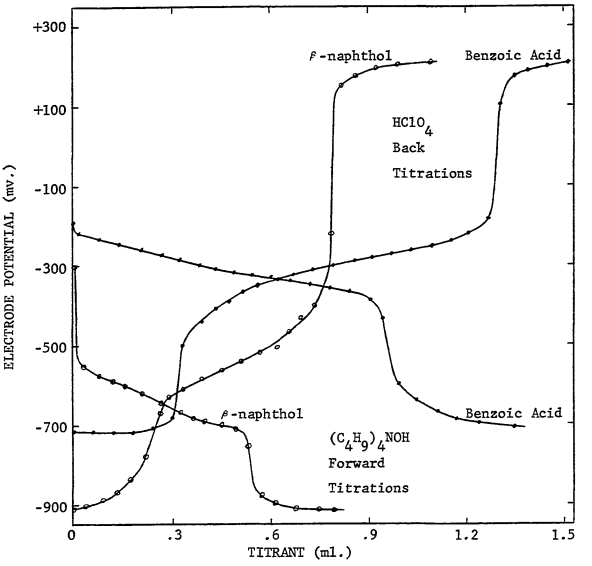

Figure 33. Forward and back titrations of DMF solutions of benzoic acid (●) and β-naphthol (○) with 0.42 N tetrabutylammonium hydroxide in 2-propanol and 0.42 N perchloric acid in 2-propanol.

300 mv for water, but no sharp equivalence points were observed. The sloping titration curves appear to be indicative of an acid mixture rather than a single weak acid such as β-naphthol where an initial sharp drop to a potential level where hydroxyl protons are removed followed by a drop to a level corresponding to an excess of titrant was observed. The equivalence point was then taken at the point where the titration curve levels off. The volume of titrant required for the polymer in the back titration was taken between the upward curvature

Reproduced with permission of the copyright owner. Further reproduction prohibited without permission.

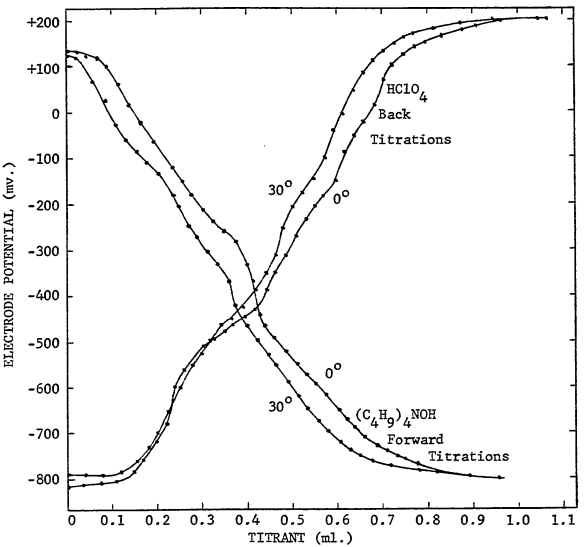

Figure 34. Forward and back titrations of DMF solutions of carbon suboxide polymers prepared at 0 and 30°C with 0.42 N tetrabutylammonium hydroxide in 2-propanol and 0.42 N perchloric acid in 2-propanol.

where the excess hydroxide titrant had been neutralized and the point where the curve levels off. The equivalent weights obtained from the back titrations averaged about 5 g/eq greater than those for the forward titrations probably due to water from the hydroxide titrant or initially present in the concentration perchloric acid. The results of the forward titrations are presented in Table VI. It is immediately seen that, like the molecular weight, the equivalent weight increases with increasing polymerization temperature and that the number of acidic

Reproduced with permission of the copyright owner. Further reproduction prohibited without permission.

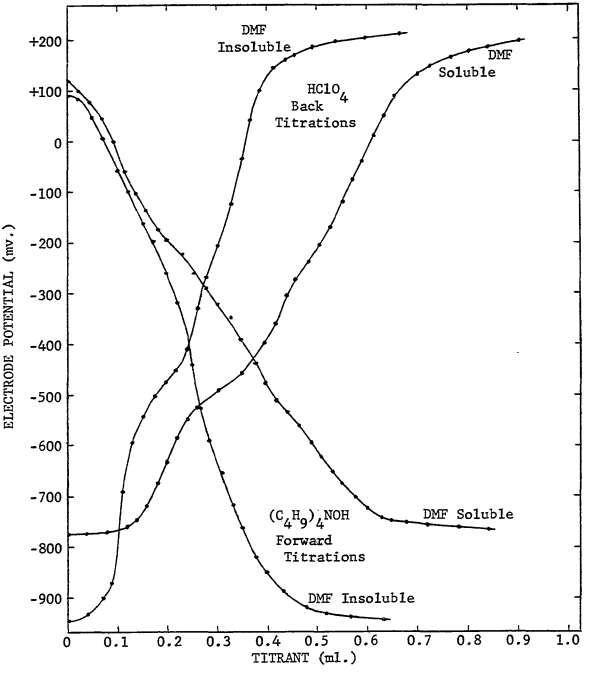

Figure 35. Forward and back titrations of DMF soluble and insoluble fractions of a carbon suboxide polymer prepared at 60°C with 0.42 N tetrabutylammonium hydroxide in 2-propanol and 0.42 N perchloric acid in 2-propanol.

protons per polymer molecule remains constant at slightly over two. It was observed that the DMF insoluble fraction of the 60°C. polymer could be titrated and went into solution as the titration proceded. Its equivalent weight would indicate that its molecular weight is also

Reproduced with permission of the copyright owner. Further reproduction prohibited without permission.

higher than that for the DMF soluble fraction. With the water extracted polymers, the equivalent weight dropped with the molecular weight. It was initially expected that water would enter the polymer first by hydrolyzing the ketenyl groups followed by hydrolyzing the lactone bonds. This would result in a small increase in the molecular weight and a large decrease in the equivalent weight at high degrees of hydrolysis. The most probable explanation for the contrary experimental result is a decarboxylation. Carboxylic acids with an olefin bond in the α-β or β-γ position are known to decarboxylate to nonacidic products (43). This could keep the equivalent weight from dropping, and the greater mass of the departing CO_2 molecules could outweigh the addition of the H_2O molecules to account for the molecular weight decrease. The hydrolysis and decarboxylation processes cause a change in the elemental composition of the polymer which is examined in the next section.

5. ELEMENTAL ANALYSIS

When the polymer is prepared from highly purified C_3O_2 and rigorously protected from moisture, it would be expected to have no hydrogen content and the same stoichiometry as the monomer. Schmidt, Boehm and Hofmann, by performing transfers and weighings in a dry box, were able to obtain an elemental analysis of 53.05% C , < 0.2% H and 46.75% O which is in good agreement with a C_3O_2 calculated analysis of 52.96% C. and 47.04% O (9). Blake and Hyde eliminated the polymer weighing and transfer operations by quantitatively analyzing the combustion products of the polymer with a known quantity of oxygen and obtained a stoichiometry of $C_3O_{1.99}$ (44). When the polymer is exposed to air, hydrogen contents up to 3% have been reported (9).

Reproduced with permission of the copyright owner. Further reproduction prohibited without permission.

Elemental analyses were performed on the extracted and unextracted 0 and 60°C. samples and on the water extracted samples. An ammonia exposed sample was also analyzed to determine what the stoichiometry is between the C_3O_2 repeat unit and the attacking NH_3 molecule. This sample was prepared by opening a sealed tube, containing polymer formed by bulk polymerization at 30°C., in a glove bag that had been flushed three times with dry nitrogen. The opened tube and polymer were immediately immersed in an ammonia saturated DMF solution and tightly stoppered. The ammonia had previously been vacuum distilled to IR purity. The polymer rapidly bleached to a light yellow powdery precipitate but was allowed to stand in the solution in a desiccator for a week. The precipitate was filtered, extracted with ether to remove the DMF and vacuum dried. The DMF filtrate was concentrated at reduced pressure and added dropwise to precipitate a small quantity of polymer. After extraction and drying, the DMF soluble portion of the ammoniated polymer was found to be 3% of the total which is a much lower solubility than for the air exposed C_3O_2 polymers. The elemental analyses were performed by Schwarzkopf Microanalytical Laboratory, Woodside, N.Y., and results are presented in Table VII.

TABLE VII

POLY(CARBON SUBOXIDE) ELEMENTAL ANALYSIS

Sample	%C	%H	%N	m	n	Mn	DP
$(C_3O_2)_n$ calculated	52.94	0	___	___	___	___	___
0° polymer unextracted	46.50	1.76	___	.65	.12		
DMF extracted	50.90	2.33	___	.69	.48	311	5.2
60° polymer unextracted	49.55	1.48	___	.50	.21		
DMF soluble	50.50	2.55	___	.75	.51	358	6.0
DMF insoluble	50.51	1.92	___	.60	.37	___	___
30° polymer H_2O soluble	53.20	3.12	___	.81	.70	281	5.4
H_2O insoluble	52.38	3.09	___	.82	.67	287	5.4
30° polymer NH_3 exposed	44.54	3.92	16.56	___	___	___	___
$C_3O_2 \cdot NH_3$ calculated	42.35	3.63	16.47	___	___	___	___

Reproduced with permission of the copyright owner. Further reproduction prohibited without permission.

The analyses show that limited air exposure resulted in an uptake of moisture sufficient to produce a hydrogen content of between 1 and 2%. The carbon content also shows a significant drop due to the added weight of the water molecule. After the polymer was extracted with DMF and worked up, the hydrogen content increased further, but the carbon content rose indicating more is occurring than just hydrolysis. A decarboxylation can account for the carbon content increase since two oxygen atoms are lost for every one carbon atom. When the polymer was extracted with water, in addition to further increases in the hydrogen and carbon contents the molecular weight dropped. This may be explained by decarboxylation occurring to an extent comparable to hydrolysis. If the polymer composition is assumed to be determined by the number of C_3O_2 and H_2O molecules that enter the polymer and the number of CO_2 molecules that depart, these quantities may be calculated from the carbon and hydrogen contents and the molecular weight. Considering the polymer to be initially composed of p C_3O_2 units, its C_3O_2 composition will be altered by the addition of m H_2O molecules per C_3O_2 unit and the loss of n CO_2 molecules per C_3O_2 unit.

$$\text{Composition} = C_3O_2 + m\,H_2O - n\,CO_2$$

The percentages of carbon and hydrogen, expressed as decimal fractions, are given by

$$\%\ C = \frac{12(\text{mole C})}{12(\text{mole C}) + 16(\text{mole O}) + 1(\text{mole H})}$$

$$\%\ H = \frac{1(\text{mole H})}{12(\text{mole C}) + 16(\text{mole O}) + 1(\text{mole H})}$$

From the stoichiometry of C_3O_2, H_2O and CO_2:

$$\text{mole C} = 3 - n \qquad \text{mole O} = 2 - 2n - m \qquad \text{mole H} = 2m$$

Reproduced with permission of the copyright owner. Further reproduction prohibited without permission.

$$\%C = \frac{36 - 12n}{68 - 44n + 18m} \qquad \%H = \frac{2m}{68 - 44n + 18m}$$

$$\text{or} \quad n = \frac{17(\%C)H - 9}{11(\%C)H - 3} \quad ; \quad H = \frac{1}{1 - 9(\%H)}$$

$$m = \frac{34 - 22n}{\frac{1}{\%H} - 9}$$

The degree of polymerization, p, is obtained from n, m and the molecular weight.

$$Mn = p(MW\ C_3O_2) + pm(MW\ H_2O) - pn(MW\ CO_2)$$

$$\text{or} \quad p = \frac{Mn}{68 + 18m - 44n}$$

Values for n, m and p(DP) based on experimental data are presented in Table VII. These results show that appreciable hydrolysis occurs only on exposure to air and that decarboxylation becomes more significant during extraction and workup. The degrees of both hydrolysis and decarboxylation become more extensive after extraction with water. The degrees of polymerization range between 5 and 6 and show a definite increase with increasing polymerization temperature. This DP size and temperature dependence are in very good agreement with the results of Blake's x-ray diffraction experiment (2). The analysis for the ammonia exposed sample is in good agreement with that calculated for one NH_3 unit reacted per C_3O_2 unit. This would correspond to an opening of the lactone bond, of which there is one per C_3O_2 unit, to form an amide functional group. This is supported by the shift of a lactone carbonyl absorption to an amide absorption in the IR (Section IV-6). Titration of this sample with tetrabutylammonium hydroxide was irreversible and accompanied by a color change to a dark brown. Smith reports the ammoniated polymer to release ammonia on hydrolysis with atmospheric

Reproduced with permission of the copyright owner. Further reproduction prohibited without permission.

moisture (1). These results would indicate that the lactone bonds of the polymer are not stable enough under workup conditions toward water or ammonia to permit determination of the number of hydrolyzed or ammoniated ketenyl groups per polymer molecule by titration or nitrogen analysis.

Another way to deal with this polymer molecule-ketenyl group functionality is to assume that the ketenyl groups are much more reactive than the lactone bonds toward water and, under mild exposure conditions, determine the quantity of water reacted with a known quantity of polymer at the point where the ketenyl groups are no longer present. This was done by simultaneously following the quantity of water uptake by weighing and the relative quantity of ketenyl groups present by ESR. These measurements have the advantage of being valid for inhomogeneous systems. A film of weighable mass was prepared by polymerizing C_3O_2 at 100°C. and 90 mm pressure over a 1-1/2 to 2 day period on the tip of a 100 ml cell similar to that in Figure 3 except that the tip was a 5mm cylindrical quartz tube. The mass of the film, obtained from evacuated cell weight differences, corresponded to 25 mg. Water weight and ESR signal intensity measurements were made after successive exposures to and evacuations of pressures of water vapor corresponding to 10 mm or less. These measurements are plotted against exposure time in Figure 36. The ESR signal intensity, which was measured against the Mn^{2+} marker and normalized to 1 before exposure, lost 95% of its intensity after 100 minutes exposure while the H_2O weight gain passed through a maxima at about 2.4 mg. Taking the 2.4 mg water as the effective hydrolyzing mass, the following degree of polymerization may be calculated assuming two ketenyl groups per polymer molecule.

Reproduced with permission of the copyright owner. Further reproduction prohibited without permission.

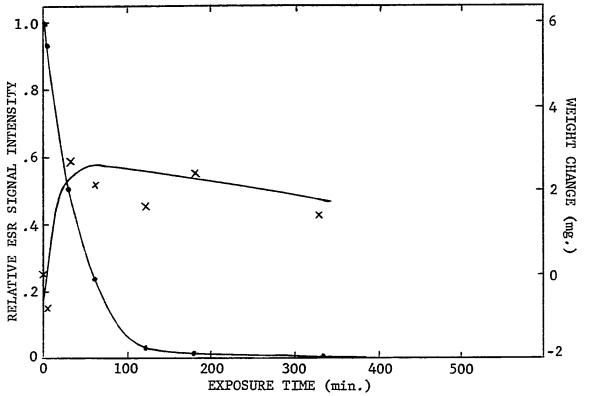

Figure 36. ESR signal decay (•) and polymer weight gain (x) as a function of water vapor exposure time for a 25 mg polymer sample.

$$DP = \frac{\left[\frac{.025g\ P + .0024g\ H_2O}{.0024g\ H_2O \times \frac{mole}{18g} \times \frac{mole\ P}{2\ mole\ H_2O}}\right] - \left[\frac{2\ mole\ H_2O}{mole\ P} \times \frac{18g\ H_2O}{mole\ H_2O}\right]}{\left[\frac{68g\ C_3O_2\ unit}{mole\ C_3O_2\ unit}\right]} = 5.5$$

This result falls well within the DP range of 5 to 6 result from the elemental analyses although it is probably a minimum since lactone hydrolysis is not taken into account. This indicates that there are two ketenyl groups per polymer molecule.

6. INFRARED, VISIBLE-ULTRAVIOLET AND FLUORESCENCE SPECTRA

Changes in the spectroscopic properties of the polymer were observed on exposure to atmospheric moisture. The elemental analysis results suggested that, for just air exposure, hydrolysis was the primary change and then, when the polymer was subjected to workup

Reproduced with permission of the copyright owner. Further reproduction prohibited without permission.

conditions, decarboxylation became significant. Spectra of the worked up polymers are examined for the effects of hydrolysis and decarboxylation. Polymer solutions, in addition to having an intense color, display a green fluorescence. The optical and fluorescence spectra and absorption and emission intensities are obtained for the different polymer samples.

Infrared spectra of the polymer samples were obtained from KBr discs and films (Figure 37). No significant differences between spectra of worked up polymers prepared at different temperatures was observed. Extraction with water had only the effect of broadening the spectra. However, with the ammoniated polymer, a shift from a lactone carbonyl at 5.85 μ to an amide carbonyl at 6.2 μ as well as an N-H stretching band at 2.96 μ was observed (Figure 37d).

The changes in the IR spectrum that accompany polymer hydrolysis are best followed in Figure 26 where a constant amount of polymer receives successive exposures to water vapor. The formation of carboxylic acid groups would be expected from two sources, the ketenyl groups and the lactone bonds. This is observed by the decay of the ketenyl band at 4.6 μ and decline of the lactone linkage absorption at 8.2 μ. Acid bands would be expected to appear at 5.85-5.95 μ (conjugated C=O stretching), 3.0-4.0 μ (O-H stretching), 7.58-8.26 μ (C-O stretching) and 6.95-7.17 μ (O-H bending) (45). A gradual shift from the α-pyrone carbonyl absorption at 5.6 μ to an acid carbonyl at 5.8-5.9 μ can readily be seen in Figure 26 and by reference to the dashed line at 5.9 μ in Figure 37. Increases in the absorption intensity are observed at wavelengths corresponding to the other acid absorptions and appear as a filling in between previously resolved absorptions of the unexposed polymer. After

Reproduced with permission of the copyright owner. Further reproduction prohibited without permission.

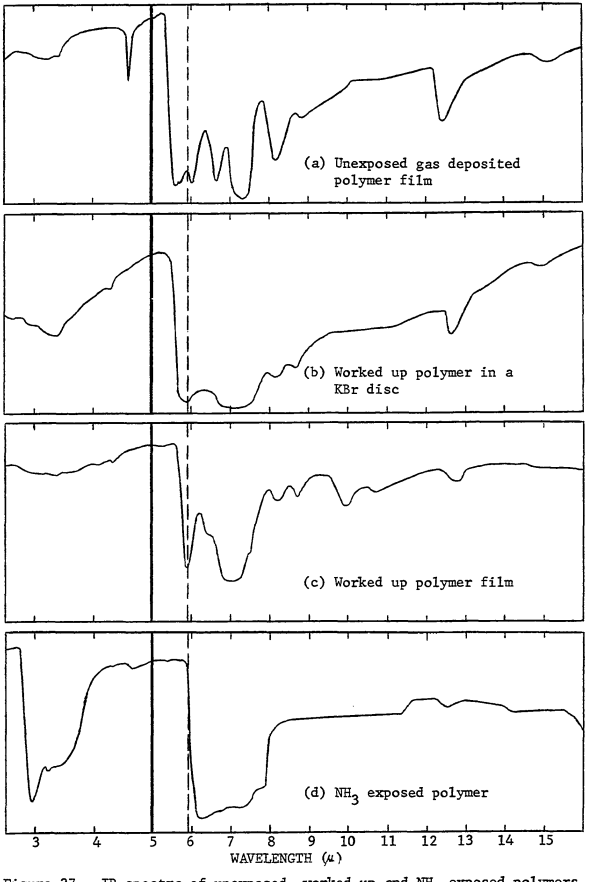

Figure 37. IR spectra of unexposed, worked up and NH_3 exposed polymers.

Reproduced with permission of the copyright owner. Further reproduction prohibited without permission.

the DMF extraction, the carbonyl shift and the 6.95 μ absorption appear more prominently, but the spectrum diffusiveness and lactone absorption at 8.2 μ do not entirely disappear.

A partially hydrolyzed, partially decarboxylated poly(α-pyrone) is also in agreement with the visible-ultraviolet and fluorescence spectra. Visible-ultraviolet spectra of the polymer samples were obtained with a Cary model 118-C spectrometer. The wavelength and optical density calibration were checked at 262 and 275.5 nm with potassium hydrogen phthalate and at 394 nm with nickel sulfate standards (46) and found to have an accuracy of better than 1%. In all cases the Beer-Lambert Law was followed by the polymer solutions. Spectra of the DMF extracted polymers in DMF have two absorption maxima at 430 and 324 nm (Figure 38). Both the wavelength maxima and specific absorbtivities were found to be independent of the polymerization temperature (Table VIII). The water extracted polymer samples showed a breaking up of the longer wavelength maxima to shorten wavelength maxima at 410 and 375 nm with a substantial decrease in intensity (Figure 39). The 324 nm wavelength also showed a slight shift to a shorter wavelength but no significant intensity change. The long wavelength absorption can be attributed to a $\pi \rightarrow \pi^*$ transition which would be expected of the conjugated polymer structure. Partial hydrolysis would not break up the polyene backbone of the polymer but lactone hydrolysis and decarbolylation would reduce the amount of ring fusion. Extensive hydrolysis and decarboxylation could result in an effective shortening of the polyene system by reducing ring fusion to an extent where coplanarity between double bonds is not maintained and produce a series of shorter polyene systems having less intense shorter wavelength maxima.

Reproduced with permission of the copyright owner. Further reproduction prohibited without permission.

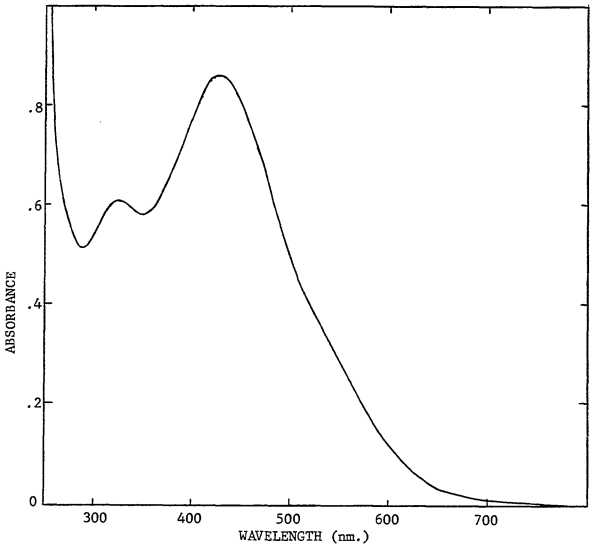

Figure 38. Visible-ultraviolet spectrum of DMF extracted poly(carbon suboxide) in DMF solution.

TABLE VIII

VISIBLE-ULTRAVIOLET AND FLUORESCENCE SPECTROSCOPIC DATA IN DMF

Sample	a_{430}(1/g cm)	a_{324}(1/g cm)	λ_{em}(nm)	Φ
0° polymer	39.9	25.6	504	.021
30° polymer	39.1	26.6	503	.022
60° polymer[a]	40.0	27.5	503	.022
	a_{410} a_{375}	a_{320}		
30° polymer H_2O soluble	29.9 30.2	28.6	487	.031
30° polymer H_2O insoluble	31.0 28.5	26.8	492	.026

[a]DMF soluble fraction.

Reproduced with permission of the copyright owner. Further reproduction prohibited without permission.

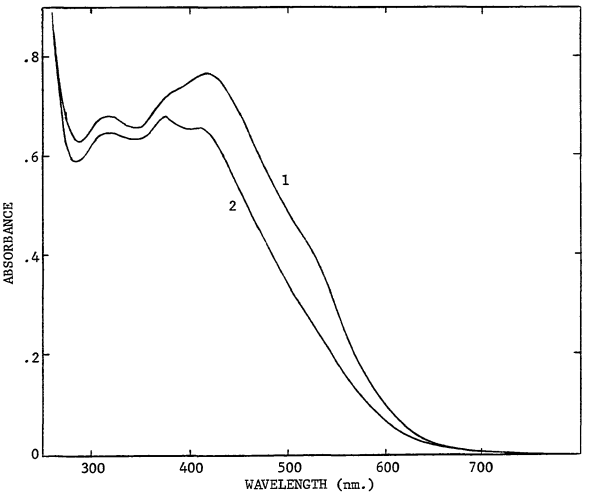

Figure 39. Visible-ultraviolet spectra of water extracted poly(carbon suboxide) in DMF solution. Curve 1 - water insoluble fraction. Curve 2 - water soluble fraction.

The long wavelength maxima is also sensitive to the polarity of the solvent. When the more polar but structurally similar N-methylformamide is substituted for DMF, a bathochromic shift characteristic of $\pi \rightarrow \pi^*$ K bands (47) is observed (Table IX). With DMSO as the solvent, a very large bathochromic shift of 55 nm is observed. This would indicate a strong interaction with the polymer, possibly a complex formation. This would also be consistent with a positive second virial coefficient (Γ_2 = 38.6 g/g) derived from the freezing point depression data (Figure 32).

Reproduced with permission of the copyright owner. Further reproduction prohibited without permission.

TABLE IX

SOLVENT EFFECTS ON VISIBLE-ULTRAVIOLET AND FLUORESCENCE SPECTRA

Solvent	Dielectric constant	λ_1(nm)	a_1	λ_2(nm)	a_2	λ_{em}(nm)	Φ
Dimethylforamide	36.7	430	39.1	324	26.6	503	.022
Methylforamide	182	435	39.1	324	26.8	503	.022
Dimethylsulfoxide	46.7	485	42.9	324	24.7	490	.012

Fluorescence spectra of the polymer samples were obtained using an Aminco-Bowman Cat. No. 4-8202 spectrofluorimeter with a xenon lamp and recorded with a Hewlett-Packard 7005B x-y recorder. The emission wavelength was calibrated with a 5 x 10^{-3}F $UO_2(NO_3)_2$ solution in 5.0 N H_2SO_4 (48) with excitation and emission slit settings of 4 and 1 mm respectively. Quantum yields, Φ, were obtained with a fluorescein standard (10^{-6}M in 0.01 N NaOH; Φ_1 = 0.85, λ_{ex} = 436 nm) by measuring the area corresponding to the emission intensity of the polymer against that of the standard at an excitation wavelength of 436 nm according to:

$$\Phi_2 = \frac{\text{area}_2}{\text{area}_1} \Phi_1 \frac{\varepsilon_1 c_1 l_1}{A_2} \frac{n_2}{n_1}$$

where the subscript 1 refers to the standard and 2 to the polymer (49). A_2 is the absorbance of the polymer solution at 436 nm, ε_1 is the molar absorbtivity of fluorescein at 436 nm (experimentally determined to be 7.85 x 10^3 l/mole cm), C_1 is the fluoroscein concentration, l_1 is the cell path length and n_1 and n_2 are the refractive indexes of the standard and polymer solvents. Fluoroscein's inner filter effect necessitated fluorescence intensity measurements at concentrations of less than 10^{-6}M which is too dilute for an accurate absorbance measurement at 436 nm. Spectra and quantum yields were obtained from solutions where the fluorescent intensity was proportional to the concentration.

Reproduced with permission of the copyright owner. Further reproduction prohibited without permission.

The uncorrected excitation and emission spectra of the 0°C. DMF extracted polymer sample in DMF is presented in Figure 40. This spectrum is typical in shape and band width of the other samples in DMF and other solvents. There is a correspondence between the excitation and absorption spectra indicated by a maxima near 430 nm and a shoulder at 320 nm which indicates that the polymer is the source of the fluorescence. That the polymer is fluorescent is evidence for a fused ring conjugated system (50). The green 500 nm emission wavelength suggests a relatively large conjugated system. There is an interesting parallel between the fluorescent emission wavelength and number of condensed rings in aromatic hydrocarbons where benzene and naphthalene fluoresce in the ultraviolet, anthracene is blue, naphthacene is green and pentacene is red (51). The α-pyrones appear to compose a similar series with dipyrone fluorescing in the ultraviolet and tripyrone fluorescing blue (52). The relatively low quantum yield may be due to the presence of carboxylic acid groups as this substituent is reported to have large decreasing effects on intensities of fluorescent molecules (53). The apparent increase in quantum yield after extraction of the polymer with water is probably due more to a smaller absorbance at 436 nm by the nonfluorescent chromophores (the absorption spectrum shifts to shorter wavelengths). The decrease in fluorescent wavelength is consistent with a shortening of the polyene length as suggested for the absorption spectrum. The decrease in quantum yield and emission wavelength with DMSO as solvent may be the result of a strong polymer-solvent interaction.

In summary, both the optical and fluorescence spectra support a poly(α-pyrone) polymer structure which undergoes partial hydrolysis on exposure to water.

Reproduced with permission of the copyright owner. Further reproduction prohibited without permission.

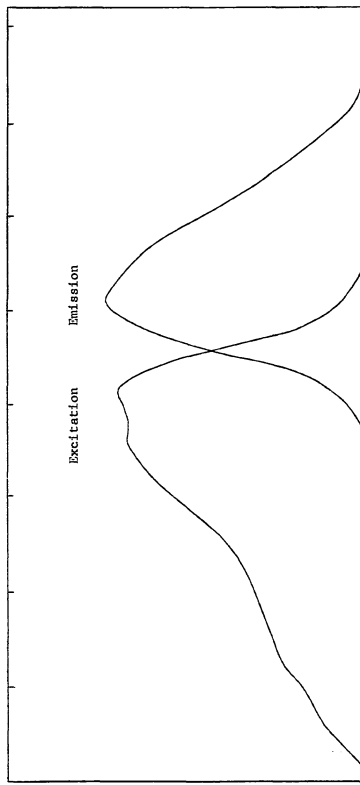

Figure 40. Uncorrected excitation (λ_{em} = 504 nm) and emission (λ_{ex} = 460 nm) of poly(carbon suboxide).

Reproduced with permission of the copyright owner. Further reproduction prohibited without permission.

7. ATTEMPTED POLYMER HYDROGENATION

The object of hydrogenation was to increase the polymer's solubility and obtain NMR structural information from the hydrogen placement. A 5% rhodium-carbon catalyst was selected on the basis of successful hydrogenations reported for coumarin derivatives at hydrogen pressures of a few atmospheres (54). Using coumarin as a model compound, it was found, when a 1:1 weight ratio of catalyst to compound in methanol was used, 5 moles of hydrogen per mole coumarin were absorbed. The product was identified as 3-cyclohexylpropanoic from the infrared spectrum. When the solvent was changed to the DMF polymer solvent, only about 2 moles of hydrogen per mole coumarin were absorbed at a much slower rate. Gas chromatography showed a mixture of at least three components two of which had retention times corresponding to dihydrocoumarin and coumarin but none corresponding to 3-cyclohexylpropanoic acid. The IR indicated the presence of an acid. This, in addition to a strong aromatic absorption in the UV, would indicate DMF inhibits the rhodium catalyst from hydrogenating the aromatic portion of coumarin. Hydrogenations of the carbon suboxide polymer were attempted at a weight ratio of 2:1 in DMF and 1:1 in methanol (although the polymer is only slightly soluble). In both cases very little drop in the hydrogen pressure was observed as well as no change in the polymer's UV spectrum. NMR scans resulted in no signals attributable to the hydrogenation of the polymer.

Reproduced with permission of the copyright owner. Further reproduction prohibited without permission.

V. REACTION PATH

The fused ring poly(α-pyrone) structure has been found to be consistent with the experimental results of this work. Experiments designed to examine what kind of process or intermediate may be involved when linear C_3O_2 molecules are incorporated in the zigzag configuration of the polymer structure are presented in this section. Two important observations of the polymerization are that it is preceded by an induction period and that it does not occur in the gas phase but proceeds by coating the walls of its container. The induction period indicates either an agent is present that retards polymerization or an agent is absent that promotes polymerization. It has been found that monomer stability toward polymerization improves with purification which suggests that the inhibition is due to lack of an initiator. That the polymerization does not occur in the gas phase indicates that monomer that monomer interaction with something other than another monomer is necessary for initiation. These interpretations are consistent with the observed dependence of the induction period on the nature of the vessel surface (1). Once an initial quantity of polymer is formed, it can serve as a site for further polymerization. This is consistent with the kinetic rate law of first order in both monomer and polymer. From the polymer's repeat unit, it appears that monomers would have to be added by a 1,3 addition to the 2,4 positions of the previously added monomer or vice versa.

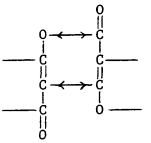

Reproduced with permission of the copyright owner. Further reproduction prohibited without permission.

This addition process was investigated by examining the effect of various inhibiting reagents and of medium polarity on the polymerization rate.

1. POLYMERIZATION INHIBITORS

The selection of inhibitors which would affect radical and ionic polymerizations was made on the basis of keeping the polymerization system as simple as possible. Such a system is a polymer formed by gas deposition. This required choosing inhibitors which have substantial vapor pressures. The polymerizations were run using a cell (Figure 3) with a cyclindrical quartz tip heated to 100°C. by immersion to a depth of 2.5 cm in a foil covered oil bath. The rate of polymer formation was followed by ESR. A carbon suboxide pressure of 330 mm Hg (vapor pressure at -13°C.) was used. Either equimolar quantities of inhibitor based on pressure measurements or room temperature vapor pressures of inhibitor if less than 330 mm Hg were used. Normally 30 to 60 minutes heating was required before a faint yellow film appeared at the tip of the cell. At this point ESR signal intensity measurements were made against the Mn^{2+} marker every 15 minutes. Measurements, which involved bringing the cell tip rapidly to room temperature with a 5 second immersion in water and scanning the signal and marker, required 4 minutes. The 4 minute measurement time was not included in the polymerization time. The inhibitors chosen were oxygen, nitric oxide, 3-methyl-1-butene, 1,3-butadiene, acetone and acetaldehyde. The results are presented in Figure 41.

The free radical inhibitors, oxygen and nitric oxide, when compared with the C_3O_2 control, appear to have little effect on the polymerization rate. This result was also observed by Blake (15) who followed the polymerization rate by the fall in monomer pressure. The presence

Reproduced with permission of the copyright owner. Further reproduction prohibited without permission.

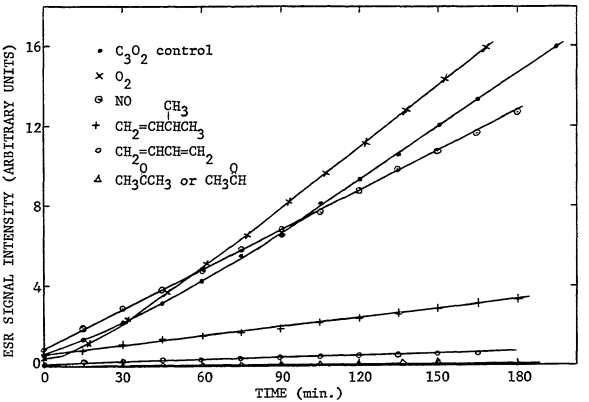

Figure 41. Effect of assorted inhibitors on the carbon suboxide polymerization rate.

of oxygen had no effect on the signal's line shape but nitric oxide produced a dramatic change. The growth of an ESR absorption with a shape illustrated in Figure 42 was observed when nitric oxide was present. It would appear that a second signal, having a central line at a lower magnetic field and some wing structure between 20 and 30 gauss on either side, has overlapped the normally observed 2.3 gauss signal. The spectrum did not change as the polymerization proceded, and no selective saturation was observed at high microwave powers. Evacuation of the cell for one hour resulted in no spectrum change indicating it is not a weak association of the nitric oxide molecule. The infrared spectrum through the quartz cell (2.5 to 4.8 μ) showed only the ketenyl absorption. When a C_3O_2 polymer is exposed to nitric oxide subsequent to polymerization a shoulder maxima on the ESR signal

Reproduced with permission of the copyright owner. Further reproduction prohibited without permission.

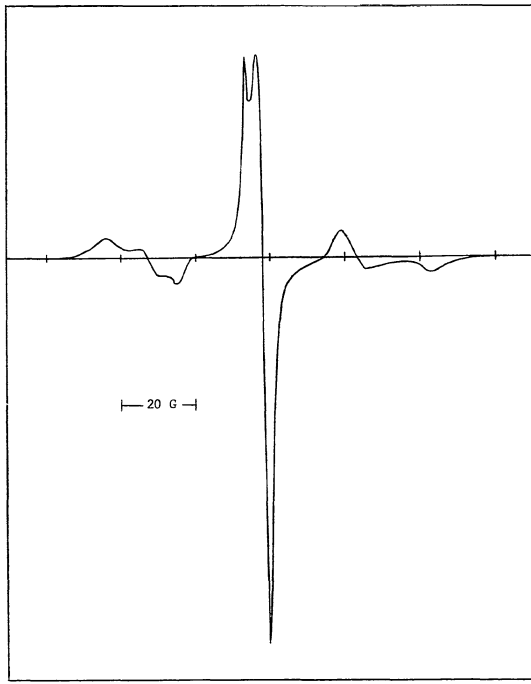

Figure 42. ESR spectrum of poly(carbon suboxide) polymerized in the presence of nitric oxide.

very slowly develops at a point corresponding to the "new" line's central maxima. The wing structure does not appear to have enough symmetry to be hyperfine structure and nitroxy radical splitting is

Reproduced with permission of the copyright owner. Further reproduction prohibited without permission.

usually on the order of 15 gauss. While a nitric oxide-polymer complex formation is suspected, the nature of it is unknown.

Carbon suboxide's susceptability to radical polymerization was also tested by an attempted copolymerization of equimolar quantities of C_3O_2 and styrene initiated by AIBN at 60°C. The infrared spectrum of the "copolymer" obtained was identical to that of a styrene homopolymer control with no carbonyl absorption detectable. When free radical initiated polymerization of C_3O_2 alone was attempted, the only product obtained was identical to the thermopolymer.

These results indicate that, although unpaired electrons are generated during the polymerization process, monomer addition is not a radical process. This conclusion is the same as that of the phenyl-tert-butylnitrone spin trap experiment in Section III where it was found that there is no radical present during the polymerization reactive enough to convert the nitrone to the nitroxy radical. It is not then probable that C_3O_2 monomer would be attacked by the polymer radical since C_3O_2 is inert to radicals as reactive as the styryl radical while the polymer radical does not possess sufficient reactivity to attack the nitrone spin trap.

There was a significant reduction in the polymerization rate when 3-methyl-1-butene was present. This monomer is susceptable to cationic polymerization but yields very low molecular weight products. The polymerization rate reduction was even more pronounced in the presence of 1,3-butadiene which also undergoes cationic polymerization. In both cases the normal ESR spectrum was observed. However, when cleaning the cell, the film from these polymerizations was insoluble in DMF and in aqueous hydroxide which is uncharacteristic of the normal poly(carbon suboxide) films. When acetone or acetaldehyde was present, the yellow

Reproduced with permission of the copyright owner. Further reproduction prohibited without permission.

film did not develop over an 8 hour period, but only a nonuniform faintly detectable brown film and an extremely weak ESR signal were observed. A particular weakness of inhibitor experiments is that they are incapable of yielding a meaningful positive result. A negative result is evidence against a polymerization mechanism, but a positive result only indicates the polymerization does not compete successfully with an inhibitor reaction. Carbon suboxide has been reported to react with aldehydes and ketones under various conditions (12,68), but nothing was found for olefins or dienes with the exception of photolysis. Blake observed no effect on the polymerization rate when ethylene was present (15) although ethylene is not an easily polymerized monomer.

The inhibition of the polymerization by acetone or acetaldehyde may well explain why the C_3O_2 derived from the diacetyltartaric anhydride pyrolysis is more stable than that from the malonic acid dehydration. In the appendix, infrared spectra of the diacetyltartaric anhydride derived C_3O_2 purification show a carbonyl band of a slightly less volatile impurity for which acetaldehyde was suggested. It would be formed according to the following reaction.

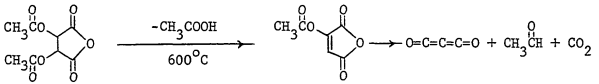

A suggested improvement for this synthetic method would be to use an anhydride which would place a longer chain acyl group on the tartaric anhydride and, after pyrolysis, yield less volatile, more easily separable by-products than acetic acid and acetaldehyde (and possibly ketene).

Reproduced with permission of the copyright owner. Further reproduction prohibited without permission.

2. EFFECT OF SOLUTION POLARITY

If the polymerization involves a charged intermediate or transition state, the polarity of the medium would be expected to have an effect on the reaction rate. Although there are reports of surface effects on the polymerization rate (1,15), no correlation has been made with the polarity at the reaction site. To determine the effect of polarity, a homogeneous system would provide a more advantageous representation than a heterogeneous system. The use of a polymer solvent such as DMF precludes using ESR to follow the polymerization because of the inability to obtain a solution spectrum as well as spectrometer tuning difficulties due to the solvent's high dielectric constant. However, the polymerization can be followed by optical density since the system is homogeneous and the monomer does not interfere in the visible region.

The optical spectrum of a DMF solution polymerization was found to be different from that of the gas deposited film having two pair of maxima centered at 420 and 320 nm instead of the one at 370 nm (Figure 43). The spectrum was independent of conversion, and a simple log A vs. time plot was not linear indicating the rate law was no longer first order with respect to polymer. Before determining what the effect of solution polarity is, it was necessary to determine the kinetic rate law.

DMF was dried and purified by stirring over P_2O_5, then over KOH pellets and distilled at reduced pressure. The polymerization was run in a 1 cm optical cell connected to a wide bore stopcock having a closed volume of 9.51 ml. The cell was filled with C_3O_2 at pressures of 590, 430 and 340 mm Hg (C_3O_2 vapor pressures at 0, -7 and -12.5°C). After condensing the C_3O_2 with a piece of dry ice, a calibrated volume

Reproduced with permission of the copyright owner. Further reproduction prohibited without permission.

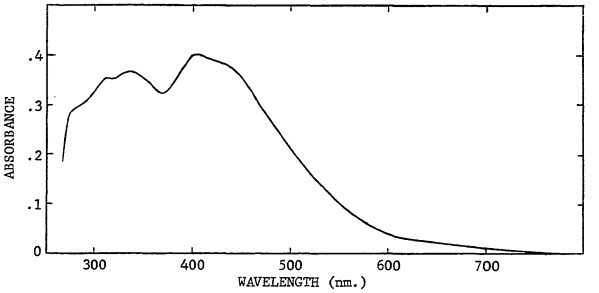

Figure 43. Visible-ultraviolet spectrum of DMF solution polymerized poly(carbon suboxide).

of 3.98 ml of DMF or DMF-toluene mixture was added. The cell was agitated by tipping but not inverting for about 20 seconds to insure mixing and placed in the Cary visible-ultraviolet spectrometer. The absorbance at 420, 500 and 600 nm against a DMF reference was recorded consecutively as a function of time.

At all three wavelengths a plot of the square root of the absorbance against time was linear indicating a reaction order of 1/2 with respect to polymer (Figure 44). The reaction order with respect to monomer was obtained by the initial rate method where the natural log of the slope of the $A^{1/2}$ vs. time plot was plotted against the log of the initial monomer pressure (Figure 45). Slopes of this plot corresponding to the 420, 500 and 600 nm measurements were 1.14, 1.03 and 1.14 respectively indicating a first order reaction with respect to monomer.

An explanation for the change in optical spectrum and reaction order with respect to polymer is the formation of a dimeric complex in

Reproduced with permission of the copyright owner. Further reproduction prohibited without permission.

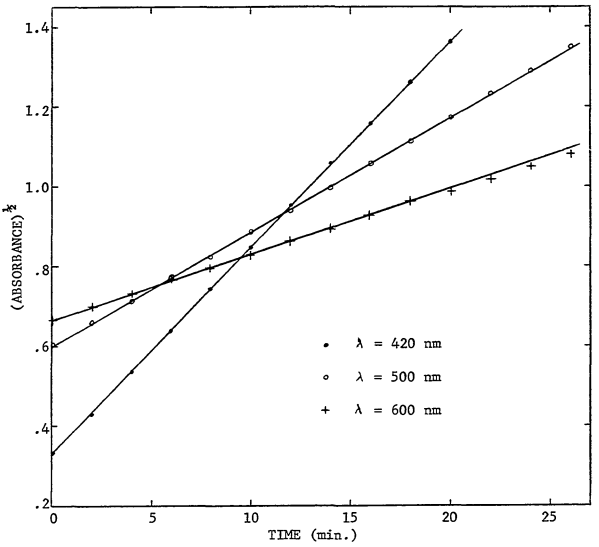

Figure 44. Half order solution polymerization rate dependence on polymer absorbance at 420, 500 and 600 nm. Initial monomer pressure - 430 mm Hg.

DMF. The following kinetic scheme can account for the change in rate law:

$$P + M \xrightarrow{k} P$$

$$P + P \underset{}{\overset{K}{\rightleftharpoons}} C \qquad K = \frac{[C]}{[P]^2}$$

where M is a C_3O_2 monomer, P is a polymer molecule and C is the complex. If the complex is the only species absorbing at the longer wavelengths where the absorbance was measured, the polymerization rate is given by

Reproduced with permission of the copyright owner. Further reproduction prohibited without permission.

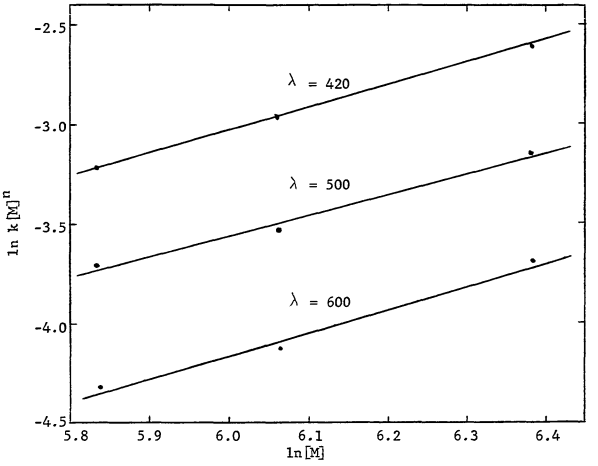

Figure 45. Solution polymerization rate dependence on monomer. Monomer concentration is expressed as initial monomer pressure.

the following expression assuming the complex equilibrium to be rapid compared to the polymerization rate and the complex to be dimeric.

$$\frac{d[P]}{dt} = k[P][M] = \frac{k}{K^{1/2}}[M][C]^{1/2}$$

When the polarity of the medium was decreased by diluting the DMF with toluene, a reduction in the polymerization rate was observed (Figure 46). This decrease varied regularly with the decreasing mole fraction of DMF. The possibility of a shift in the complex equilibrium to favor the shorter wavelength absorping species was ruled out since the opposite spectrum change was observed. The intensity of the 420 nm absorption was observed to increase rather than decrease relative to the one at 320 nm with increasing toluene concentration. The polymerization

Reproduced with permission of the copyright owner. Further reproduction prohibited without permission.

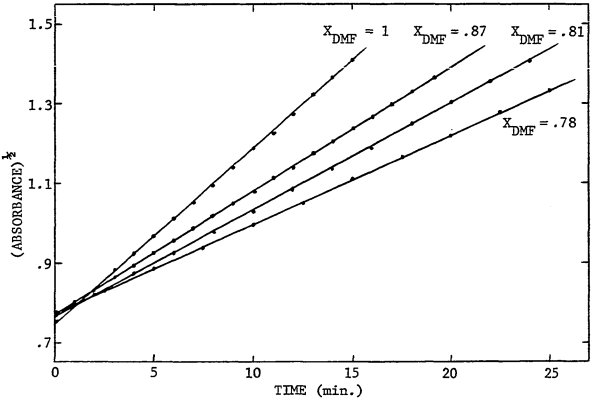

Figure 46. Effect of solution polarity on the polymerization rate followed by polymer optical density at 500 nm for varying DMF - toluene compositions. X_{DMF} - mole fraction DMF.

rate dependence on solution polarity is interpreted that the polymerization passes through a polar or ionic intermediate or transition state which would be stabilized by an increasingly polar medium. This is consistent with the inhibition results where the strongest inhibitors (the carbonyl compounds) are known to be more susceptable to ionic rather than free radical addition. A mechanism taking this into account will be presented in the next section.

Reproduced with permission of the copyright owner. Further reproduction prohibited without permission.

VI. CONCLUSION

In this section proposals for the structure of the poly(carbon suboxide) radical and the polymerization mechanism are made.

1. POLYMER RADICAL STRUCTURE

Before proposing a structure for the poly(carbon suboxide) radical, the criteria it should satisfy will be reviewed.

First, it is necessary to consider that the polymer is composed of only oxygen and carbon atoms which are even electron atoms. To have an unpaired electron, it is necessary to have a triplet state or an electron transfer between polymer molecules. An electron transfer is favored since no evidence of a triplet state was observed. No half field transition or zero field splitting were observed in the ESR spectrum at room temperature or at temperatures as low as 5°K. The constant line width down to 5°K and the resolution of carbon 13 hyperfine structure preclude the possibility of an exchange narrowed triplet. The lack of an anisotropic ESR signal response to illumination with polarized light also discounts the triplet state. Photomagnetic behavior where only signal intensity is affected has been characterized as a property of charge transfer donor acceptor pairs in the solid state (55). The greater susceptability of the polymer to the more polar spin quenching nucleophiles suggests the polymer possesses some ionic character. Attributing the paramagnetism to electron transfer requires the polymer molecule be provided with donor and acceptor sites to stabilize either a positive or negative charge.

The second criteria is that there must be two ketenyl groups per polymer molecule and the unpaired electron's existance must be dependent on their presence.

Reproduced with permission of the copyright owner. Further reproduction prohibited without permission.

Third is that the carbon 13 coupling constant stipulates that the unpaired electron must be in a pi delocalized system with an appreciable spin density at the carbon atom corresponding to the monomer's central carbon atom.

Fourth, the g-value indicates that oxygen must be an important constituent of this pi delocalized system.

Finally, the ketenyl group should be conjugated with the pi system to account for the visible-ultraviolet spectrum change on exposure to water.

Starting with the polymer's repeat unit structure, it is necessary to supply two end groups. Since each polymer molecule must have two ketenyl groups, the end groups are the logical places for them. These can be formed with C_3O_2 additions by opening just one double bond resulting in a five membered terminal ring as in the top of Figure 47. Since each molecule must have a donor and acceptor site to stabilize a positive or negative charge, it is important how the ketenyl groups are placed. A close examination of this structure shows a polyene chain running through the ladder structure, and the end groups have been placed in such a way that one end is terminated by a ketenyl group and the other by a carbonyl group. For an acceptor site a carbonyl group is proposed and for a donor site a ketenyl group. Dipole moments for the analogous small molecules of formaldehyde (2.3 D) and ketene (1.4 D) indicate that the charged resonance structures in Figure 47 make a reasonable contribution (56). Since oxygen carries a charge better than carbon, a carbonyl group will more readily accept an electron, and a ketenyl group will more readily release one. Connecting these two groups with a polyene chain creates a pathway for this transfer to occur resulting in a stable charged resonance structure (center of Figure 47).

Reproduced with permission of the copyright owner. Further reproduction prohibited without permission.

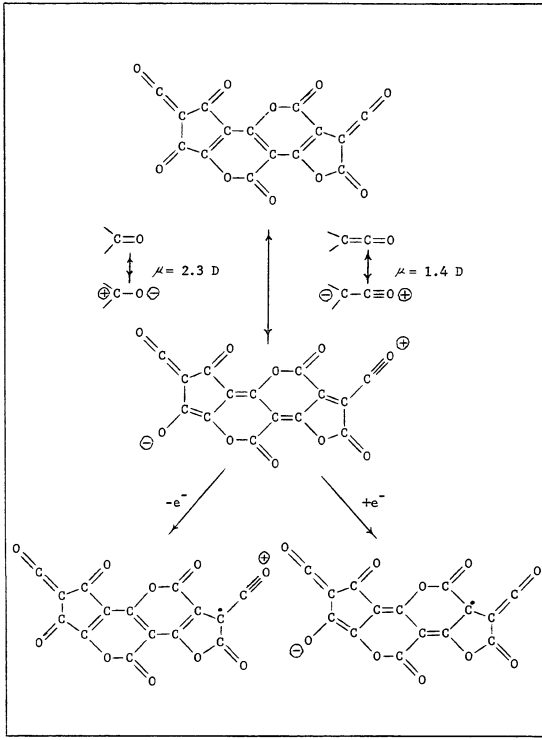

Figure 47. Proposed Lewis structures for poly(carbon suboxide) resonance forms and radical ions.

Reproduced with permission of the copyright owner. Further reproduction prohibited without permission.

Electron transfer can be pictured as occurring from this charged resonance structure, and the resultant radical ions may be stabilized by resonance with the polyene chain. A better representation of the charge and electron delocalization is obtained using Linnett structures (57) which is illustrated in Figure 48 where the double headed arrows show the corresponding resonant Lewis structures.

Nonstoichiometry between the spin density and the molecular density is commonly observed with organic donor acceptor charge transfer systems (32,35,36,55). For the poly(carbon suboxide) system, a spin density of 2.5×10^{18} spin/gram and degree of polymerization of six give a relation of one spin for every 600 polymer molecules. The explanation for this appears to be that there is a limit to the amount of charge an organic matrix can support. Kearns and Calvin (55) have proposed a mechanism for donor acceptor charge transfer composites which appears to be applicable to homogeneous systems as well. Charge transfer is proposed to occur by the following equilibrium:

$$D_i + A_i \rightleftharpoons \underset{\text{singlet or triplet}}{[D_i^{\delta+} - A_i^{\delta-}]} \rightleftharpoons \underset{\text{doublet doublet}}{D^+ + A^-}$$

where D_i and A_i represent neutral donor and acceptor molecules, $[D_i^{\delta+} - A_i^{\delta-}]$ represents a charge transfer complex and D^+ and A^- are singly charged donor and acceptor molecules. As the extent of electron transfer increases, the distance between neighboring charge centers decreases, and the amount of energy required to maintain mobile charges against attracting and repelling coulombic forces increases. A point is reached where the energy gained by charge transfer is balanced by the energy required to overcome the coulombic forces in the matrix, and electron transfer ceases. This applies to the poly(carbon suboxide) system as follows. The complex has a singlet multiplicity consistent with the

Reproduced with permission of the copyright owner. Further reproduction prohibited without permission.

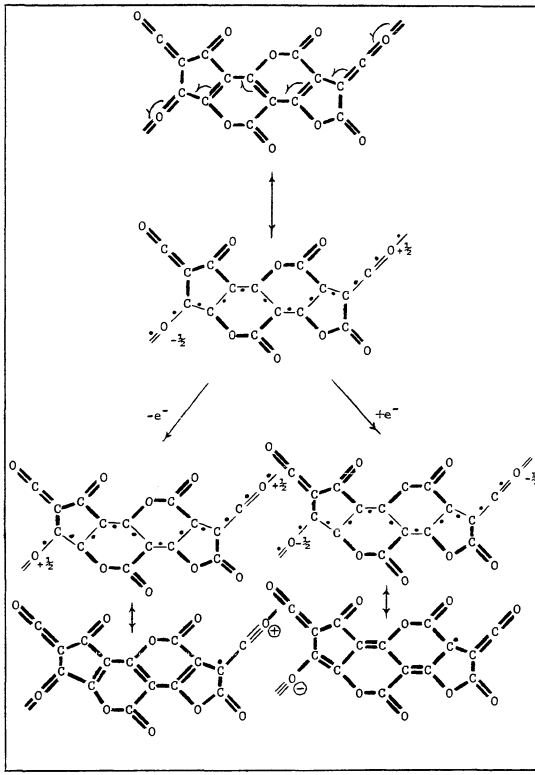

Figure 48. Proposed Linnett structures illustrating electron and charge delocalization for the poly(carbon suboxide) neutral molecule and radical ions.

Reproduced with permission of the copyright owner. Further reproduction prohibited without permission.

absence of an ESR triplet spectrum. The energy required for further complex ionization is greater than can be supplied thermally without disrupting the polymer structure as observed by the Curie law behavior. The energy can be supplied by irradiating with light. The photogenerated unpaired electrons may recouple immediately or be transferred to adjacent unionized polymer molecules to couple later with an unpaired electron on an oppositely charged molecule. This would be consistent with the indistinguishability of the photogenerated and residual unpaired electrons in the ESR spectrum, the square root dependence on the light intensity and the complicated decay kinetics.

In conclusion, it is proposed that the origin of the paramagnetism is an electron transfer between polymer structures stabilized by a planar polyene chain terminated by carbonyl and ketenyl functional groups.

2. POLYMERIZATION MECHANISM

In proposing a polymerization reaction path, the following experimental observations and results should be accounted for.

First, the polymerization does not occur in the gas phase and is preceded by an induction period.

Second, a polymer structure having 1,3 - 2,4 C_3O_2 repeat unit linkages and two ketenyl end groups as in Figure 47 should be the product.

Third, a termination step which can effectively compete with propagation is necessary to account for the low molecular weight.

Fourth, the rate determining step must be first order with respect to monomer and to polymer.

Fifth, the polymerization should be a non-free radical process.

Reproduced with permission of the copyright owner. Further reproduction prohibited without permission.

Sixth, the presence of an aldehyde or ketone should inhibit the formation of polymer.

Seventh, the polymerization procedes more rapidly in a more polar medium.

A zwitterionic mechanism taking these points into consideration is proposed in Figure 49. In the initial step, a C_3O_2 monomer is complexed in a bent conformation by a complexing agent, S. Bending at the central carbon atom has been found to be remarkably easy as indicated by an observed bending frequency of 63 cm^{-1} (58). Carbon 13 NMR has shown the central carbon atom to have a very high electron density (59). The molecule is also calculated to have high electron densities at the terminal oxygen and central carbon atoms (60) which could facilitate complexing in a bent conformation by attraction of S for the oxygen atoms and nucleophilic attack by the central carbon atom. The identity of S would initially be a site on the container surface or the polymer once an initial quantity has been formed. A monomer-polymer complex is supported by the observation that there is a significant attraction between monomer and polymer as reported in section III-5. A polymerization induction period and polymer formation on the vessel surface can be explained by a poor complexing ability of a surface site compared with the polymer. The complexation step is proposed to be the rate determining step and would account for the first order dependencies on monomer and polymer. Nucleophilic attack by the central atom of the complexed monomer is proposed to be the initiating step. The presence of an aldehyde or ketone carbonyl that could react with the complexed monomer to prevent polymer formation and prolong the induction period can account for their inhibiting effect. Once the two initiation steps are

Reproduced with permission of the copyright owner. Further reproduction prohibited without permission.

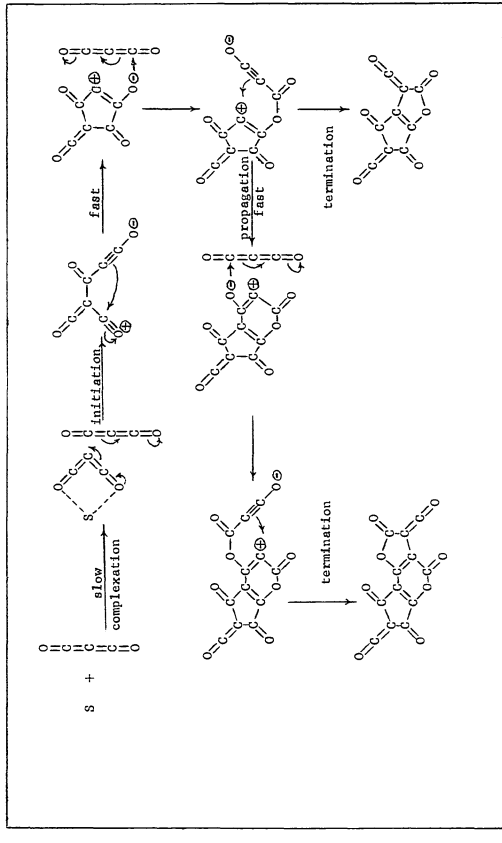

Figure 49. Zwitterionic mechanism for carbon suboxide polymerization.

Reproduced with permission of the copyright owner. Further reproduction prohibited without permission.

accomplished, propagation procedes rapidly by a 1,3-dipolar addition of the propagating end to the 2,4-positions of the monomer, and termination by a 1,3-dipolar addition to the 2,3-positions of the monomer as illustrated. This sequence leads to the polymer structure with the proposed end groups of the structure in Figure 47. The energy required to form a polarized initiating complex would be expected to be lowered by a polar environment and account for the polarity effect on the polymerization rate. A carbene resonance structure may be drawn for the propagating end, but the importance of its contribution is probably small since oxygen is reported to retard the rates of both triplet and singlet carbene reactions (61).

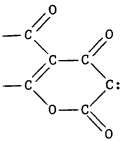

The propagation and termination may also be written as a concerted bond opening and ring closure rather than the two step process of Figure 49. The degree of polymerization result of between 5 and 6 would indicate that propagation and termination are quite competitive. A rough degree of polymerization calculation may be performed assuming propagation and termination to be equally probable. However, termination at the dimer or trimer stage would result in a four membered ring or two fused five membered rings respectively. The structures would be highly strained since all of the ring carbon atoms are sp^2 bonded, so termination is assumed to be non-competitive at these stages. The calculation is performed beginning at the tetramer stage according to:

Reproduced with permission of the copyright owner. Further reproduction prohibited without permission.

$$\overline{X}_n = \sum X_i N_i$$

where N_i is the number fraction and X_i is the degree of polymerization of that fraction.

X_i	N_i	$X_i N_i$
4	.500	2.00
5	.250	1.25
6	.125	.75
7	.062	.43
8	.031	.25
9	.015	.14
10	.007	.07
11	.003	.03
	$\overline{X}_n$ =	4.92

If the calculation is started at the pentamer stage, a result of $\overline{X}_n = 5.93$ is obtained.

The characteristics of this C_3O_2 polymerization are similar to those reported for the ketene thermopolymerization although no mechanism was proposed (62). In the ketene case, the following observations and results were reported. Polymerization does not occur in the gas phase but appears as brown spots on the vessel walls. It follows a bimolecular rate law with respect to ketene, and the rate increases with increasing solvent dielectric constant. The polymerization rate is independent of the presence of oxygen. The dimer of ketene has been determined to have a lactone structure (63). Carbenes are proposed to undergo a 1,3-dipolar addition with ketene from a zwitterionic resonance form (64).

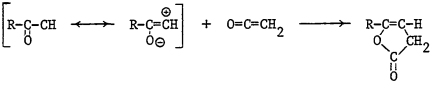

Reproduced with permission of the copyright owner. Further reproduction prohibited without permission.

This zwitterionic resonance form is very similar to that proposed for the C_3O_2 polymerization and attacks the ketene carbonyl from the negatively charged oxygen atom as well.

In conclusion, a zwitterionic dipolar addition mechanism is consistent with the experimental results and appears to be related to the mechanism for the addition of a keto-carbene to ketene.

Reproduced with permission of the copyright owner. Further reproduction prohibited without permission.

APPENDIX

Synthesis of Carbon Suboxide

The principal laboratory preparations of C_3O_2 are the dehydration of malonic acid (4) and the pyrolysis of diacetyltartaric anhydride (5). While other preparations have better yields, starting materials are not as easily obtained and apparatus is more complicated (12).

The dehydration of malonic acid was carried out in the apparatus pictured in Figure 50 as follows.

$$HOOC\text{-}CH_2\text{-}COOH \xrightarrow[140°C]{P_2O_5} O{=}C{=}C{=}C{=}O + H_2O + CH_3COOH + CO_2$$

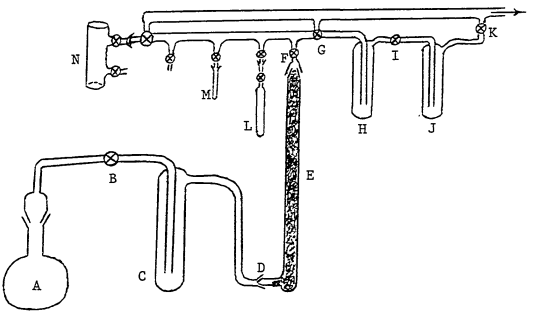

Figure 50. Vacuum system and malonic acid dehydration apparatus.

A 1 liter flask	E $CaCO_3$ column
B,F,G,I,K stopcocks	L storage vessel
C,H,J traps	M small holding vessel
D ∓10/30 joint	N 100 mm IR gas cell

Reproduced with permission of the copyright owner. Further reproduction prohibited without permission.

Flask A is filled with 40 g calcined sand, 20 g dried, ground malonic acid and 200 g phosphorous pentoxide. It is necessary to work rapidly with the P_2O_5 to keep moisture absorption at a minimum. The malonic acid is finely ground with a mortar and pestle to insure intimate mixing with the P_2O_5. The flask is tightly stoppered and shaken vigorously for 5 minutes. It is then connected to the trap and vacuum line, pumped out and allowed to stand overnight with stopcock B closed. The system is then reevacuated, stopcock B opened, trap C cooled with liquid nitrogen and flask A is heated to 140°C. with an oil bath. After 1 to 1-1/2 hour, when the reactant mixture has turned dark brown, the oil bath is removed, stopcocks B and K are closed and the liquid nitrogen is removed from trap C and used to cool trap J. As trap C warms to room temperature, CO_2 and C_3O_2 are transferred through calcium carbonate column E to trap J. When the frost has melted on trap C, stopcock F is closed, trap C and flask A are removed from the system at joint D and allowed to vent in a hood. Stopcocks I and K are opened and traps H and J are evacuated. Stopcocks G and K are then closed and liquid nitrogen is transferred to cooling trap H while trap J is cooled with a carbon disulfide slush bath (-110°C.). The bulk of the CO_2, which has a vapor pressure 33 mm at -110°C., is transferred to trap H while C_3O_2, which has a vapor pressure of ~ 0.1 mm at -110°C., is retained in trap J. When nearly all of the solid white CO_2 is no longer visible in trap J, stopcock I is closed and the CO_2 in trap H is transferred to vessel L which is removed from the system and vented in a hood. The CO_2 transfer takes 4 to 5 hours and minimizes C_3O_2 loss while removing the bulk of the CO_2. The crude C_3O_2 (~ 1.5 ml, 13% yield) may now be packed in a dry ice bath prior to subsequent purification by distillation.

Reproduced with permission of the copyright owner. Further reproduction prohibited without permission.

To obtain C_3O_2 by pyrolyzing diacetyltartaric anhydride, it is first necessary to obtain the anhydride by acetylating and dehydrating tartaric acid.

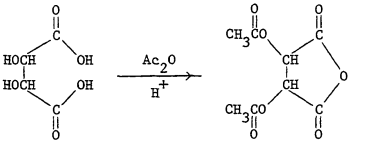

To a 2 l erlenmeyer are added 500 g tartaric acid and 1100 ml acetic anhydride. The mixture is heated to 50°C., and 1.5 ml conc. H_2SO_4 is a added. The tartaric acid rapidly dissolves, and temperature rises to 120°C. After an hour the diacetyltartaric anhydride begins to precipitate as crystalline needles. After standing over night the flask is cooled in an ice bath, filtered and washed with benzene until the wash is clear and free of acetic acid odor. The crystalline diacetyltartaric anhydride is dried in a vacuum oven at 60°C. until weight loss is negligible (yield 585 g, 81%, MP 132°C.).

The diacetyltartaric anhydride is pyrolyzed in apparatus illustrated in Figure 51 which is nearly identical to that of Hegar (5).

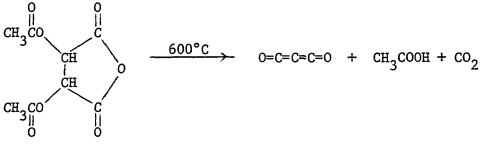

The mercury level in reservoir D is adjusted to just above the lower edge of the heated area, and reservoir D is preheated to 140-150°C. Through a wide stem funnel, 150 g molten diacetyltartaric anhydride is added to reservoir D. Mercury is allowed to pass through capillary B at

Reproduced with permission of the copyright owner. Further reproduction prohibited without permission.

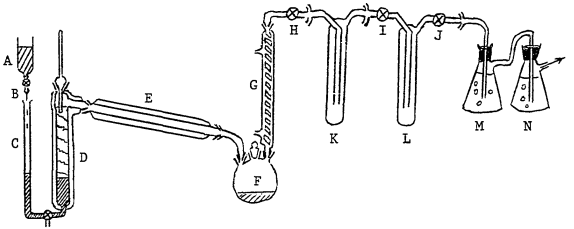

Figure 51. Diacetyltartaric anhydride pyrolysis apparatus.

A mercury reservoir	F trap flask
B capilliary	G Graham condenser
C mercury counter column	H,I,J stopcocks
D anhydride reservoir	K,L traps
E pyrolysis tube	M,N analine solution traps

a rate such that its level in C rises about 1 cm per 3 minutes. The molten anhydride is gradually passed through the side arm of the anhydride reservoir to pyrolysis tube E which is heated to 575-600°C. The pyrolysis tube consists of a 60 cm length of 25 mm ID Corning Vicor glass tube of which 40 cm is wrapped with a Cole-Palmer electrical heating tape and covered with asbestos cloth. Temperature is monitored with iron-constantan thermocouples. The pyrolysis products pass through a trap flask and a Graham condenser of 50 cm jacket length which condenses the acetic acid. The C_3O_2 is condensed in traps K and L which are cooled to -78°C. with dry ice baths. Carbon dioxide and any escaping C_3O_2 are passed through DMF solutions of aniline to extinguish the C_3O_2. When nearly all of the anhydride has passed from the reservoir, the mercury level is dropped, the heat to the pyrolysis tube is shut off and stopcocks H and J are closed. The dry ice bath is removed from trap K, and the C_3O_2 distills to trap L leaving a dark

Reproduced with permission of the copyright owner. Further reproduction prohibited without permission.

brown liquid residue of about 1-2 ml in trap K. The crude C_3O_2 in trap L has a light brown tinge and a volume of about 15 ml (35% yield). Stopcock I is closed, trap L is removed and connected to the vacuum system in Figure 50. The trap is immersed in a carbon tetrachloride slush bath (-23°C.), and about 80% of the C_3O_2 is rapidly distilled to a storage vessel or to trap J for subsequent purification.

Purification of Carbon Suboxide

Depending on the synthetic method, there is a marked difference in the stability toward polymerization. The crude C_3O_2 derived from diacetyltartaric anhydride may be stored for at least several weeks in a freezer (-16°C.) with only a faint yellow color developing. That derived from malonic acid will have undergone a large conversion to polymer after just a few days storage in the freezer, but will remain colorless for several weeks in a dry ice bath. The malonic acid derived C_3O_2 becomes more stable with purification, and trace quantities of P_2O_5 particles, acetic acid, water and other proton releasing and nucleophilic substances have been proposed as sources of the instability (10,12,65). While the diacetyltartaric anhydride derived C_3O_2 is generally acknowledged to be less pure (1,65,66), the greater stability is unexplained.

Purification is performed by vacuum distillation at 10^{-5} mm Hg between traps J and H in Figure 50 where trap J is maintained at -110°C and trap H at -195°C. Purity was monitored by taking infrared spectra of successive 0.1 ml fractions. Spectra of each fraction's vapor at pressures corresponding to -23°C. were obtained using a 100 mm NaCl Perkin-Elmer gas cell on a Beckman IR 8 spectrophotometer. IR spectra of selected fractions prepared from both methods are presented in Figures 52 and 53.

Reproduced with permission of the copyright owner. Further reproduction prohibited without permission.

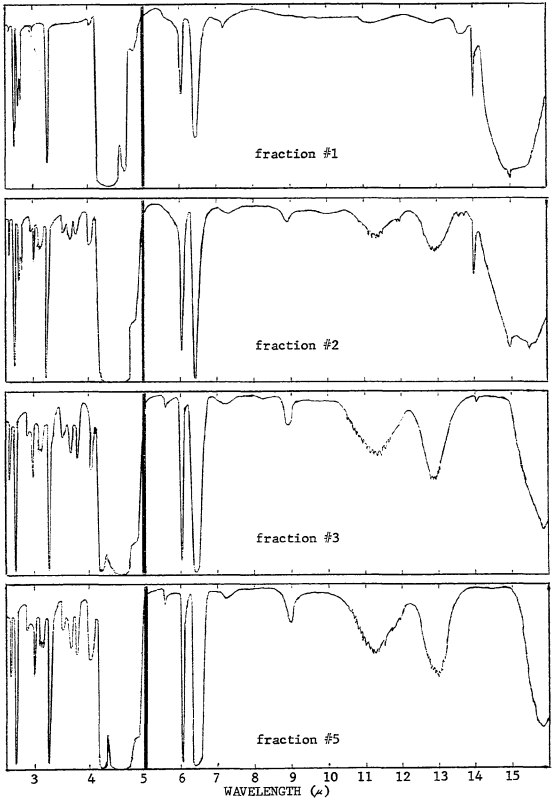

Figure 52. Infrared spectra of malonic acid derived carbon suboxide.

Reproduced with permission of the copyright owner. Further reproduction prohibited without permission.

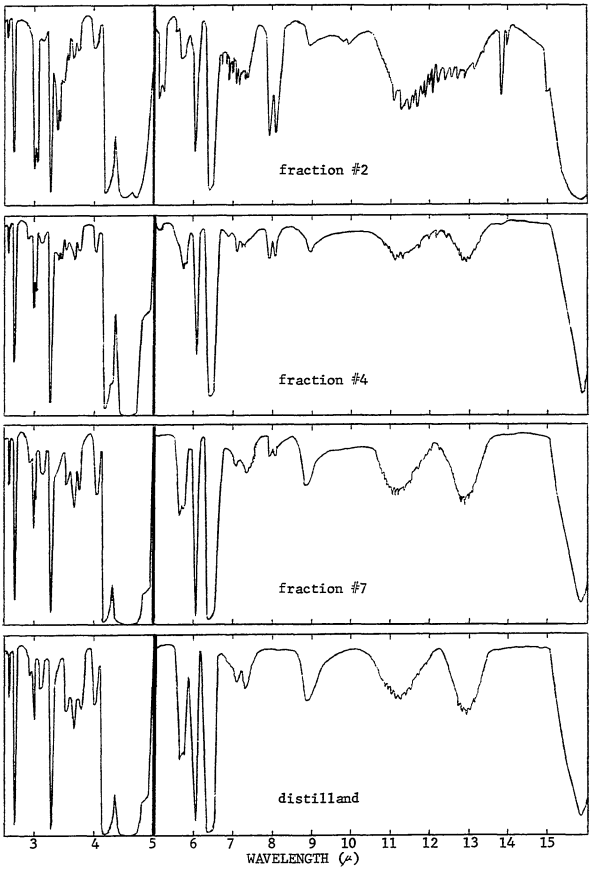

Figure 53. Infrared spectra of diacetyltartaric anhydride derived C_3O_2.

Reproduced with permission of the copyright owner. Further reproduction prohibited without permission.

The only impurity observed in the IR spectra of the C_3O_2 obtained from malonic acid (Figure 52) was carbon dioxide as comparison with a spectrum of CO_2 (Figure 54-a) shows. The best band to follow the CO_2 depletion is the sharp one occurring at 14 μ as C_3O_2 is the most transparent at this wavelength. After this band had disappeared completely and one additional fraction had been distilled and discarded, about 90% of the remaining C_3O_2 was distilled at -110°C. and transferred to storage vessel L. This storage vessel should be scrupulously cleaned and dried by flamming out under vacuum. The spectrum of this C_3O_2 distillate (Figure 52-bottom) could be matched band for band with that obtained by Long, Merfin and Williams (65) with the exception of a weak band at 5.5 μ. This band was later attributed to C_3O_2 by Smith and Leroi (58). The weak band at 7.3 μ is a cell absorption. There was no trace of acetic acid bands (Figure 54-b) in the distillate, however, if the remaining 10% residue is allowed to warm to room temperature, acetic acid bands are observed in its spectrum.

There are many impurity bands observed in the spectra of early fractions of the C_3O_2 obtained from diacetyltartaric anhydride pyrolysis (Figure 53). The most frequently mentioned impurity by-product of this synthesis is ketene (1,65,66) based on a band at 5.2 μ. Comparing the spectrum of ketene (Figure 54-C (67)) with the spectra in Figure 53, this appears to be questionable since ketene has stronger bands at 7.2 and 8.8 μ which are not proportionately as strong in the C_3O_2 spectrum. Sharp bands at 3.05, 3.4 and 13.8 μ as well as the jagged fine structure between 11 and 13 μ appear to decrease proportionately with the 5.2 μ band and are similar in shape to the ketene spectrum. The doublet band at 8.0 μ decreases more slowly and is of

Reproduced with permission of the copyright owner. Further reproduction prohibited without permission.

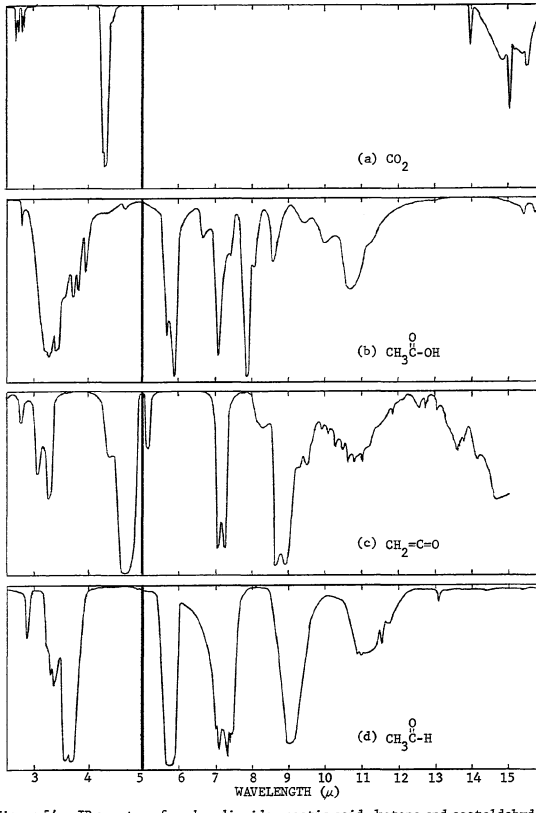

Figure 54. IR spectra of carbon dioxide, acetic acid, ketene and acetaldehyde.

Reproduced with permission of the copyright owner. Further reproduction prohibited without permission.

unknown origin. Bands at 14 and 15 μ correspond to CO_2. Increasing bands of a less volatile impurity at 5.75, 7.2 and 9.0 μ correspond well with those of acetaldehyde (Figure 54-d) which has a boiling point only 13°C. above that of C_3O_2. The symmetry of the three C_3O_2 bands near 3.7 μ is different from that of the more pure malonic acid derived C_3O_2 and can be accounted for by an overlapping with an acetaldehyde absorption at 3.6 μ.

In summary, the malonic acid preparation has the advantage that the C_3O_2 can be distilled to good purity but the disadvantage that large quantities of P_2O_5 are required, the yield is very low, and the crude product's stability toward polymerization is poor. The diacetyltartaric anhydride pyrolytic method has the advantage that a much larger quantity of C_3O_2 can be obtained in a shorter time, and the crude product is much more stable. Its disadvantage is that good purity cannot be readily obtained by distillation. For physical chemical studies requiring high C_3O_2 purity, the best synthesis is the malonic acid route, while for synthesis, where quantity is more important than purity, the pyrolytic method is best.

Physical Properties of Carbon Suboxide

Carbon suboxide is a gas at room temperature with the following physical data (68-70).

Melting point = -112°C.
Boiling point = 6.8°C.
Vapor pressure = 587 - 589 mm Hg at 0°C.
Density = 1.114 g/cm^3 at 0°C.
Refractive index n_D^0 = 1.45538 at 0°C.
Carbon-carbon bond length = 1.28 Å
Carbon-oxygen bond length = 1.16 Å

Reproduced with permission of the copyright owner. Further reproduction prohibited without permission.

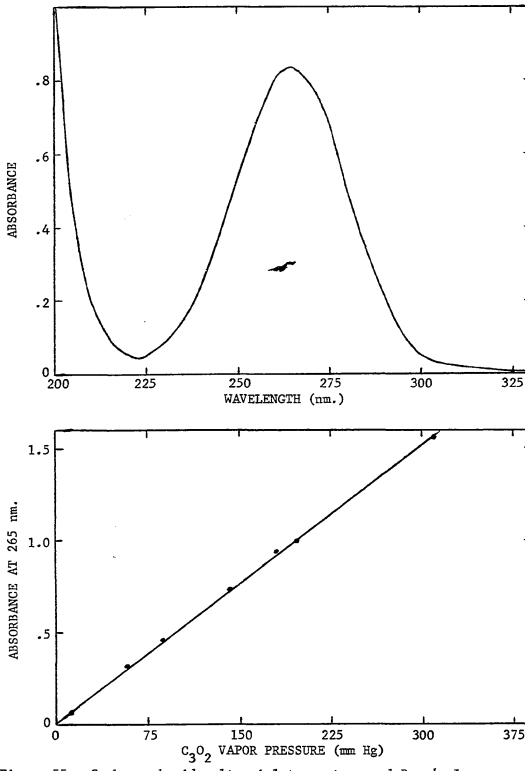

Figure 55. Carbon suboxide ultraviolet spectrum and Beer's Law dependence at 265 nm.

Reproduced with permission of the copyright owner. Further reproduction prohibited without permission.

Carbon suboxide has a weak absorption in the ultraviolet at 265 nm (Figure 55) which is particularly convenient for monitoring C_3O_2 concentrations in the gas phase. A molar extinction coefficient of 93 liter/(mole cm) was determined from vapor pressure and 265 nm absorbance measurements assuming ideal gas behavior. This is in good agreement with ε_{max} = 94 liter/mole cm reported by Bayes (71).

Reproduced with permission of the copyright owner. Further reproduction prohibited without permission.

IX. REFERENCES

1. R.N. Smith, D.A. Young, E.N. Smith and C.C. Carter, Inorg. Chem. 2, 829 (1963).
2. A.R. Blake, W.T. Eeles and P.P. Jennings, Trans. Faraday Soc. 60, 691 (1964).
3. O. Diels and B. Wolf, Ber. 39, 689 (1906).
4. G. Brauer, "Handbook of Preparative Inorganic Chemistry," Second edition, p. 648, Academic Press, N.Y. (1963).
5. G. Hegar, "Beitrag zur Chemie des Kohlensuboxides," Ph.D. thesis, Zurich (1961).
6. A. Klemenc, R. Wechsberg and G. Wagner, Monatsh. Chem. 66, 337 (1935).
7. O. Diels, R. Beckman and C. Tonnies, Ann. Chem. 439, 76 (1924); O. Diels, Z. Angew. Chem. 39, 1025 (1926).
8. W. Reid and H. Mengler, Ann. Chem. 678, 113 (1964).
9. V.L. Schmidt, H.P. Boehm and U. Hofmann, Z. annorg. allgem. Chem. 282, 16 (1955); V.L. Schmidt, H.P. Boehm and U. Hofmann, "Proc. Third Carbon Conf.," p. 235, Pergamon Press, London (1959).
10. E. Ziegler, H. Junek and H. Bieman, Monatsh. Chem. 92, 927 (1961); H. Sterk, P. Tritthart and E. Ziegler, Monatsh. Chem. 101, 1851 (1970).
11. R.N. Jones, C.L. Angell, T. Ito and R.J.D. Smith, Canadian J. Chem. 37, 2007 (1959).
12. T. Kappe and E. Ziegler, Angew. Chem. (International edition) 13, 491 (1974).
13. T. Money, Chem. Rev. 70, 553 (1970).
14. R.N. Smith, Trans. Faraday Soc. 62, 1881 (1966).
15. A.R. Blake, J. Chem. Soc. 3866 (1965).

Reproduced with permission of the copyright owner. Further reproduction prohibited without permission.

16. T. Kunitake and S. Murakami, J. Poly. Sci. 12, 67 (1974).

17. E.G. Janzen, Accounts Chem. Res. 4, 31 (1971).

18. S.J. Wyard, J. Sci. Instr. 42, 769 (1965).

19. C.P. Pool, "Electron Paramagnetic Resonance," p. 806, Interscience Publishers, New York (1967).

20. C.P. Pool, "Electron Paramagnetic Resonance," pp. 129 and 716, Interscience Publishers, New York (1967).

21. C.P. Pool, "Electron Paramagnetic Resonance," pp. 706-709, Interscience Publishers, New York 1967; C.P. Pool and H.A. Farach, "Relaxation in Magnetic Resonance," p. 20, Academic Press, New York (1971).

22. T.G. Castner, Phys. Rev. 115, 1506 (1959).

23. N. Bloembergen, E.M. Purcell and R.V. Pound, Phys. Rev. 73, 679 (1948); L.S. Singer, W.J. Spry and W.H. Smith, "Proc. Third Carbon Conf.," pp. 121-128, Pergamon Press, London (1959).

24. N. Bloembergen and S. Wang, Phys. Rev. 93, 72 (1954).

25. J.P. Lloyd and G.E. Pake, Phys. Rev. 92, 1576 (1953).

26. M. Bersohn and J.L. Baird, "An Introduction to Electron Paramagnetic Resonance," pp. 69-70, W.A. Benjamin, Inc., New York (1966).

27. D.C. Reitz, F. Dravnicks and J.E. Wertz, J. Chem. Phys. 33, 1880 (1960).

28. M.S. Blois, "Free Radicals in Biological Systems," p. 117, Academic Press, New York (1961).

29. G. Vinco and D.C. Fraenkel, J. Chem. Phys. 34, 1333 (1961).

30. L.S. Singer, "Proc. Fifth Carbon Conf.," pp. 37-64, Pergamon Press (1962).

Reproduced with permission of the copyright owner. Further reproduction prohibited without permission.

31. G.M. Holob, P. Ehrlich and R.R. Allendoerfer, Macromolecules 5, 569 (1972); L.S. Singer, W.J. Spry and W.H. Smith, "Proc. Third Carbon Conf.," pp. 121-128, Pergamon Press, London (1959).

32. D. Bijl, H. Kainer and A.C. Rose-Innes, J. Chem. Phys. 35, 765 (1959).

33. D.B. Chesnut and W.D. Phillips, J. Chem. Phys. 35, 1002 (1961).

34. B.M. Hoffman and R.C. Hughes, J. Chem. Phys. 52, 4011 (1970).

35. J.W. Eastman, G.M. Androes and M. Calvin, J. Chem. Phys. 36, 1197 (1962).

36. L.S. Singer and J. Kommandeur, J. Chem. Phys. 34, 133 (1961).

37. G. Wagoner, "Proc. Fourth Carbon Conf.," pp. 197-206, Pergamon Press (1961); L.S. Singer and G. Wagoner, "Proc. Fifth Carbon Conf.," pp. 65-71, Pergamon Press, London (1962).

38. Iscotables - "Handbook of Data for Biological and Physical Scientists," fifth edition, p. 43 (1975).

39. P.B. Ayscough, "Electron Spin Resonance in Chemistry," pp. 401-422, Methuen, London (1967).

40. R.N. Lacey, "The Chemistry of Alkenes," S. Patai editor, Chapter 14, Interscience Pub., New York (1964).

41. G.S. Ross and A.R. Glasgow, Analytical Chem. 36, 700 (1964).

42. J.S. Fritz, "Acid-Base Titrations in Nonaqueous Solvents," p. 33, Allyn and Bacon Inc., Boston (1973).

43. J. March, "Advanced Organic Chemistry: Reactions, Mechanisms and Structure," pp. 477-478, McGraw-Hill, New York (1968).

44. A.R. Blake and A.F. Hyde, Trans. Faraday Soc. 60, 1775 (1964).

45. R.M. Silverstein and G.C. Bassler, "Spectroscopic Identification of Organic Compounds," second edition, p. 90, J.Wiley & Son, New York (1967).

Reproduced with permission of the copyright owner. Further reproduction prohibited without permission.

46. R. Marvodineanu, J.I. Schultz and O. Menis, "Accuracy in Spectrophotometry and Luminescence Measurements," pp. 104-105, NBS Special Publication 378 (1973).

47. R.M. Silverstein and G.C. Bassler, "Spectroscopic Identification of Organic Compounds," second edition, p. 152, J. Wiley & Son, New York (1967).

48. C.A. Parker, "Photoluminescence of Solutions," p. 472, Elsevier Pub. Co., New York (1968).

49. C.A. Parker, "Photoluminescence of Solutions," p. 262, Elsevier Pub. Co., New York (1968).

50. C.A. Parker, "Photoluminescence of Solutions," p. 430, Elsevier Pub. Co., New York (1968).

51. D.M. Hercules, "Fluorescence and Phosphorescence Analysis," p. 85, Interscience Publishers, Inc., New York (1966).

52. unpublished data.

53. D.M. Hercules, "Fluorescence and Phosphorescence Analysis," p. 89, Interscience Publishers, Inc., New York (1966).

54. K.J. Liska and L. Salerni, J. Org. Chem. 25, 124 (1960).

55. D.R. Kearns and M. Calvin, J. Am. Chem. Soc. 83, 2110 (1961).

56. C.L. Angyal, G.A. Barclay, A.A. Hurkins and R.J.W. LeFevre, J. Chem. Soc. 2583 (1951); K. Ingold, Chem. Rev. 15, 552 (1947).

57. J.W. Linnett, "The Electronic Structure of Molecules," J. Wiley & Son, Inc., New York (1966).

58. W.H. Smith and G.E. Leroi, J. Chem. Phys. 45, 1767 (1966).

59. E.A. Williams, J.D. Cargiola and A. Ewo, Chem. Comm. 366 (1975).

60. J.F. Olsen and L. Burnelle, J. Phys. Chem. 73, 2298 (1967); J.R. Sabin and H. Kim, J. Chem. Phys. 56, 2195 (1972).

Reproduced with permission of the copyright owner. Further reproduction prohibited without permission.

61. R.A. Moss and M. Jones, "Carbenes," Vol. 2, p. 319, J. Wiley & Son, Inc., New York (1975).

62. F.O. Rice and J. Greenberg, J. Am. Chem. Sco. 56, 2132 (1934).

63. R.N. Lacey, Advan. Org. Chem. 2, 213 (1960).

64. J. March, "Advanced Organic Chemistry: Reactions, Mechanisms and Structure," p. 625, McGraw Hill, New York (1968).

65. D.A. Long, F.S. Murfin and R.L. Williams, Proc. Roy. Soc. 223, 25 (1954).

66. B.D. Kybett, G.K. Johnson, C.K. Barker and J. Margrave, J. Phys. Chem. 69, 3603 (1965).

67. W.H. Harp and R.S. Rasmussen, J. Chem. Phys. 15, 778 (1947).

68. L.B. Dashkevich and V.G. Berlin, Russian Chemical Review 36, 391 (1967).

69. L.A. MacDougall and J.E. Kilpatrick, J. Chem. Phys. 42, 2311 (1965).

70. R.L. Livingston and C.N.R. Rao, J. Am. Chem. Soc. 81, 285 (1959).

71. K.D. Bayes, J. Am. Chem. Soc. 84, 4077 (1962).

Reproduced with permission of the copyright owner. Further reproduction prohibited without permission.

Research Proposal

Synthetic Control of Polyynes Produced by Oxidative Coupling of Diynes

Submitted by Arthur Snow

August 1, 1974

A proposition submitted to the Graduate Faculty in Chemistry in partial fulfillment of the requirements for the degree of Doctor of Philosophy, The City University of New York

Reproduced with permission of the copyright owner. Further reproduction prohibited without permission.

ABSTRACT

Terminal diynes can be polymerized into a linear polyyne in the presence of a copper-amine catalyst.

$$n\ H\text{-}C{\equiv}C\text{-}R\text{-}C{\equiv}C\text{-}H \xrightarrow{Cu\ amine} H\{C{\equiv}C\text{-}R\text{-}C{\equiv}C\}H + (2n-2)\ H^{+}$$

Two aspects of this polymerization to be explored from a synthetic control angle are the absence of a stoichiometric restriction and the high sensitivity of the reactivity of the terminal triple bond to the identity of R. The lack of a stoichiometric restriction in comparison with conventional step polymerizations will not alter the relation between the degree of polymerization and extent of reaction, but will affect molecular weight control by addition of monofunctional species and the gel point when a multifunctional species is added. The sensitivity of the terminal triple bond to R will be reflected in the degree of blocking of two comonomers in a copolymerization, the degree of which is determined by the relative reactivities of the two differently affected triple bonds. Block lengths within the copolymer are calculated by assuming the copolymerization to pass through three stages; (1) self-coupling of the more reactive triple bonds, (2) cross-coupling between the more reactive and less reactive triple bonds, and (3) self-coupling between the less reactive triple bonds. The possibility of an azeotrope exists when both relative reactivities are less than one.

Reproduced with permission of the copyright owner. Further reproduction prohibited without permission.

PROPOSAL

Introduction:

Molecules possessing two terminal triple bonds will couple in the presence of an amine complexed cupric ion or cuprous ion plus oxidizing agent to yield a linear polyyne.

$$n\ H\text{-}C{\equiv}C\text{-}R\text{-}C{\equiv}C\text{-}H \xrightarrow[\text{or } Cu^{+}/O_2 \text{ amine}]{Cu^{2+} \text{ amine}} H\text{-}\left[C{\equiv}C\text{-}R\text{-}C{\equiv}C\right]_n\text{-}H + (2n-2)H^{+}$$

It is somewhat puzzling that this reaction has been employed in only a scant few polymerizations [R = p,mC_6H_4, -C≡C-, -Hg-, -$Si(C_2H_5)_2$-, -$As(C_6H_5)$-, (1); R = 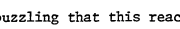 (2); R = $\{CH_2\}_n$, n = 3,4,5 (3); R = $-CH_2O-R'-OCH_2-$, R' = 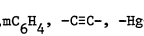 , 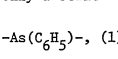 , 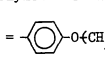 , 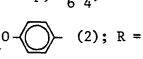 , 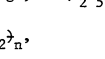 , 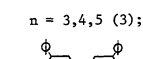 (4); R = 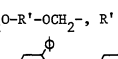 (5); R = 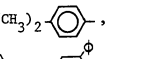 (6)]

as the reaction has been known for over a century (7), and practically quantitative yields can be obtained fulfilling the requirement for production of high polymer (8). The polyyne structure, which consists of two adjacent triple bonds at regular intervals within the polymer chain presents interesting and unique possibilities. From such a structure, one might expect the adjacent triple bonds to act as rigid segments within the chain and result in a poorly soluble, brittle material. Low solubility, probably caused by reduced conformational freedom, has been observed with several structures (1,9). However, the triple bond has been found to be less rigid than a double bond which in turn is found to be less rigid than a single bond as evident from the

Reproduced with permission of the copyright owner. Further reproduction prohibited without permission.

bending force constants obtained from IR spectra (10). It has been rationalized that the important factor is the crowding of substituents attached to the deforming bond (11). Thus, with this chain flexibility one might expect a low Tg and a soft or rubbery material, if crystallinity is low. Surprisingly, the crystallinity of poly (metadiethynylbenzene) has been observed to be as high as 90 per cent (12). Such a high crystallinity may lead to interesting solid-state, photolyzed, crosslinking reactions since conjugated diynes are quite photolabile and produce highly colored polymeric products (13,14,15).

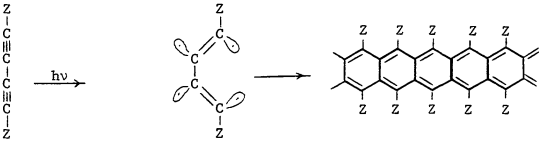

Another possibility is that of hydrogenating the triple bonds to study the effect of various structures incorporated into a polyethylene chain. Coupled alkynes have been observed to add 3 moles of hydrogen rapidly and a fourth mole slowly. The identity of the structure, R, between the triple bonds should be quite variable as the coupling reaction has been found to be insensitive to most functional groups including aliphatic and aromatic hydrocarbons, heterocyclic derivatives, eneynes, alcohols, ethers, ketones, acids, esters, amines, nitriles, thio and silicon derivatives and organo-metalic bonds. Copolymerization adds even another dimension to the possibilities.

To study such possibilities it would be of great importance to have synthetic control over the molecular weight. This involves knowledge of the acetylenic coupling mechanism. Two important steps within the mechanism are believed to be the dissociation of an acetylenic hydrogen

Reproduced with permission of the copyright owner. Further reproduction prohibited without permission.

(with or without cuprous ion assistance) and the collapse of a dimeric cupric complex to yield the diyne.

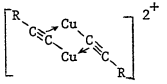

$$\longrightarrow \quad R\text{-}C{\equiv}C\text{-}C{\equiv}C\text{-}R \; + \; 2\ Cu^{+}$$

For a discussion of evidence and various proposed mechanisms see appendix I. Though the importance of the two steps is dependent on reaction conditions, an experiment, yet to be performed, that may determine the relative importance of the two steps would be the observation of an isotopic effect with R-C≡C-D. The lack of an isotopic effect would indicate that the rate determining step occurs prior to dissociation of the acetylenic hydrogen.

Since the polymerization involves stepwise coupling between terminal alkyne functional groups, this polymerization may be referred to as an A-A step polymerization where A represents a terminal triple bond. This step polymerization differs from the more common A-B and A-A + B-B polymerizations in that like functional groups react to form polymer instead of different functional groups reacting. In other words there is no A-B stoichiometric restriction to attain polymer in this A-A system.

It has been noted in the mechanism (Appendix I) that coupling reactivity of a terminal alkyne group is strongly dependent on how the remainder of the molecule perturbs the electronic structure of the terminal triple bond as well as on reaction conditions. Thus in a copolymerization system, there should be a more reactive monomer, M_1, and a less reactive one, M_2, and the greater the reactivity difference between the two, the longer should be the block sequences in the copolymer.

Reproduced with permission of the copyright owner. Further reproduction prohibited without permission.

The proposed work is three fold; (I) to attempt to observe a hydrogen-deuterium isotope effect for a dimeric coupling and a polymeric coupling employing Hay's polymeric coupling conditions (8,9); (II) to develop and test step polymerization equations relating (i) number and weight average degrees of polymerization to extent of conversion, (ii) degree of polymerization to amount of monofunctional reagent added, and (iii) gel point to amount of multifunctional reagent (f>2) added, and (III) to develop and test copolymerization parameters and equations for the relative reactivities and block lengths of the two monomers.

I. Mechanism:

A consideration of the overall reaction for the coupling of two alkynes with oxygen as oxidizing agent (8)

$$2\ R\text{-}C{\equiv}C\text{-}H\ +\ \tfrac{1}{2}O_2 \longrightarrow R\text{-}C{=}C\text{-}C{\equiv}C\text{-}R\ +\ H_2O$$

which is a summation of

$$2\ R\text{-}C{\equiv}C\text{-}H\ +\ 2\ Cu^{2+} \longrightarrow R\text{-}C{\equiv}C\text{-}C{\equiv}C\text{-}R\ +\ 2H^{+}\ +\ 2Cu^{+}$$

$$2\ Cu^{+}\ +\ \tfrac{1}{2}O_2\ +\ H_2O \longrightarrow 2Cu^{2+}\ +\ 2OH^{-}$$

shows that somewhere in the reaction's path a C-H bond must be broken. A discussion of the reaction mechanism (Appendix I) indicates the C-H bond breaking may be an important step. If the rate determining step occurs before the carbon-hydrogen bond breaking, then substitution of deuterium for hydrogen should result in no lowering of the reaction rate.

Reaction conditions (complexing amine, oxidizing agent, solvent, pH) for this experiment would be the same as those employed for a polymerization. Hay has demonstrated that a copper(I)-N,N,N',N'-tetramethylethylene diamine-oxygen system in neutral solvent promotes much more rapid coupling than other popular coupling systems.

Reproduced with permission of the copyright owner. Further reproduction prohibited without permission.

Comparative Half Reaction Times of Three Copper Catalyzed Acetylenic Oxidative Coupling Systems (8)

Cu ($M \times 10^{-3}$)	R-C≡C-H*	A#	B#	C#
5	phenylacetylene	270	96	10
15	1-ethynylcyclohexanol	420	360	13
60	1-hexyne	550	950	55

* R-C≡C-H = 0.4 M. in all cases
\# Half reaction time in minutes
A Cu(II) acetate/pyridine
B Cu(I) chloride-oxygen/pyridine
C Cu(I) chloride-N,N,N',N'-tetramethylethylene diamine-oxygen/2-propanol

Hay's system has also been employed in the successful polymerization of several monomers (1,3,4,9). The reaction may be followed by oxygen uptake or spectrophotometrically (In the UV region for -C≡C-C≡C-, λ_{max} = 227 nm. and ε_{max} = 360 (16). In the IR region the stretching of ≡C-H and ≡C-D occur at 3333-3267 $cm.^{-1}$ and 2400 $cm.^{-1}$ respectively (16). Phenylacetylene and m-diethynylbenzene would be the alkynes chosen for the experiment since coupling work previously done on these two molecules shows them to be highly reactive and phenylacetylene is commercially available while m-diethynylbenzene may be synthesized conveniently from m-divinylbenzene (17).

II. Homopolymerization:

Equations presented here are derived in appendix II.

In choosing a monomer one should be selected which will produce a reasonably soluble polymer in order to maintain a homogeneous system and to easily determine molecular size. Monomers of the type H-C≡C-R-C≡C-H where R = $(CH_2)_n$ n = 3,4,5 have been polymerized (3), but details of polymer solubility and size are not given. Hay's comparative half reaction times show when R = alkane, the reaction is relatively sluggish. In cases where R is a rigid group such as m,p, or o-C_6H_4, -$Si(\phi)_2$-, or

Reproduced with permission of the copyright owner. Further reproduction prohibited without permission.

-C≡C-, the resulting polymers are poorly soluble or insoluble (1). Soluble polymers of reasonable molecular weight (>18,000) have been obtained when the ether group is incorporated into R (2,4). Thus, a logical monomer choice would be one containing an ether group with enough insulation to prevent one functional group from affecting the reactivity of another. The monomer should also be relatively uncomplicated to synthesize, if not commercially available. Such choices are

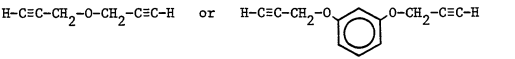

For the aromatic choice, Hay has shown similar compounds can be synthesized from propargyl bromide and resorcinol or bisphenols (4).

i. Degree of polymerization:

Following Flory's derivations for the number and weight average degrees of polymerization (18), their dependences on the extent of reaction (p = number of linkages formed/total pairs of functional groups) for this A-A system should be the same as for the A-B or the A-A + A-B systems in spite of the absence of the A-B strochiometric restriction.

$$\bar{X}n = \frac{1}{1-p} \qquad \bar{X}w = \frac{1+p}{1-p} \qquad \frac{\bar{X}w}{\bar{X}n} = 1 + p$$

Using Hay's coupling reaction conditions, the coupling rate has been demonstrated to be second order with respect to alkyne. Letting A represent the terminal triple bond concentration, the derived relation between the number average degree of polymerization and reaction time is

$$\bar{X}n = k'A^{o}t + 1 \qquad A = A^{o} \text{ at } t = 0$$

A plot of $\bar{X}n$ vs. t should be linear with slope of $k'A^{o}$.

Reproduced with permission of the copyright owner. Further reproduction prohibited without permission.

ii. Molecular weight control by addition of monofunctional reagent:

The equations for $\bar{X}n$ and $\bar{X}w$ are the same as for the A-B and A-A + B-B systems except for the stoichiometric ratio, r.

$$\bar{X}n = \frac{r + 1}{r + 1 - 2rp'} \qquad \bar{X}w = \frac{r + 1 + 2rp'}{r - 1 - 2rp'} \qquad r = \frac{A^o}{A^o + A^o u} \qquad p' = \frac{2(A^o - A)}{2A^o + A^o u}$$

$A^o u$ = concentration of monofunctional reagent.

Addition of Ch_3-O-CH_2-C≡C-H to the H-C≡C-CH_2-O-CH_2-C≡C-H system or m-CH_3-O-C_6H_4-O-CH_2-C≡C-H to the m-H-C≡C-CH_2-O-C_6H_4-O-CH_2-C≡C-H system with measurement of $\bar{X}n$ and $\bar{X}w$ would test these equations.

A very similar experiment has been performed by Hay (1) with an m-diethynyl-benzene-phenylacetylene system. His results were as follows:

$C_6H_5C{\equiv}CH$ (mole %)	[η](dl/g)	MW calculated by Hay	MW from above equation with p=1
25	0.12	1200	868
11	0.16	2480	2130
5	0.22	5080	4840
2.5	0.27	10200	9800
1.25	0.29	20000	19700

Hay admits his calculated molecular weights do not match the intrinsic viscosities (Where $\bar{M}n$ can be determined by IR absorption of ≡C-H stretching, the correlation between [η] and Mn is [η] = .19, Mn = 8700; [η] = .35, Mn = 12400; [η] = .41, Mn = 30000). Hay does not present his method of calculation. Foreseeable complications are precipitation of the polymer as it is formed and the non-equivalency of a meta diethynylbenzene alkyne group with a phenylacetylene triple bond.

iii. Gel point:

When a reagent with functionality greater than two is added to an A-A system, the Carothers equation (19) predicts the same gel point, Pc, as in an A-A + B-B + A-A system while the statistical approach (18) predicts an earlier one.

Reproduced with permission of the copyright owner. Further reproduction prohibited without permission.

The equations for the Carothers gel point are

$$P_c = \frac{2}{favg} \qquad favg = \frac{\Sigma M_i f_i}{\Sigma M_i}$$

The statistical equations are

$$\alpha = \sum_{n=o}^{\infty} (P\rho)((1-\rho)P)^n = \frac{P\rho}{1-(1-\rho)P} \qquad \rho = \frac{A^o_{f>2}}{A^o + A^o_{f>2}}$$

$$\alpha_c = 1-f \qquad f = \text{functionality of } M_{f>2}$$

$$P_c = \frac{1}{\rho(f-2)+1} \qquad P_{c_{\rho=1}} = \frac{1}{f_1 - 1}$$

Multifunctional monomers to be tested are

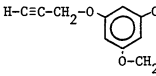

and $CH(CH_2\text{-}O\text{-}CH_2\text{-}C\equiv C\text{-}H)_3$

III. Copolymerization:

The equations presented here are derived in appendix III.

Crosscoupling experiments have shown that the rate which different terminal alkynes couple may vary substantially (20).

Cross Coupling at Low Conversion in Pyridine

Component	% AA	% AB	% BB
A = $C_6H_5C\equiv C\text{-}C\equiv C\text{-}H$ B = $HO\text{-}CH_2\text{-}CH{=}CH\text{-}C\equiv C\text{-}H$	99.6	0.3	0.1
A = $C_6H_5C\equiv C\text{-}H$ B = $HO\text{-}CH_2\text{-}CH{=}CH\text{-}C\equiv C\text{-}H$	51	38.1	10.5

Bohlman has shown a very useful empiracle relation between an alkyne's coupling reactivity and its NMR chemical shift of the acetylenic proton. Expressing the coupling reactivity as the log of the half reaction time, he obtained the following (20).

Reproduced with permission of the copyright owner. Further reproduction prohibited without permission.

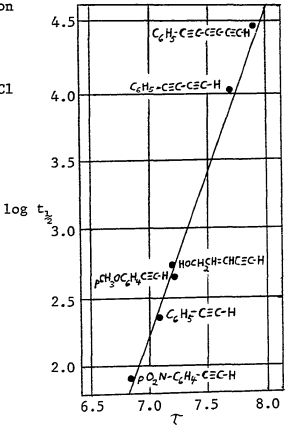

Logarithm of dimerization half reaction time vs. NMR chemical shift of the acetylenic proton. $t_{\frac{1}{2}}$ was determined in a methanol-ethanolamine-HCl system at pH = 3. τ was determined in a CCl_4 solution.

These results indicate the closer the chemical shifts of the two alkynes, the more crosscoupling that will occur.

When the coupling mechanism is divided into two stages, the following results. (Derivations are in appendix III) The first stage is that of preparing the alkyne for entry into the dimeric copper complex. In Bohlman's mechanism (20) (see appendix I) this would involve the reversable cuprous assisted or unassisted dissociation of the acetylenic hydrogen. In the proposed mechanism at the end of appendix I it would involve the creation of the species, $[R\text{-}C{\equiv}C\text{-}Cu]^+$, where the third reaction is not slow. This stage may be represented by

$$A + C \underset{\leftarrow}{\overset{K}{\rightleftharpoons}} A^* \qquad K = \frac{A^*}{A \cdot C}$$

Reproduced with permission of the copyright owner. Further reproduction prohibited without permission.

$A = -C\equiv C-H \qquad C = Cu^{+} \qquad A^{*} = -C\equiv C(\overset{\uparrow}{Cu^{+}})-H \text{ or } -C\equiv C(\overset{\uparrow}{Cu^{+}})O \text{ or } [R-C\equiv C-Cu]^{+}$

The second stage and presumed rate determining one is the formation and irreversible collapse of the dimeric copper complex. It can be represented by

$$A^{*} + A^{*} \xrightarrow{k} P(AA)$$

$P(AA)$ is a polymer of $\bar{X}n \geq 2$

Where two different monomers are present, there are two different alkyne functional groups represented by A_1 and A_2. The subscript 1 is used for the more reactive alkyne.

The relative rates which the two alkynes enter into the copolymer is

$$(1) \qquad \frac{dA_1^{*}}{dA_2^{*}} = \frac{K_1' \frac{A_1}{A_2} + 1}{K_2' \frac{A_2}{A_1} + 1} \qquad K_1' = \frac{k_{11}K_1}{k_{12}K_2} \qquad K_2' = \frac{k_{22}K_2}{k_{12}K_1}$$

The instantaneous mole fraction of A_1 in the copolymer is

$$(2,3) \qquad F_1 = \frac{dA_1^{*}}{dA_1^{*} + dA_2^{*}} = \frac{f_1(K_1' - 1) + 1}{f_1(K_1' + K_2' - 2) + \frac{K_2'}{f_1} - 2K_2' + 2}$$

$$f_1 = \frac{A_1}{A_1 + A_2} = \text{mole fraction of } A_1 \text{ in the feed}$$

As the polymeric coupling proceeds to higher extents of reaction, the feed composition drifts in favor of monomer 2. To obtain the feed composition as a function of extent of reaction, the differential equation is set up as follows (21). At some point in the reaction dA moles of $-C\equiv C-H$ are copolymerized. The copolymer contains $F_1 dA$ moles of A_1 and the feed contains $(A-dA)(f_1 - df_1)$ moles of A_1. Then

Reproduced with permission of the copyright owner. Further reproduction prohibited without permission.

A_1 copolymerized = A_1 before reaction − A_1 after reaction

$$F_1 dA = Af_1 - (A-dA)(f_1-df_1)$$

or $$\frac{dA}{A} = \frac{df_1}{(F_1-f_1)}$$ assuming $df_1 dA$ to be neglectable

$$(4) \quad \frac{A}{A^o} = \left[\left(\frac{\delta f_1 - 1}{\delta f_1^o - 1}\right)\left(\frac{f_1^o - 1}{f_1 - 1}\right)\right]^{\varepsilon} \left[\frac{\Delta_2 - (\Delta_1+2\Delta_2)f_1 + (\Delta_1+\Delta_2)f_1^2}{\Delta_2 - (\Delta_1+2\Delta_2)f_1^o + (\Delta_1+\Delta_2)(f_1^o)^2}\right]^{\mu} \left[\frac{f_1}{f_1^o}\right]^{\eta}$$

$$\Delta_1 = (1-K_1'), \qquad \Delta_2 = (1-K_2'), \qquad \delta = \frac{\Delta_2}{\Delta_1} + 1$$

$$\varepsilon = 1 - \frac{1}{\Delta_1} - \frac{1}{2\Delta_2}, \qquad \mu = \frac{-1}{2\Delta_2}, \qquad \eta = \frac{1}{\Delta_2} - 1$$

By determining the extent of reaction and knowing the initial feed composition, f_1^o, the feed composition may be calculated. Knowledge of p and f_1 will permit determination of $\bar{X}n$, copolymer composition and a measure of the block sequence length in the copolymer. To check the above equation, one of the monomers could have its acetylenic hydrogen replaced by deuterium and the reaction quenched at various points by withholding oxidizing agent (O_2). The concentration of uncoupled triple bonds, A, could be determined by a titration with a heavy metal ion and f_1 by IR absorption of -C≡C-D (about 2400 cm^{-1}) or by deuterium content in the form of HDO or D_2O. To obtain the parameters Δ_1, Δ_2, δ, ε, μ, and η it is necessary to determine K_1' and K_2'. One way to accomplish this is to measure the amounts of self-coupling and crosscoupling at low degrees of conversion. Equations for these two rates are

$$\frac{dP(A_1A_1)}{dP(A_1A_2)} = \frac{k_{11}A_1^{*2}}{k_{12}A_1^*A_2^*} = \frac{k_{11}K_1^2A_1^2}{k_{12}K_1K_2A_1A_2} = K_1' \cdot \frac{A_1}{A_2} = \left(\frac{P(A_1A_1)}{P(A_1A_2)}\right)_{\text{low conversion}}$$

Reproduced with permission of the copyright owner. Further reproduction prohibited without permission.

and analogously $K_2' \cdot \frac{A_2}{A_1} = \left(\frac{P(A_2A_2)}{P(A_1A_2)}\right)_{\text{low conversion}}$

For example using Bohlman's data on page 7 assuming $A_1^o = A_2^o$

$C_6H_5C\equiv C\text{-}C\equiv C\text{-}C\equiv C\text{-}H \qquad K_1' = \frac{99.6}{.3} = 332$

$HOCH_2\text{-}CH{=}CH\text{-}C\equiv C\text{-}H \qquad K_2' = \frac{.1}{.3} = .333$

$C_6H_5C\equiv C\text{-}H \qquad K_1' = \frac{51}{38.5} = 1.33$

$HOCH_2\text{-}CH{=}CH\text{-}C\equiv C\text{-}H \qquad K_2' = \frac{10.5}{38.5} = .367$

Another way is to rearrange equation (3) to

$$(5) \qquad \left[\frac{F_1 + f_1}{f_1^2(1-F_1)}\right] = \left[\frac{F_1\left(f_1 - \frac{1}{f_1} - 2\right)}{f_1(F_1 - 1)}\right]\Delta_2 + \Delta_1$$

By holding $p < .05$ and approximating $f_1 \cong f_1^o$ and $F_1 = A_1'/(A_1' + A_2')$ (A' represents a reacted $-C\equiv C\text{-}H$ group), a plot of the first bracketed term against the second in equation (5) should yield a straight line of slope Δ_2 and intercept Δ_1.

The copolymer composition at various extents of reaction is given by the accumulated copolymer mole fraction, C.

$$(6) \qquad C_1 = \frac{A_1^o - Af_1}{A_1^o - A}$$

A may be determined by heavy metal ion titration or by IR absorption of uncoupled $-C\equiv C\text{-}H$ and f_1 from equation (4) or by acetylenic deuterium substitution on one of the monomers.

It is contended that the greater the difference in acetylenic reactivity between monomers, the longer will be the monomer blocks composing the copolymer. Appendix III pages 8 to 17 shows four ways of

Reproduced with permission of the copyright owner. Further reproduction prohibited without permission.

obtaining measures of amounts of block placement.

The first involves a plot of the accumulative copolymer mole fractions against the extent of reaction. The more rapidly C_1 and C_2 converge, the shorter the blocks of M_1 and M_2 and the more random the placement in the copolymer.

The second is to find the feed mole fraction where both monomers are entering the copolymer at an equal rate ($F_1 = F_2$). At this point in the reaction ($f_1 = f_{1\ F_1 = F_2}$) the value of f_1 is used to calculate the amount of unreacted functional groups, A, from equation (4). Then $f_{1\ F_1 = F_2}$ and A are used to calculate the mole fraction of M_1 in the copolymer, C_1, at this extent of reaction using equation (6). The value of $f_{1\ F_1 = F_2}$ is obtained from the following equation.

$$(7) \qquad f_{1\ F_1 = F_2} = \frac{(K_2')^{1/2}}{(K_1')^{1/2} + (K_2')^{1/2}}$$

The larger the value of $C_{1\ F_1 = F_2}$, the greater the degree of blocking in the copolymer. This would be a simpler method than constructing a copolymer composition-extent of reaction curve.

The third way is to employ Flory's statistical method in an almost identical manner as it is used to calculate degrees of polymerization when monofunctional reagent is added. Instead of replacing the extent of reaction, p, by p', the probability a functional group has formed a linkage with bifunctional monomer, for copolymerization it is replaced by Q, the probability a functional group has formed a linkage with the more reactive monomer, M_1.

Reproduced with permission of the copyright owner. Further reproduction prohibited without permission.

$$(8) \quad Q = \frac{A_1'A_1'}{2A_1^o + \phi A_2^o}$$

$A_1'A_1'$ = a linkage between two M_1 monomers

ϕ = ratio of accumulation rates of A_2 to A_1 on coupling with A_1 end groups

$$(9) \quad \phi = \frac{f_1^o \cdot C_{12}}{f_2^o \cdot C_{11}}$$

C_{12} = mole fraction of A_1A_2 linkages in the copolymer

C_{11} = mole fraction of A_1A_1 linkages in the copolymer

The equations for calculating C_{11} and C_{12} require numerical values of K_1' and K_2' for integration as well as iteration and graphical integration procedures.

By making the approximations $A_1A_1 >> A_1A_2$ $A_1A_2 >> A_2A_2$

ϕ and Q are obtained as $\phi = \frac{2C_2f_1^o}{C_1f_2^o}$, $Q = \frac{P_1}{1 + r_c}$

where $P_1 = \frac{A_1^o - A_1}{A_1^o}$ and $r_c = \frac{C_2}{C_1}$

The number and weight average block lengths, $\bar{X}_{b1}$ and $\bar{X}_{wb1}$ are given by

$$(11) \quad \bar{X}_{b1} = \frac{1 + r_c}{1 + r_c - P_1} \qquad \bar{X}_{wb1} = \frac{1 + r_c + P_1}{1 + r_c - P_1}$$

The approximation $A_1A_2 >> A_2A_2$ breaks down when the extent of reaction has passed through the stage where crosscoupling is predominent and a plot of $\bar{X}_{b1}$ vs. p will go through a maxima. It is proposed to determine how well this maximum $\bar{X}_{b1}$ approximates the true $\bar{X}_{b1}$.

The fourth way is to calculate $\bar{X}_{b1}$ from its definition.

$$\bar{X}_{b1} = \frac{\text{number of } M_1 \text{ units}}{\text{number of } M_1 \text{ blocks}} = \frac{\text{initial concentration of } M_1}{\text{half concentration of } M_1 \text{ block ends}}$$

Reproduced with permission of the copyright owner. Further reproduction prohibited without permission.

The prime superscript distinguishes this $\bar{X}_{b1}$ from that derived by Flory's method. During the course of the reaction an M_1 block end must either be an unreacted M_1 end group, A_1, or a reacted M_2 end group, A_2', up to the point where M_2 predominently reacts with itself. Hence the approximation $A_1A_2 >> A_2A_2$ is also involved and a plot of X_{b1} vs. p will yield a maximum X_{b1}'. X_{b1}' is given by

$$(12) \qquad \bar{X}_{b1}' = \frac{1}{1 + r_A P_2 - P_1} \qquad P_2 = \frac{A_2^o - A_2}{A_2^o} \qquad r_A = \frac{A_2^o}{A_1^o}$$

The existance of an azeotrope will require

$$(13) \qquad f_1 = \frac{1 - K_2'}{1 - K_1' + 1 - K_2'} = \frac{\Delta_2}{\Delta_1 + \Delta_2}$$

To obtain such a feed composition the relative reactivities will be restricted to

$$\left\{ \begin{array}{l} 1 > K_1' > 0 \\ 1 > K_2' > 0 \end{array} \right\}$$

If such a set of K_1', K_2' is found, X_{b1} may be calculated exactly since

$$\phi = \frac{dA_2}{dA_1} = \frac{A_2}{A_1}.$$

To experimentally test these copolymer equations it would be advantageous to have two monomers which vary significantly in reactivity but not so much that a situation of sequential polymerization is incurred. It was observed on page 9 that the NMR chemical shift of the acetylenic proton will give an indication of the relative reactivities of the triple bonds. In Bohlman's crosscoupling experiment it is seen that self-coupling of the more reactive monomer occurred to a much greater extent when the τ values differed by 0.5 units than when they differed by 0.1

Reproduced with permission of the copyright owner. Further reproduction prohibited without permission.

The monofunctional counterparts of the two monomers already proposed for homopolymerization experiments have the following chemical shifts.

$CH_3-O-CH_2C\equiv C-H$ = 7.63
$C_6H_5-O-CH_2-C\equiv C-H$ = 7.99

Should the relative reactivities of these two monomers converge or diverge using Hay's coupling conditions, other possibilities are

$HOCH_2-C\equiv C-H$ = 7.16
$(CH_3)_2CH-C\equiv C-H$ = 8.18
$C_6H_5-C\equiv C-H$ = 7.07
$CH_3-O-C\equiv C-H$ = 8.67
$C_2H_5-O_2C-C\equiv C-H$ = 7.25
$CH_3-CO-C\equiv C-H$ = 6.82

Once K_1' and K_2' are determined either from equation (5) or (1), equation (4) can be checked and cross-checked with equation (10) (appendix III) by plotting the appropriate quantities. The number of uncoupled triple bonds can be determined by either IR absorption of the acetylenic hydrogen or heavy metal ion titration and f_1 can be determined roughly by NMR absorption or by deuteration of M_1. Measurement of these quantities also permits characterization of the copolymer by the C_1 and C_2 vs. p plot, f_1 $F_1=F_2$, $\bar{X}_{bl}$, $\bar{X}_{wbl}$, and $\bar{X}_{bl}$.

To experimentally determine the number average block length, one of the monomers' structures will contain a glycol unit such that the polymer backbone can be cleaved by the addition of periodic acid. The simplest and initial choice of such a monomer is bispropargyl alcohol.

The reactions for monomer and polymer block cleavage are

Reproduced with permission of the copyright owner. Further reproduction prohibited without permission.

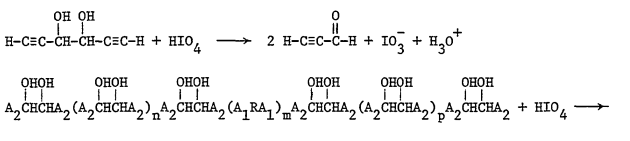

where $A_1 \approx A_2 = -C\equiv C-$

A copolymer of numerous M_1 and M_2 blocks will be cleaved into F fragments. The number of fragments per polymer molecule containing M_1 blocks is designated F_1. The remaining fragments will be of the type

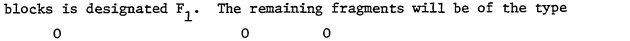

per polymer molecule is F_2. The total number of monomeric units per polymer molecule is M', while M_1' and M_2' are the number of units of each monomer. As demonstrated in appendix III, the number average block lengths are given by

$$\bar{X}_{b1} = \frac{M_1'}{F-F_2} \qquad \bar{X}_{b2} = \frac{M_2'}{F-F_2+1} \qquad \text{where } F_2 = A_2A_2 + A_2$$

M' is determined as $\bar{X}n$. Since the cleavage is quantitative, M_2' can be obtained by a gravimetric titration of the cleavage mixture with $AgNO_3$ which yields a white $AgIO_3$ precipitate. M_1' is obtained as the difference between M' and M_2' or spectrophotometrically by inclusion of a chromophore (eg. aromatic ring) into M_1''s structure. A_2A_2 and A_2 (which may be assumed to be two if M_2 is much less reactive than M_1) can be obtained from quantitative gas chromatographic measurements. F can be determined by measuring the aldehyde concentration by C=O or C-H aldehyde stretching in the infrared or by oxidation of the aldehyde to an acid followed by an acid base titration.

Reproduced with permission of the copyright owner. Further reproduction prohibited without permission.

The weight average block length may be measured by light scattering measurements if a solvent can be found where its refractive index matches that of one of the polymer blocks.

In the absence of experimental data it is possible to examine the predictability of the copolymer equations by supplying the four experimental quantities which these equations require. The four quantities are the two relative reactivities, K_1' and K_2', and the initial monomer concentrations, M_1^o and M_2^o, or initial functional group concentrations, A_1^o and A_2^o.

To demonstrate the integrated copolymer equation a plot of feed mole fraction, f_1, predicted by equation (4) vs. extent of reaction, p, for equimolar concentrations of A_1^o and A_2^o is used. In one case the product of $K_1'K_2'$ is held at 1, and in the other case K_2' is held constant and K_1' is varied from 1000 to 2. See figure 1 in appendix IV for the plots of these two cases. These plots show the expected result that the greater the difference between relative reactivities, the faster the feed is depleted of monomer 1.

Equation (4) and equation (10) (Appendix III) can be used to cross check each other by calculating f_1 and A (which is the sum of A_1 and A_2) for a given p with equation (4), then using equation (10) to calculate a matching A_2 from the value of A_1 obtained through equation (4). Equations (4) and (10) were found to yield matching values of A_2.

On page 13 four methods of obtaining monomer block lengths were proposed. Predicted results for assumed values of K_1', K_2', A_1^o and A_2^o can be obtained through application of the equations in this section. The first method proposed that the rapidity of convergence of C_1 and C_2 in a plot of C_1 and C_2 vs. p would be a qualitative measure of the shortness

Reproduced with permission of the copyright owner. Further reproduction prohibited without permission.

of the monomer block length, $\bar{X}_b$. Figure 2 in appendix IV shows as K_1' and K_2' become closer in size, C_1 and C_2 converge more rapidly. The third and fourth methods contend that $\bar{X}_{b1}$ and $\bar{X}_{b1}'$ would pass through maxima as p increases and these maxima can be taken as the monomer block lengths. Figure 3 in appendix IV shows $\bar{X}_{b1}$ and $\bar{X}_{b1}'$ passing through maxima for two cases. Table 1 in appendix IV gives $\bar{X}_{b1\ max}$ and $\bar{X}_{b1\ max}'$ and the corresponding extents of reaction, p_{max} and p_{max}', at which they occur for several varying cases of K_1', K_2', A_1^o, and A_2^o. The second method involves obtaining f_1 where the rates of addition of the two monomers are equal (equation (7)). An $\bar{X}_{b1}$ and $\bar{X}_{b1}'$ can be calculated from this value of $f_{1\ F_1 = F_1}$ and compared with those of $\bar{X}_{b1\ max}$ and $\bar{X}_{b1\ max}'$. It is surprising to note that the agreement is exact for $\bar{X}_{b1}'$ and close for $\bar{X}_{b1}$. This second method would be the most efficient since it requires only one calculation of $\bar{X}_{b1}$ or $\bar{X}_{b1}'$.

Finally it was stated that for an azeotrope to exist both K_1' and K_2' must be less than one. Figure 4 in appendix IV shows this to be the case.

The figures and table in appendix IV were obtained by means of a Fortran computer program. This program is available on request as well as output for additional cases.

Reproduced with permission of the copyright owner. Further reproduction prohibited without permission.

APPENDIX I

The Reaction Mechanism

Solely from stoichiometric considerations the reaction can be perceived as follows

$$2\ R\text{-}C{\equiv}C\text{-}H + 2\ Cu^{2+} \longrightarrow R\text{-}C{\equiv}C\text{-}C{\equiv}C\text{-}R + 2\ Cu^{+} + 2H^{+}$$

However it is observed that different substituents adjacent to the triple bond produce a large variation in the relative reactivities of terminal alkynes (20). The reactivity differences can be traced to how the substituent affects the acidity of the acetylenic hydrogen and the electrophilic susceptability of the triple bond. Because of these two factors, the reaction conditions dictate whether a coupling will proceed at a reasonable rate. The important reaction conditions are acidity or basisity of the medium, solvent and cuprous ion presence. To be able to create the proper conditions for a coupling it is necessary to have some knowledge of the reaction mechanism.

From the stoichiometric reaction, one can preceive that a mechanism must account for two events; the removal of the acetylenic hydrogen and the oxidative coupling of the alkyne. While no completely satisfactory and varified mechanism exists, substantial work has been done by Westcott and Baxendale (22), Klebanski (22), Clifford and Waters (23), Bohlman (20), and Hay (8). Since these workers used widely varying reaction conditions as well as ethynyl compounds, it is necessary to keep reaction conditions in mind when generalizing their observations.

Acetylenic Oxidative Coupling Observations:

1. The cupric ion is the true mechanistic oxidizing agent as demonstrated by Westcott and Baxendale using a stoichiometric quantity of the cupric ion with dimethylethynylcarbinol (22).

Reproduced with permission of the copyright owner. Further reproduction prohibited without permission.

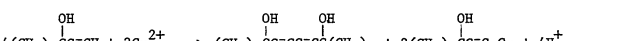

2. Coupling is more rapid and higher yields are produced when a cuprous ion-oxidizing agent (usually oxygen) combination is used in place of the cupric ion.
3. In alkaline media (aqueous-ammonia, ammonia, pyridine)
   (a) Coupling reactivity parallels acetylenic acidity.
   (b) Reaction rate increases with increasing pH.
   (c) Reaction will proceed without cuprous ion initially present.
   (d) Presence of cuprous ion accelerates the reaction rate.
   (e) Reaction is first order with respect to alkyne (With pyridine solvent and a piperidine buffer present first order was observed after a cuprous ion alkyne complex equilibrium was taken into account (23). But with pyridine alone a second order alkyne dependence was observed (20).)
4. In acidic media (hydrochloric acid-methanol)
   (a) Coupling reactivity increases as acetylenic acidity decreases.
   (b) Coupling reactivity increases as the olefinic character of the triple bond increases.
   (c) Cuprous ion is essential for the reaction to proceed and accelerates the reaction with increasing concentration.
   (d) Reaction is second order with respect to alkyne.
5. In neutral media (acetone, alcohols, ether) the coupling is second order with respect to alkyne employing a Cu^{+}/O_2 redox system.
6. The presence of vinyl cyanide during the coupling of propargyl alcohol in a copper(II)-copper(I)-piperidine-pyridine system resulted in no poly(vinylcyanide) formation.

Reproduced with permission of the copyright owner. Further reproduction prohibited without permission.

Mechanisms:

Various mechanisms have been advanced, but none have been flexible enough to be applicable under all the conditions which the reaction has been run. To account for the alkaline first order kinetics Klebanski (22) proposed

$$R\text{-}C{\equiv}C\text{-}H \underset{}{\overset{\text{slow}}{\rightleftharpoons}} R\text{-}C{\equiv}C^{\ominus} + H^{+}$$

$$R\text{-}C{\equiv}C^{\ominus} + Cu^{2+} \xrightarrow{\text{fast}} R\text{-}C{\equiv}C\cdot + Cu^{+}$$

$$2\ R\text{-}C{\equiv}C\cdot \xrightarrow{\text{fast}} R\text{-}C{\equiv}C\text{-}C{\equiv}C\text{-}R$$

The mechanism suffers in that it cannot account for the cuprous ion accelerating effect, the rate dependence on the copper ions nor the second order acidic kinetics.

Clifford and Waters (23) proposed a mechanism which fits their data for a cupric-cuprous ion-piperidine-pyridine system remarkably well especially the rate dependence on piperidine and copper.

$$R\text{-}C{\equiv}C\text{-}H + B \underset{}{\overset{\text{slow}}{\rightleftharpoons}} R\text{-}C{\equiv}C^{\ominus} + BH^{+}$$

$$R\text{-}C{\equiv}C\text{-}H + Cu^{+} \underset{}{\overset{K}{\rightleftharpoons}} \underset{\downarrow +}{R\text{-}C{\equiv}C\text{-}H\ Cu^{+}} \quad \text{(inert complex)}$$

$$R\text{-}C{\equiv}C^{\ominus} + Cu^{+} \underset{}{\overset{\text{slow}}{\rightleftharpoons}} R\text{-}C{\equiv}C\text{-}Cu$$

$$R\text{-}C{\equiv}C\text{-}Cu + Cu^{2+} \xrightarrow{\text{fast}} R\text{-}C{\equiv}C\cdot + 2Cu^{+}$$

$$2\ R\text{-}C{\equiv}C\cdot \xrightarrow{\text{fast}} R\text{-}C{\equiv}C\text{-}C{\equiv}C\text{-}R$$

This mechanism does not cover the cases where there is no cuprous ion present or the second order acidic kinetics.

The most encompassing mechanism is that advanced from Bohlman's work (20).

Reproduced with permission of the copyright owner. Further reproduction prohibited without permission.

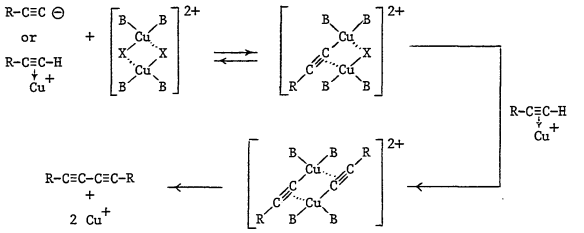

By choosing the proper step as rate determining a rate law can be expressed as unimolecular of bimolecular with respect to alkyne. If formation of the acetylide ion or cuprous acetylene complex is rate determining the reaction is unimolecular, but if formation of the dimeric cupric acetylene complex is rate determining, the reaction is bimolecular. In addition to accounting for the different kinetic orders of the alkyne in acidic and basic media, the inverted relative reactivities of the alkynes in the two media as well as the cuprous ion accelerating effect can be rationalized. Bohlman reports the following reactivity order as determined by half reaction times.

In pyridine:

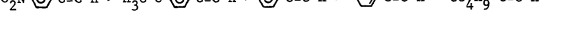

In methanol acidified with HCl to pH = 3:

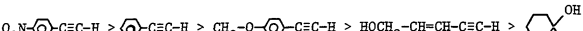

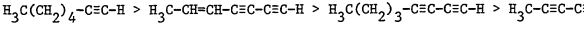

Reproduced with permission of the copyright owner. Further reproduction prohibited without permission.

In basic media the acetylenic proton may dissociate forming the acetylide ion and a protonated base, typical of acid base equilibrium. The more that the charge on the acetylide part of the molecule can be stabilized, the more acidic the alkyne. It is primarily an inductive rather than a conjugated resonance effect which stabilizes the acetylide anion. The lack of resonance interaction is evidenced in that triple and adjacent single bond lengths show little variation between isolated triple bonds in an alkyl chain and those conjugated with an unsaturated group (alkene, alkyne, carbonyl, or phenyl) (24). Also triple bonds usually react independently of other conjugated groups within the molecule. The inductive effect is evidenced in the relative coupling reactivity sequence in pyridine above by noting that the reactivity parallels the electronegativity of the group attached to the terminal triple bond. (The -C≡C- group has an electronegativity approximately equal to bromine and much greater than ϕ-, -C=C-, or -C-C- as seen by the dipole moments; H-C≡C-Br μ=0, CH_2=CHBr μ=1.42, CH_3CH_2Br μ=2.04, ϕ-Br μ=1.52 (25).)

The effect of making the medium acidic is to decrease the degree of acetylenic hydrogen dissociation. No reaction occurs at all for the less acidic acetylenes when the cuprous ion is absent. Bohlman demonstrated the cuprous ion accelerating effect with the following data (20).

Half Reaction Time Dependence on Cu^+ Concentration

Temperature = 20 °C, $C_{R-C\equiv C-H}$ = 8mMol/l, $C_{Cu^{2+}}$ = 100mMol/l, Solvent - Pyridine

Compound	$t_{1/2}$(min.)	C_{Cu^+}(mMol/l)	Compound	$t_{1/2}$(min.)	C_{Cu^+}(mMol.
C_6H_5-C≡C-H	35000	0	CH_3-C≡C-C≡C-H	200	0
	9000	2		90	100
	1500	8			
	50	100			

Reproduced with permission of the copyright owner. Further reproduction prohibited without permission.

The cuprous ion has a more pronounced accelerating effect on the less acidic alkyne. Changing to acidic media necessitates the presence of the cuprous ion, and its accelerating effect is again more pronounced with the less acidic alkyne. It is believed that the cuprous ion, by an electrophilic association with the triple bond, forms a complex from which the acetylenic hydrogen more easily dissociates or which promotes formation of the cupric dimeric complex. The existence of three cuprous acetylene complexes, described as $[C_2H_2Cu]^+$, $[C_2H_2CuCl]$ and $[C_2H_2CuCl_2]^-$, in solution has been demonstrated (26). Infrared evidence for such a complex consists of a triple bond stretching frequency decrease from the normal 2190-2260 cm^{-1} to 1920-1960 cm^{-1} for the complex (27). Why the lesser acidic acetylenes should be more susceptable to the electrophilic attack of the cuprous ion may be attributed to the perturbed nature of the triple bond. Considering the relative reactivity order in acidic media where the normal acetylenic dissociation is surpressed, it is observed that an adjacent phenyl group promotes the fastest complex formation followed by the alkene group, the saturated alkyl group and finally the alkyne group. It is known that olefin bonds are much more susceptable to electrophilic attacks than triple bonds (28) and has been rationalized by applying the Linnet double quartet bonding system (29). This system shows the triple bond to be cyclindrically symmetric and delocalized about the carbon-carbon axis of the triple bond. Anything, such as an adjacent phenyl group or olefin bond, might perturb this cyclindrical symmetry and result in electron localization in the triple bond-hence a site for electrophilic attack. Any disruption in this cyclindrical electron symmetry would be reflected in a negative or olefinic NMR chemical shift of the

Reproduced with permission of the copyright owner. Further reproduction prohibited without permission.

acetylenic protron. (Acetylenic hydrogens appear at τ of 4.1 to 5.4) Bohlman's work (20) shows a linear dependence between the logarithm of the half reaction time and the acetylenic chemical shift indicating the greater the olefinic chemical shift, the faster the acidic coupling. Thus, the acidity of the acetylenic hydrogen is determined by the electronegativity of the triple bond substituent, and the cuprous complex formation by the "olefinic character" of the triple bond. The reaction conditions and the nature of the alkyne molecule determine which is the more important factor in the coupling reaction.

Concerning the dimeric copper complex, evidence for it exists in both the cuprous and cupric cases (27, 30). In the cupric case the complex examined was

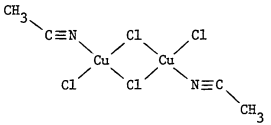

The configuration about the cupric ion is nearly square planear. The Cu-Cl bridge bond distance is 2.3 Å and the Cu-N distance is 2.0 Å. The Cu bond angles are about 90° while the N-C-C angle is 170 $\pm$ 6° and Cu-N-C angle is 165 $\pm$ 4°. Thus, "it appears that the nitrogen atom does not use pure sp hybrid orbitals but that the orbitals have partial sp^2 character" (30). This can be accounted by a Linnet double quartet bond structure (29).

Reproduced with permission of the copyright owner. Further reproduction prohibited without permission.

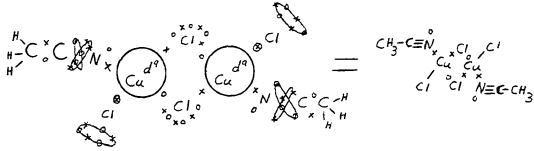

This structure by transferring an electron to the nitrogen atom leaves nitrogen with a formal charge of $+\frac{1}{2}$ and Cu with $-\frac{1}{2}$ and accounts for the Cu-N-C and N-C-C bond angles while a Lewis structure gives nitrogen a +1 formal charge, Cu a -2 charge, and the bridging Cl a +1 charge and linear Cu-N-C and N-C-C bonds. The same bonding can be applied to Bohlman's dimeric cupric complex.

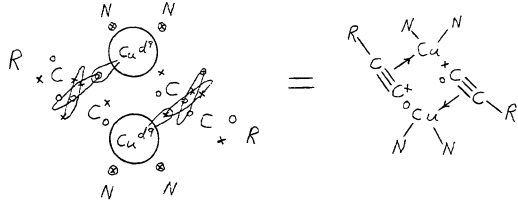

This structure with the electron transferred to carbon gives it a formal charge of $-\frac{1}{6}$, for the other carbon $+\frac{1}{6}$, and for copper $-\frac{2}{3}$. Crystal field theory would also predict the dsp^2 square planar configuration.

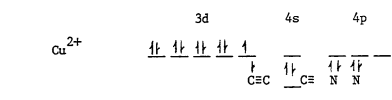

Reproduced with permission of the copyright owner. Further reproduction prohibited without permission.

By localizing an electron on the carbon atom, one can picture a coupling occurring diagonally across the complex with the simultaneous production of two cuprous ions. Thus there is no free acetylide radical in solution which may explain the lack of the vinyl cyanide polymerization in the coupling medium.

One minor difficulty with Bohlman's mechanism would be in explaining Westcott and Baxendale's observation (22) in an acidic aqueous cupric-cuprous system that the coupling rate was observed to be proportional to [R-C≡C-H], [Cu^{+}], [Cu^{2+}] and inversely proportional to [H^{+}]. Bohlman's mechanism would predict zero or second order kinetics with respect to cupric ion. In aqueous media the cuprous ion is unstable and disproportionates with the following equilibrium (31).

$$2\ Cu^{+} \rightleftharpoons Cu^{2+} + Cu^{o} \qquad K_{eq} = \frac{[Cu^{2+}][Cu^{o}]}{[Cu^{+}]} = \frac{[Cu^{2+}]}{[Cu^{+}]} = 10^{5.8}$$

A complexing amine would undoubtedly affect this constant (32) but no mention is made of any complexing ligand. Considering production of the cuprous ion to be rate determining, Bohlman's mechanism may be modified to take this observation into account.

$$R\text{-}C{\equiv}C\text{-}H + Cu^{+} \rightleftharpoons \left[\begin{array}{c} R\text{-}C{\equiv}C\text{-}H \\ \downarrow \\ Cu \end{array}\right]^{+}$$

$$\left[\begin{array}{c} R\text{-}C{\equiv}C\text{-}H \\ \downarrow \\ Cu \end{array}\right]^{+} + B \rightleftharpoons [R\text{-}C{\equiv}C\text{-}Cu] + BH^{+}$$

$$[R\text{-}C{\equiv}C\text{-}Cu] + Cu^{2+}(\text{or } \tfrac{1}{2}O_2 + H^{+}) \xrightarrow{\text{slow}} [R\text{-}C{\equiv}C\text{-}Cu]^{+} + Cu^{+}(\text{or } \tfrac{1}{2}H_2O)$$

Reproduced with permission of the copyright owner. Further reproduction prohibited without permission.

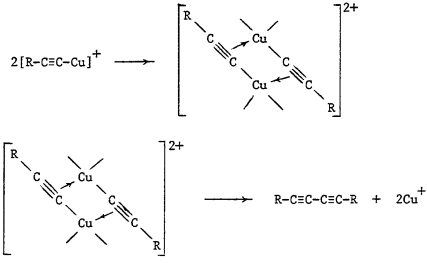

Assuming the third reaction to be rate determining

$$R = k[R\text{-}C{\equiv}C\text{-}Cu][Cu^{2+}] = k' \frac{[R\text{-}C{\equiv}C\text{-}H][Cu^{+}][Cu^{2+}]}{[H^{+}]}$$

In this case an oxidizing agent other than the cupric ion (O_2, $Fe(CN)_6^{3-}$, NaOCl) would play a more active part in the mechanism, i.e., other than regenerating cupric ion.

Reproduced with permission of the copyright owner. Further reproduction prohibited without permission.

APPENDIX II
Homopolymerization

The majority of work on the acetylenic coupling mechanism shows the coupling rate to be second order with rexpect to terminal triple bond concentration, A, expecially in neutral and acidic media. The time dependence of the degree of polymerization can be shown as follows.

$$-\frac{dA}{dt} = k'A^2$$

$$-\int_{A^o}^{A} \frac{dA}{A^2} = \int_0^t k'dt$$

$$\frac{1}{A} - \frac{1}{A^o} = k't \qquad A = A^o - pA^o = A^o(1-p)$$

$$\frac{1}{A^o(1-p)} - \frac{1}{A^o} = k't$$

$$\frac{1}{1-p} = k'A^o t + 1 \qquad \overline{X}n = \frac{A^o}{A} = \frac{A^o}{A^o(1-p)} = \frac{1}{(1-p)}$$

$$\overline{X}n = k'A^o t + 1$$

Thus, a plot of $\overline{X}n$ vs. t should be linear with slope equal to $k'A^o$.

The most probable number average, $\overline{X}n$, and weight average, $\overline{X}w$, chain length distributions can be calculated by following Flory's method (18).

H-C≡C-R-C≡C-C≡C-R-C≡C-C≡C-R-C≡C-·····-C≡C-R-C≡C-C≡C-R-C≡C-H
1 2 3 x-1 x

Instead of having two different functional groups forming a chain linkage (~~~A-B~~~, ie. ~~~C(=O)-O~~~) in this case two identical functional groups form the chain linkage (~~~A-A~~~ ie. ~~~C≡C-C≡C~~~) as shown above. Using Flory's convention;

p = fraction of functional groups reacted = probability two functional groups have reacted to produce a closed linkage.
A' = a reacted functional group (R-C≡C-).
A'A' = a closed linkage (R-C≡C-C≡C-R).

$$p = \frac{A'A'}{2A^o} = \frac{\text{number of closed linkages formed}}{\text{total number of functional group pairs}}$$

$$p = \frac{2A'}{2A^o} = \frac{A'}{A^o}$$

x = number of monomeric groups in the molecule.
x-1 = number of closed linkages in a polymer molecule.
p^{x-1} = probability of a sequence of x-1 closed linkages.
1-p = probability of a sequence terminated by two unreacted end groups = one open linkage.

Reproduced with permission of the copyright owner. Further reproduction prohibited without permission.

$\bar{N}_x = (1-p)p^{(x-1)}$ = probability a molecule is composed of x monomeric units.

$N_x = \bar{N}_x N$ = number of molecules in a fraction containing x units.

$N = N_o(1-p)$ = total number of molecules in the system.

N_o = total number of monomeric units in the system.

$N_x = N_o(1-p)^2 p^{(x-1)}$

w_x = weight fraction

$w_x = \frac{xM_o N_x}{M_o N_o} = \frac{xN_x}{N_o}$ $\qquad M_o$ = molecular weight of a monomeric unit.

$w_x = (1-p)^2 x p^{(x-1)}$

Degree of polymerization:

$$\bar{X}n = \frac{\sum xN_x}{\sum N_x} = \frac{\sum xN_o(1-p)^2 p^{x-1}}{\sum N_o(1-p)^2 p^{x-1}} = \frac{\sum xp^{x-1}}{\sum p^{x-1}}$$

$$\sum_{1}^{\infty} xp^{x-1} = Sn_1 = 1 + 2p + 3p^2 + 4p^3 + 5p^4 + \cdots\cdots\cdots$$

$$-[pSn_1 = \quad p + 2p^2 + 3p^3 + 4p^4 + \cdots\cdots\cdots]$$

$$(1-p)Sn_1 = 1 + p + p^2 + p^3 + p^4 + \cdots\cdots\cdots$$

$$-[p(1-p)Sn_1 = \quad p + p^2 + p^3 + p^4 + \cdots\cdots\cdots]$$

$$(1-p)^2 Sn_1 = 1$$

$$Sn_1 = \frac{1}{(1-p)^2}$$

$$\sum_{1}^{\infty} p^{x-1} = Sn_2 = 1 + p + p^2 + p^3 + p^4 + \cdots\cdots\cdots\cdots$$

$$-[pSn_2 = \quad p + p^2 + p^3 + p^4 + \cdots\cdots\cdots\cdots]$$

$$(1-p)Sn_2 = 1$$

$$Sn_2 = \frac{1}{(1-p)}$$

$$\bar{X}n = \frac{Sn_1}{Sn_2} = \frac{\frac{1}{(1-p)^2}}{\frac{1}{(1-p)}} = \frac{1}{(1-p)}$$

Reproduced with permission of the copyright owner. Further reproduction prohibited without permission.

$$\bar{X}w = \sum xw_x = \sum x(1-p)^2 xp^{x-1} = (1-p)^2 \sum x^2 p^{x-1}$$

$$\sum x^2 p^{x-1} = Sn_3 = 1 + 4p + 9p^2 + 16p^3 + 25p^4 + \ldots\ldots\ldots\ldots$$

$$-[pSn_3 = \quad p + 4p^2 + 9p^3 + 16p^4 + \ldots\ldots\ldots\ldots.]$$

$$(1-p)Sn_3 = 1 + 3p + 5p^2 + 7p^3 + 9p^4 + \ldots\ldots\ldots\ldots$$

$$-[p(1-p)Sn_3 = \quad p + 3p^2 + 5p^3 + 7p^4 + \ldots\ldots\ldots\ldots.]$$

$$(1-p)^2 Sn_3 = 1 + 2p + 2p^2 + 2p^3 + 2p^4 + \ldots\ldots\ldots\ldots$$

$$-[p(1-p)^2 Sn_3 = \quad p + 2p^2 + 2p^3 + 2p^4 + \ldots\ldots\ldots\ldots.]$$

$$(1-p)^3 Sn_3 = 1 + p$$

$$Sn_3 = \frac{(1+p)}{(1-p)^3}$$

$$\bar{X}w = (1-p)^2 Sn_3 = \frac{(1+p)}{(1-p)}$$

Breadth of Chain Distribution:

$$\frac{\bar{X}w}{\bar{X}n} = \frac{\frac{(1+p)}{(1-p)}}{\frac{1}{(1-p)}} = 1 + p$$

These results for $\bar{X}n$ and $\bar{X}w$ are the same as those for A-B and A-A+B-B polymerizations, since their derivations are dependent on the relation between the number of linkages and number of monomeric units within the molecule.

Molecular Weight Control with Addition of a Monofunctional Species:

One may want to cap the terminal acetylenic groups not so much to prevent further polymerization as the absence of copper would accomplish that, but to prevent possible formation of heavy metal acetylides as when dried some are known to be explosive. Here the equations governing the number and weight average degree of polymerization for acetylenic coupling system differ from the A-B and A-A+B-B systems. The reason is that in the A-B or A-A+B-B systems there is an average of one end group per molecule identical to the functional group on the monofunctional

Reproduced with permission of the copyright owner. Further reproduction prohibited without permission.

species while in the acetylenic coupling system there are two end groups per molecule identical to the monofunctional species.

To obtain the $\bar{X}n$ and $\bar{X}w$ dependence on the monofunctional species, it is necessary to replace the extent of reaction ($p = \frac{A'A'}{2A^o}$ with the probability, p', that a given functional group has formed a linkage with a bifunctional monomer (18).

$A'A'$ = number of linkages formed from bifunctional species.

A^o = number of functional groups on bifunctional species.

A^o_u = number of functional groups on monofunctional species.

$$p' = \frac{A'A'}{2A^o + A^o_u} = \frac{2A'}{2A^o + A^o_u} = \frac{A'}{A^o + \frac{1}{2}A^o_u}$$

The factor of $\frac{1}{2}A^o_u$ appears because there are half as many A functional groups on a monofunctional monomer as on a bifunctional monomer as opposed to an A-B or A-A+B-B system. For the A-B and A-A+B-B system; $p' = \frac{A'}{A^o + A^o_u}$.

$$p' = \frac{A'}{A^o + \frac{1}{2}A^o_u} = \frac{2A'}{2A^o + A^o_u} = \frac{2\frac{A'}{A^o}A^o}{A^o + A^o + A^o_u} = \frac{2\frac{A'}{A^o}\frac{A^o}{A^o+A^o_u}}{\frac{A^o}{A^o+A^o_u} + 1}$$

$$p = \frac{A'}{A^o} \qquad r = \frac{A^o}{A^o+A^o_u}$$

$$p' = \frac{2rp}{(r+1)}$$

$$\bar{X}n = \frac{1}{1-p'} = \frac{1}{1 - \frac{2rp}{r+1}} = \frac{r+1}{r+1-2rp}$$

Reproduced with permission of the copyright owner. Further reproduction prohibited without permission.

$$\bar{X}w = \frac{1 + p'}{1 - p'} = \frac{1 + \frac{2rp}{r+1}}{1 - \frac{2rp}{r+1}} = \frac{r + 1 + 2rp}{r + 1 - 2rp}$$

The equations for $\bar{X}n$ and $\bar{X}w$ are the same as for those applying to A-B and A-A+B-B systems except there $r = \frac{A^o}{A^o + 2A^o_u}$

Crosslinking:

Since there is no stoichiometric requirement in this A-A system as there is in an A-B or A-A+B-B system, branching must lead to crosslinking and both the Carothers (19) and statistical (18) calculations of the gel point are simpler as only one functional group is involved.

The equations leading to the gel point in the Carothers calculation are the same as those for A-A+$A_{f>2}$+B-B or A-A+$A_{f>2}$+A-B systems where A and B are present in equivalent amounts.

$f_{avg} = \frac{M_i f_i}{M_i}$ M_i = number of monomers of type i with functionality f_i

$p_c = \frac{2}{f_{avg}}$ p_c = critical extent of reaction at the gel point

The statistical gel point equation is different from that of bifunctional systems due to no stoichiometric restriction.

$\alpha_c = \frac{1}{f - 1}$ = critical branching coefficient

f = functionality of M_f with f>2

$p = \frac{A'}{A^o}$ = extent of reaction = probability two A groups react

$\rho = \frac{A^o_{f>2}}{A^o + A^o_{f>2}}$ = ratio of functional groups attached to $M_{f>2}$ to total functional groups

p = probability two A groups (-C≡C-H) of a trifunctional monomer have reacted

Reproduced with permission of the copyright owner. Further reproduction prohibited without permission.

$p(1-\rho)$ = probability two A groups (-C≡C-H) of a bifunctional monomer have reacted

For crosslinking to occur there must be two or more units of $M_{f>2}$ in a polymeric molecule. The probability of obtaining a chain segment terminated by two $M_{f>2}$ units is given by α (equal to the probability of such a sequence).

$$\top AA-AA-AA-AA-AA-AA-AA-AA-AA\top$$
$$1 \quad 2 \quad 3 \quad 4 \ldots\ldots\ldots n-2 \quad n-1 \quad n$$

$$\alpha = \sum_n (p\rho)((1-\rho)p)^n = (p\rho)\sum_n((1-\rho)p)^n = \frac{p\rho}{1-(1-\rho)p}$$

At the gel point $p = p_c$

$$\alpha = \alpha_c = \frac{1}{f-1} = \frac{p_c\rho}{1-(1-\rho)p_c}$$

$$p_c = \frac{1}{\rho(f-2)+1}$$

$$p_{c\rho=1} = \frac{1}{f-1}$$

This result predicts that the gel point in an acetylenic coupling system will occur earlier than in an A-A+A$\overset{A}{\perp}$A+B-B system (where [A] = [B], $p_c = \frac{1}{((f-2)+1)}$ ½. This difference arises from α being two combinations of three different probabilities in the A-A+A$\overset{A}{\perp}$A+B-B system.

i.e., p_A = probability two A groups react or the A halves of two linkages are formed

p_Ap_B = probability two AB linkages are formed

$p_Ap_B\rho$ = probability two AB linkages are formed and the A groups belong to A$\overset{A}{\perp}$A

$p_Ap_B(1-\rho)$ = probability two AB linkages are formed and the A groups belong to A-A

The probability of a linear chain segment of n bifunctional units capped by two trifunctional monomers is then

Reproduced with permission of the copyright owner. Further reproduction prohibited without permission.

$$\alpha = \sum P_A P_B \rho [P_A P_B (1-\rho)]^n = \sum P^2 \rho [P^2 (1-\rho)]^n \qquad P_A = P_B = P \text{ or } A = B$$

In the A-A+A$\overset{A}{\perp}$A system any bifunctional molecule (A-A) may react with a trifunctional molecule but in the A-A+A$\overset{A}{\perp}$A+B-B system only one half the bifunctional molecules (B-B) may react with the trifunctional molecule (A$\overset{A}{\perp}$A). Consequently polymer molecules with two trifunctional units should be formed earlier in the A-A+A$\overset{A}{\perp}$A system than the A-A+A$\overset{A}{\perp}$A+B-B system.

Reproduced with permission of the copyright owner. Further reproduction prohibited without permission.

APPENDIX III
Copolymerization

Copolymer Equation:

$A = -C\equiv C-H \qquad C = Cu^+ \qquad A^* = \overset{-C\equiv C-H}{\underset{Cu^+}{}} \quad \text{or} \quad [-C\equiv C:]^-Cu^+$

A_1 = more reactive alkyne group

A_2 = less reactive alkyne group

P(AA) = polymer of n≥2 units

$$A_1 + C \underset{}{\overset{K_1}{\rightleftharpoons}} A_1^* \qquad K_1 = \frac{A_1^*}{A_1 C}$$

$$A_2 + C \underset{}{\overset{K_2}{\rightleftharpoons}} A_2^* \qquad K_2 = \frac{A_2^*}{A_2 C}$$

$$A_1^* + A_1^* \xrightarrow{k_{11}} P(A_1A_1)$$

$$\left.\begin{aligned} A_1^* + A_2^* &\xrightarrow{k_{12}} P(A_1A_2) \\ A_2^* + A_1^* &\xrightarrow{k_{21}} P(A_2A_1) \end{aligned}\right\} \text{ same reaction}$$

$$A_2^* + A_2^* \xrightarrow{k_{22}} P(A_2A_2)$$

$$\frac{dA_1^*}{dt} = k_1A_1C - k_{-1}A_1^* - k_{11}A_1^{*2} - k_{12}A_1^*A_2^*$$

$$= k_1A_1C - k_{-1}K_1A_1C - k_{11}K_1^2A_1^2C^2 - k_{12}K_1K_2A_1A_2C^2$$

$$= -k_{11}K_1^2A_1^2C^2 - k_{12}K_1K_2A_1A_2C^2$$

$$\frac{dA_2^*}{dt} = -k_{22}K_2^2A_2^2C^2 - k_{12}K_1K_2A_1A_2C^2$$

$$\frac{dA_1^*}{dA_2^*} = \frac{k_{11}K_1^2A_1^2C^2 + k_{12}K_1K_2A_1A_2C^2}{k_{22}K_2^2A_2^2C^2 + k_{12}K_1K_2A_1A_2C^2} = \frac{\frac{k_{11}}{k_{12}}\frac{K_1}{K_2}\frac{A_1}{A_2} + 1}{\frac{k_{22}}{k_{12}}\frac{K_2}{K_1}\frac{A_2}{A_1} + 1}$$

$$K_1' = \frac{k_{11}}{k_{12}}\frac{K_1}{K_2} \qquad K_2' = \frac{k_{22}}{k_{12}}\frac{K_2}{K_1}$$

(1) $$\frac{dA_1^*}{dA_2^*} = \frac{K_1'\frac{A_1}{A_2} + 1}{K_2'\frac{A_2}{A_1} + 1}$$

Reproduced with permission of the copyright owner. Further reproduction prohibited without permission.

Instantaneous Copolymer Mole Fraction:

F_1 = instantaneous mole fraction of A_1 in copolymer

$$(2)\quad F_1 = \frac{dA_1^*}{dA_1^* + dA_2^*}$$

$$\frac{1}{F_1} = \frac{dA_2^*}{dA_1^*} + 1 = \frac{K_2' \frac{A_2}{A_1} + 1}{K_1' \frac{A_1}{A_2} + 1} + 1$$

f_1 = mole fraction of A_1 in feed

$$f_1 = \frac{A_1}{A_1 + A_2} \qquad \frac{1}{f_1} = \frac{A_2}{A_1} + 1 \qquad f_2 = 1 - f_1$$

$$\frac{A_2}{A_1} = \frac{1}{f_1} - 1 \qquad \frac{A_1}{A_2} = \frac{1}{f_2} - 1 = \frac{1}{(1-f_1)} - 1$$

$$\frac{1}{F_1} = \frac{K_2'(\frac{1}{f_1} - 1)+1}{K_1'\left(\frac{1}{1-f_1}\right) - 1 + 1} + 1 = \frac{K_2'(\frac{1}{f_1} - 1)(1-f_1)+(1-f_1)}{K_1'(1-(1-f_1))+(1-f_1)} + 1$$

$$= \frac{K_2'(\frac{1}{f_1} - 1 - 1 + f_1)+(1-f_1)}{K_1'f_1 + (1-f_1)} + 1 = \frac{\frac{K_2'}{f_1} - 2K_2' + K_2'f_1 - f_1 + 1}{K_1'f_1 - f_1 + 1} + 1$$

$$= \frac{f_1(K_2'-1)+\frac{K_2'}{f_1}-2K_2'+1}{f_1(K_1'-1) + 1} = \frac{f_1(K_2'-1)+\frac{K_2'}{f_1}-2K_2'+1+f_1(K_1'-1)+1}{f_1(K_1'-1) + 1}$$

$$\frac{1}{F_1} = \frac{f_1(K_1' + K_2' - 2) + \frac{K_2'}{f_1} + 2}{f_1(K_1'-1) + 1}$$

$$(3)\quad F_1 = \frac{f_1(K_1'-1) + 1}{f_1(K_1' + K_2' -2) + \frac{K_2'}{f_1} - 2K_2' + 2}$$

Intergrated Copolymer Equation:

At some point in the reaction dA moles of -C≡C-H are copolymerized. The polymer contains $F_1 dA$ moles of A_1 and the feed contains $(A-dA)(f_1-df_1)$ moles of A_1.

mass balance requires

Reproduced with permission of the copyright owner. Further reproduction prohibited without permission.

A_1 copolymerized = A_1 before reaction - A_1 after reaction

$$F_1 dA = Af_1 - (A-dA)(f_1-df_1)$$

$$F_1 dA = Af_1 - Af_1 + Adf_1 + f_1 dA - df_1 dA$$

$df_1 dA$ is negligibly small

$$F_1 dA = Adf_1 + f_1 dA$$

$$(F_1-f_1)dA = Adf_1$$

$$\frac{dA}{A} = \frac{df_1}{(F_1-f_1)}$$

$$\frac{dA}{A} = \frac{df_1}{\frac{f_1(K_1'-1)+1}{f_1(K_1'+K_2'-2)+(K_2'/f_1)-2K_2'+2} - f_1}$$

$$\frac{dA}{A} = \left[\frac{f_1(K_1'+K_2'-2)+(K_2'/f_1)-2K_2'+2}{f_1(K_1'-1)+1-(f_1^2(K_1'+K_2'-2)+K_2'-2K_2'f_1+2f_1)}\right]df_1$$

$$\frac{dA}{A} = \left[\frac{f_1(K_1'+K_2'-2)+(K_2'/f_1)-2K_2'+2}{(1-K_2')+f_1(K_1'+2K_2'-3)+f_1^2(-K_1'-K_2'+2)}\right]df_1$$

$a = (1-K_1')$ $\quad b = (K_1'+2K_2'-3)$ $\quad c = (-K_1'-K_2'+2)$

$g = K_2'$ $\quad h = (-2K_2'+2)$ $\quad f_1 = x$

$$\frac{dA}{A} = \left[\frac{-cx+(g/x)+h}{a+bx+cx^2}\right]dx$$

$$\int\frac{dA}{A} = -c\int\frac{xdx}{a+bx+cx^2} + g\int\frac{dx}{x(a+bx+cx^2)} + h\int\frac{dx}{a+bx+cx^2}$$

Integral Tables CRC Handbook 34, 252

$X = a + bx + cx^2$ $\quad q = 4ac - b^2$

integral 83 $\quad \int\frac{dx}{X} = \frac{1}{-q}\ln\frac{2cx+b-\sqrt{-q}}{2cx+b+\sqrt{-q}}$

integral 87 $\quad \int\frac{xdx}{X} = \frac{1}{2c}\ln X - \frac{b}{2c}\int\frac{dx}{X}$

integral 93 $\quad \int\frac{dx}{xX} = \frac{1}{2a}\ln\frac{x^2}{X} - \frac{b}{2a}\int\frac{dx}{X}$

$$\int\frac{dA}{A} = -c\left(\frac{1}{2c}\ln X - \frac{b}{2c}\int\frac{dx}{X}\right) + g\left(\frac{1}{2a}\ln\frac{x^2}{X} - \frac{b}{2a}\int\frac{dx}{X}\right) + h\int\frac{dx}{X}$$

Reproduced with permission of the copyright owner. Further reproduction prohibited without permission.

$$\int \frac{dA}{A} = -\frac{1}{2}\ln X + \frac{b}{2}\int \frac{dx}{X} + \frac{g}{2a}\ln x^2 - \frac{g}{2a}\ln X - \frac{gb}{2a}\int \frac{dx}{X} + h\int \frac{dx}{x}$$

$$= \left(\frac{b}{2} - \frac{gb}{2a} + h\right)\int \frac{dx}{X} - \left(\frac{g}{2a} + \frac{1}{2}\right)\ln X + \frac{g}{2a}\ln x^2$$

$$\int \frac{dA}{A} = \alpha\int \frac{dx}{X} - \beta \ln X + \gamma \ln x^2$$

$$\alpha = \left(\frac{b}{2} - \frac{gb}{2a} + h\right) = \frac{K_1' + 2K_2' - 3}{2} - \frac{K_2'(K_1' + 2K_2' - 3)}{2(1 - K_2')} + (-2K_2' + 2)$$

$$= \frac{1}{2}\left[\frac{(K_1' + 2K_2' - 3)(1 - K_2')}{(1 - K_2')} - \frac{K_2'(K_1' + 2K_2' - 3)}{(1 - K_2')} + \frac{(-4K_2' + 4)(1 - K_2')}{(1 - K_2')}\right]$$

$$= \frac{1}{2}\left[\frac{K_1' - K_1'K_2' + 2K_2' - 2K_2'^2 - 3 + 3K_2' - K_1'K_2' - 2K_2'^2 + 3K_2' - 4K_2' + 4K_2'^2 + 4 - 4K_2'}{(1 - K_2')}\right]$$

$$\alpha = \frac{1}{2}\left[\frac{K_1' - 2K_1'K_2' + 1}{1 - K_2'}\right]$$

$$\beta = \left(\frac{g}{2a} + \frac{1}{2}\right) = \frac{1}{2}\left(\frac{g}{a} + 1\right) = \frac{1}{2}\left(\frac{K_2'}{1 - K_2'} + 1\right) = \frac{1}{2}\left(\frac{K_2' + 1 - K_2'}{1 - K_2'}\right)$$

$$\beta = \frac{1}{2}\left(\frac{1}{1 - K_2'}\right)$$

$$= \frac{g}{2a} = \frac{1}{2}\left(\frac{K_2'}{1 - K_2'}\right)$$

$$X = a + bx + cx^2 = (1 - K_2') + (K_1' + 2K_2' - 3)f_1 - (K_1' + K_2' - 2)f_1^2$$

$$\int \frac{dx}{X} = \frac{1}{(-q)^{\frac{1}{2}}}\ln \frac{2cx + b - (-q)^{\frac{1}{2}}}{2cx + b + (-q)^{\frac{1}{2}}}$$

$$-q = b^2 - 4ac = (K_1' + 2K_2' - 3)^2 - 4(1 - K_2')(-K_1' - K_2' + 2)$$

$$= K_1'^2 + 2K_1'K_2' - 3K_1' + 2K_1'K_2' + 4K_2'^2 - 6K_2' - 3K_1' - 6K_2' + 9 - (-4K_1' - 4K_2' + 8 + 4K_1'K_2' + 4K_2'^2 - 8K_2')$$

$$= K_1'^2 + 4K_1'K_2' - 6K_1' + 4K_2'^2 - 12K_2' + 9 + 4K_1' + 4K_2' - 8 - 4K_1'K_2' - 4K_2'^2 + 8K_2'$$

$$-q = K_1'^2 - 2K_1' + 1 = (K_1' - 1)^2$$

$$(-q)^{\frac{1}{2}} = (K_1' - 1)$$

$$b - (-q)^{\frac{1}{2}} = K_1' + 2K_2' - 3 - (K_1' - 1) = 2(K_2' - 1)$$

Reproduced with permission of the copyright owner. Further reproduction prohibited without permission.

$$b + (-q)^{\frac{1}{2}} = K_1' + 2K_2' - 3 + (K_1' - 1) = 2(K_1' + K_2' - 2)$$

$$\frac{2cx + (b-(-q)^{\frac{1}{2}})}{2cx + (b+(-q)^{\frac{1}{2}})} = \frac{2(-K_1'-K_2'+2)f_1+2(K_2'-1)}{2(-K_1'-K_2'+2)f_1+2(K_1'+K_2'-2)} = \frac{-(K_1'+K_2'-2)f_1+(K_2'-1)}{-(K_1'+K_2'-2)f_1+(K_1'+K_2'-2)}$$

$$= \frac{-f_1 + (K_2'-1)/(K_1'+K_2'-2)}{-f_1+1} = \frac{-f_1+(-a/-c)}{-f_1+1} = \frac{f_1 - (a/c)}{f_1 - 1}$$

$$= \frac{f_1 - \left(\frac{1 - K_2'}{2 - K_1' - K_2'}\right)}{f_1 - 1} = \frac{f_1 - \frac{(1-K_2')}{(1-K_1')+(1-K_2')}}{f_1 - 1}$$

$$= \frac{f_1 - \frac{1}{\left(\frac{1-K_1'}{1-K_2'}\right)+1}}{f_1 - 1}$$

$$\int \frac{dx}{X} = \frac{1}{(K_1'-1)} \ln \left[\frac{f_1 - \frac{1}{\left(\frac{1-K_1'}{1-K_2'}\right)+1}}{f_1 - 1} \right]$$

$$\int \frac{dA}{A} = \alpha \int \frac{dx}{X} - \beta \ln X + \gamma \ln x^2$$

The expressions $(1-K_1')$ and $(1-K_2')$ appear very frequently, and the final equation for $\int \frac{dA}{A}$ will be much less cumbersome if the constants of its terms are conglomerated into the constants:

$$\Delta_1 = (1-K_1') \qquad \text{and} \qquad \Delta_2 = (1-K_2')$$

Rewriting the terms with Δ_1 and Δ_2:

$$\alpha = \frac{K_1'-2K_1'K_2'+1}{2(1-K_2')} = \frac{2-K_2'-K_1'+(-2K_1'+1)(K_2'-1)}{2(1-K_2')} = \frac{-2K_1'K_2'+2K_1'+K_2'-1-K_1'-K_2'+2}{2(1-K_2')}$$

$$= \frac{(1-K_1')+(1-K_2')+(1-K_1'-K_1'+1-1)(K_2'-1)}{2(1-K_2')} = \frac{\Delta_1+\Delta_2(\Delta_1+\Delta_1-1)(-\Delta_2)}{2\Delta_2}$$

$$= \frac{\Delta_1+\Delta_2(1-(2\Delta_1-1))}{2\Delta_2} = \frac{\Delta_1+2\Delta_2(1-\Delta_1)}{2\Delta_2}$$

$$\alpha = \frac{\Delta_1}{2\Delta_2} + 1 - \Delta_1 = \Delta_1\left(\frac{1}{2\Delta_2} - 1\right) + 1$$

Reproduced with permission of the copyright owner. Further reproduction prohibited without permission.

$$\beta = \frac{1}{2(1 - K_2')} = \frac{1}{2\Delta_2}$$

$$\gamma = \frac{K_2'}{2(1 - K_2')} = \frac{-1 + K_2' + 1}{2(1 - K_2')} = \frac{-\Delta_2 + 1}{2\Delta_2} = \frac{1 - \Delta_2}{2\Delta_2}$$

$$\gamma = \frac{1}{2}\left(\frac{1}{\Delta_2} - 1\right)$$

$$\int \frac{dx}{X} = \frac{1}{(K_1' - 1)} \ln \left[\frac{f_1 - \dfrac{1}{\left(\dfrac{1 - K_1'}{1 - K_2'}\right) + 1}}{f_1 - 1} \right] = \frac{1}{-\Delta_1} \ln \left[\frac{f_1 - \dfrac{1}{\dfrac{\Delta_1}{\Delta_2} + 1}}{f_1 - 1} \right]$$

$$X = (1 - K_2') + (K_1' + 2K_2' - 3) f_1 - (K_1' + K_2' - 2) f_1^2$$

$$= \Delta_2 + (K_1' - 1 + 2K_2' - 2) f_1 - (K_1' - 1 + K_2' - 1) f_1^2$$

$$= \Delta_2 + (-\Delta_1 - 2\Delta_2) f_1 - (-\Delta_1 - \Delta_2) f_1^2$$

$$X = \Delta_2 - (\Delta_1 + 2\Delta_2) f_1 + (\Delta_1 + \Delta_2) f_1^2$$

substituting into

$$\int \frac{dA}{A} = \alpha \int \frac{dx}{X} - \beta \ln X + \gamma \ln x^2$$

$$\int \frac{dA}{A} = \left[\Delta_1 \left(\frac{1}{2\Delta_2} - 1\right) + 1\right] \left[\frac{1}{-\Delta_1} \ln \left(\frac{f_1 - \dfrac{1}{\dfrac{\Delta_1}{\Delta_2} + 1}}{f_1 - 1} \right) \right] - \left[\frac{1}{2\Delta_2} \ln (\Delta_2 - (\Delta_1 + 2\Delta_2) f_1 + (\Delta_1 + \Delta_2) f_1^2) \right]$$
$$+ \frac{1}{2}\left(\frac{1}{\Delta_2} - 1\right) \ln f_1^2$$

$$\int \frac{dA}{A} = \left(1 - \frac{1}{\Delta_1} - \frac{1}{2\Delta_2}\right) \ln \left[\frac{f_1 - \dfrac{1}{\dfrac{\Delta_1}{\Delta_2} + 1}}{f_1 - 1} \right] - \frac{1}{2\Delta_2} \ln (\Delta_2 - (\Delta_1 + 2\Delta_2) f_1 + (\Delta_1 + \Delta_2) f_1^2) + \left(\frac{1}{\Delta_2} - 1\right) \ln f_1$$

Reproduced with permission of the copyright owner. Further reproduction prohibited without permission.

Applying integration limits of A^o to A and f_1^o to f_1:

$$\ln \frac{A}{A^o} = \left(1 - \frac{1}{\Delta_1} - \frac{1}{2\Delta_2}\right)\left[\ln \frac{\left(\frac{\Delta_1}{\Delta_2}+1\right) f_1 - 1}{\left(\frac{\Delta_1}{\Delta_2}+1\right) f_1^o - 1} + \ln \frac{f_1^o - 1}{f_1 - 1}\right] - \frac{1}{2\Delta_2} \ln \left(\frac{\Delta_2 - (\Delta_1+2\Delta_2) f_1 + (\Delta_1+\Delta_2) f_1^2}{\Delta_2 - (\Delta_1+2\Delta_2) f_1^o + (\Delta_1+\Delta_2) f_1^{o2}}\right)$$

$$+\left(\frac{1}{\Delta_2} - 1\right) \ln \frac{f_1}{f_1^o}$$

$$\frac{A}{A^o} = \left[\frac{\left(\frac{\Delta_1}{\Delta_2}+1\right) f_1 - 1}{\left(\frac{\Delta_1}{\Delta_2}+1\right) f_1^o - 1}\right]\left(\frac{f_1^o - 1}{f_1 - 1}\right)^{\epsilon} \left[\frac{\Delta_2 - (\Delta_1+2\Delta_2) f_1 + (\Delta_1+\Delta_2) f_1^2}{\Delta_2 - (\Delta_1+2\Delta_2) f_1^o + (\Delta_1+\Delta_2) (f_1^o)^2}\right]^{\mu} \left[\frac{f_1}{f_1^o}\right]^{\eta}$$

(4)

$$\delta = \left(\frac{\Delta_1}{\Delta_2}+1\right), \qquad \epsilon = \left(1 - \frac{1}{\Delta_1} - \frac{1}{2\Delta_2}\right), \qquad \mu = \left(-\frac{1}{2\Delta_2}\right), \qquad \eta = \left(\frac{1}{\Delta_2} - 1\right)$$

While in chain polymerization polymer molecules of fixed size are are produced during the entire duration of the reaction, in step polymerizations polymer molecules are produced only as the extent of reaction approaches one. (At p=.90 one only has decamer.) Consequently, in chain polymerization, to keep the polymer composition constant one would have to keep the feed composition constant as the reaction proceeds. This cannot be done in step polymerization as one would never obtain polymer. Thus, in step copolymerization the polymer composition is determined by the initial feed composition. Assigning the more reactive monomer the subscript 1, as the extent of reaction approaches 1, the feed mole fraction of monomer 1 approaches 0.

$$\lim_{p \to 1} f_1^o = C_1^o \qquad \text{and} \qquad f_1 = 0$$

C_1 = accumulative mole fraction of A_1 in copolymer

To use either of the two preceeding equations it is necessary to obtain values for Δ_1 and Δ_2. This can be done in an analogous manner to that for chain copolymerization. From equation (3) the expression for the instantaneous copolymer mole fraction, F_1 is

$$F_1 = \frac{f_1(K_1'-1)+1}{f_1(K_1'+K_2'-2)+(K_2'/f_1)-2K_2'+2} = \frac{f_1(-\Delta_1)+1}{f_1(-\Delta_1-\Delta_2)+(1/f_1)(\Delta_2-1)+2\Delta_2}$$

$$F_1 = \frac{\Delta_1 f_1 - 1}{(\Delta_1+\Delta_2) f_1 + (1/f_1)(1-\Delta_2) - 2\Delta_2}$$

$$\Delta_1 f_1 F_1 + \Delta_2 f_1 F_1 + (F_1/f_1)(1-\Delta_2) - 2\Delta_2 F_1 = \Delta_1 f_1 - 1$$

Reproduced with permission of the copyright owner. Further reproduction prohibited without permission.

$$\Delta_1(f_1F_1-f_1)+\Delta_2(f_1F_1-(F_1/f_1)-2F_1)+(F_1/f_1)+1 = 0$$

$$\Delta_1 f_1(F_1-1)+\Delta_2 F_1(f_1-(1/f_1)-2)+(F_1/f_1)+1 = 0$$

$$\Delta_1+\Delta_2\left[\frac{F_1(f_1-(1/f_1)-2}{f_1(F_1-1)}\right]+\frac{F_1+f_1}{f_1^2(F_1-1)} = 0$$

$$(5)\quad \left[\frac{F_1+f_1}{f_1^2(1-F_1)}\right] = \left[\frac{F_1(f_1-(1/f_1)-2)}{f_1(F_1-1)}\right]\Delta_2+\Delta_1$$

By holding $p<.05$, $f_1=f_1^o$ and $F_1=\frac{A_1'}{A_1'+A_2'}$ (A' = R-C≡C-H reacted), a plot of the first bracketed term against the second in equation (5) should yield a straight line of slope Δ_2 and intercept Δ_1. Δ_1 and Δ_2 can also be obtained from K_1' and K_2' which can be determined as demonstrated on page 12.

The copolymer composition at various extents of reaction is given by the accumulative copolymer mole fraction, C.

$$C_1 = \frac{A_1'}{A_1'+A_2'} \qquad A_1' = A_1^o - A_1 = A_1^o - (A_1+A_2)f_1 = A_1^o - Af_1$$
$$A_2' = A_2^o - A_2 = A_2^o - (A_1+A_2)f_2 = A_2^o - Af_2$$

$$C_1 = \frac{A_1^o - Af_1}{A_1^o - Af_1 + A_2^o - Af_2} = \frac{A_1^o - Af_1}{A_1^o + A_2^o - A(f_1+(1-f_1))}$$

$$(6)\quad C_1 = \frac{A_1^o - Af_1}{A^o - A}$$

By constructing plots of C_1 and C_2 vs. p, one can determine the microstructure nature of the copolymer composition - whether it is random or blocky.

ie. $M_1M_1M_2M_1M_2M_1M_2M_2M_2M_1$ or $M_1M_1M_1M_1M_2M_2M_2M_1M_1M_1M_1$

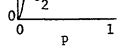

random

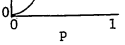

small amount of blocking

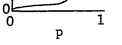

large amount of blocking

Another way of obtaining the degree of random or block placement in the copolymer is to determine the feed mole fraction where rates of coupling of A_1 and A_2 are equal.

Reproduced with permission of the copyright owner. Further reproduction prohibited without permission.

$$\frac{dA_1^*}{dA_2^*} = 1 = \frac{K_1' \frac{A_1}{A_2} + 1}{K_2' \frac{A_2}{A_1} + 1} = \frac{K_1' \frac{f_1}{(1-f_1)} + 1}{K_2' \frac{(1-f_1)}{f_1} + 1}$$

$$K_1' \frac{f_1}{(1-f_1)} + 1 = K_2' \frac{(1-f_1)}{f_1} + 1$$

$$\frac{f_1^2}{(1-f_1)^2} = \frac{K_2'}{K_1'}$$

$$\frac{f_1}{(1-f_1)} = \left(\frac{K_2'}{K_1'}\right)^{\frac{1}{2}}$$

$$f_1 = (K_2'/K_1')^{\frac{1}{2}} - (K_2'/K_1')^{\frac{1}{2}} f_1$$

$$f_1(1 + (K_2'/K_1')^{\frac{1}{2}}) = (K_2'/K_1')^{\frac{1}{2}}$$

$$f_1 = \frac{K_2'^{\frac{1}{2}}}{K_1'^{\frac{1}{2}}(1+(K_2'/K_1')^{\frac{1}{2}})} = \frac{K_2'^{\frac{1}{2}}}{K_1'^{\frac{1}{2}} + K_2'^{\frac{1}{2}}}$$

(7) $$f_{1\ F_1=F_2} = \frac{K_2'^{\frac{1}{2}}}{K_1'^{\frac{1}{2}} + K_2'^{\frac{1}{2}}}$$

Thus, the more reactive A_1 than A_2 (the greater K_1' than K_2'), the more quickly the feed is depleted of A_1 relative to A_2 and the longer the blocks of M_1 in the copolymer. (When; $K_1'=K_2'$, $f_1=.500$; $K_1'=2K_2'$, $f_1=.415$; $K_1'=10K_2'$, $f_1=.240$; $K_1'=100K_2'$, $f_1=.091$; $K_1'=1000K_2'$, $f_1=.032$.) The extent of reaction, degree of polymerization and copolymer composition at which this point occurs can be calculated by substituting the value of $f_{1\ F_1=F_2}$ for f_1 in the equations for $\frac{A}{A^0}$ and C_1.

To calculate the number average block length of the more reactive monomer, $\overline{X}_{b1}$, Flory's method for the determination of $\overline{Xn}$ in a homopolymerization can be modified in a similar way as it was to determine the degree of polymerization when monofunctional reagent was added. There the extent of reaction, p, was replaced by the probability that a functional group has formed a linkage with a bifunctional monomer, p'. For this case of copolymerization, the extent of reaction will be replaced by Q, the probability that a functional group has formed a linkage with the more reactive monomer.

Reproduced with permission of the copyright owner. Further reproduction prohibited without permission.

$$Q = \frac{A_1'A_1'}{2A_1^o + A_2^o}$$

(The A_2 groups play the same role as A_u does when monofunctional reagent is added.)

However, the expression is not correct as written above because the reactivity of A_1 and A_2 functional groups is not equal. Since A_2 is less reactive it is necessary to multiply A_2^o by an accumulative rate of entry coefficient, ϕ, which will reflect the greater probability of the more reactive functional group, A_1, reacting with the more reactive monomer.

$$(8) \qquad Q = \frac{A_1'A_1'}{2A_1^o + \phi A_2^o} \qquad 0 < \phi < 1$$

Thus, ϕ is the ratio of the accumulation of A_2 into the copolymer relative to that of A_1 and is normalized to the relative quantities of monomer initially present. Initially the relative rate of accumulation would be the same as the relative rate of dissappearance of the two monomers.

$$\phi = \frac{dA_2/A_2^o}{dA_1/A_1^o} = \frac{A_1^o dA_2}{A_2^o dA_1} = \frac{f_1^o dA_2}{f_2^o dA_1}$$

However, as the reaction proceeds from its starting point, the equality becomes invalid since ϕ is an accumulative rate and dA_2/dA_1 is an instanteneous rate. For this same reason C_1 and F_1 are inequalities. They could be made equal by maintaining a constant feed ratio by addition of less reactive monomer as in chain copolymerization, however, if one did this in step copolymerization, polymer would never be attained. Using $\phi^o = f_1^o dA_2/f_2^o dA_1$ at $A_1 = A_1^o$ and $A_2 = A_2^o$ will yield an extreme upper limit of the M_1 block length. As the reaction proceeds past its zero point the greater reactivity of A_1 is counterbalanced by the numerical superiority of A_2 and eventually dA_2/dA_1 becomes greater than one which is beyond the limit of ϕ.

Since ϕ is an accumulative ratio, it should be examined how A_1 and A_2 accumulate in the copolymer. The three possible ways are two self-couplings and one cross-coupling - that is an $\sim\sim A_1A_1\sim\sim$, $\sim\sim A_2A_2\sim\sim$, and an $\sim\sim A_1A_2\sim\sim$ linkage denoted by $A_1'A_1'$, $A_2'A_2'$ and $A_1'A_2'$. Only the $A_1'A_1'$ linkage is found within an M_1 block, and A_2 may accumulate in the copolymer as either an $A_1'A_2'$ or $A_2'A_2'$ linkage. ϕ is then the ratio of linkages which cap the M_1 block to those inside an M_1 block.

Reproduced with permission of the copyright owner. Further reproduction prohibited without permission.

$$(9) \qquad \Phi = \frac{(f_1^o)A_1'A_2'}{(f_2^o)A_1'A_1'} = \frac{f_1^o C_{12}}{f_2^o C_{11}}$$

C_{nn} is the mole fraction of various linkages within the copolymer

$$C_{11} = \frac{A_1'A_1'}{A_1'A_1'+A_1'A_2'+A_2'A_2'} \qquad C_{12} = \frac{A_1'A_2'}{A_1'A_1'+A_1'A_2'+A_2'A_2'} \qquad C_{22} = \frac{A_2'A_2'}{A_1'A_1'+A_1'A_2'+A_2'A_2'}$$

To find Φ it is necessary to know the relative amount of cross-coupling compared with the amount of self-coupling of the more reactive monomer that will occur. To determine C_{11} it is necessary to determine the number of $A_1'A_1'$ linkages and the total number of linkages (equal to $\frac{1}{2}(A_1'+A_2')$ or $\frac{1}{2}\overline{X}n-1$).

From the chemical equations

$$\frac{dA_1'A_1'}{dt} = k_{11}K_1^2A_1^2C^2$$

using the chain rule

$$\frac{dA_1'A_1'}{dt} = \frac{dA_1'A_1'}{dp_1}\frac{dp_1}{dt} = k_{11}K_1^2C^2A_1^2$$

$$dA_1'A_1' = k_{11}K_1^2C^2A_1^2\frac{dt}{dp_1}dp_1$$

$$p_1 = \frac{A_1^o - A_1}{A_1^o} \qquad \frac{dp_1}{dt} = -\frac{1}{A_1^o}\frac{dA_1}{dt} \qquad \frac{dt}{dp_1} = -A_1^o\frac{dt}{dA_1}$$

$$dA_1'A_1' = k_{11}K_1^2C^2A_1^2 - A_1^o\frac{dt}{dA_1}dp_1$$

$$-\frac{dA_1}{dt} = k_{11}K_1^2C^2A_1^2 + k_{12}K_1K_2C^2A_1A_2$$

At this point a complicated mathmatical problem occurs. It is necessary to express A_2 as a function of A_1. This is accomplished by integrating equation (1).

For simplification of following expressions

$$x = A_1 \qquad y = A_2$$

Reproduced with permission of the copyright owner. Further reproduction prohibited without permission.

equation (1)

$$\frac{dA_1}{dA_2} = \frac{\dot{x}}{\dot{y}} = \frac{K_1'(x/y)+1}{K_2'(y/x)+1}$$

$$v = (x/y) \qquad G(v) = (\dot{x}/\dot{y})$$

$$G(v) = \frac{K_1'v+1}{K_2'/v+1} = \frac{K_1'v^2+v}{K_2'+v}$$

for homogeneous differential equations

$$\frac{\dot{x}}{\dot{y}} = G\left(\frac{x}{y}\right) = G(v)$$

$$v = x/y \qquad x = vy$$

$$\frac{\dot{x}}{\dot{y}} = v + y\frac{v}{y} = G(v)$$

$$\frac{\dot{y}}{y} + \frac{\dot{v}}{v - G(v)} = 0$$

Substituting into the homogeneous differential equation form

$$0 = \frac{\dot{y}}{y} + \frac{\dot{v}}{v - \left(\frac{K_1'v^2+v}{K_2'+v}\right)} = \frac{\dot{y}}{y} + \frac{\dot{v}}{\frac{K_2'v+v^2-K_1'v^2-v}{K_2'+v}}$$

$$0 = \frac{\dot{y}}{y} + \frac{K_2'\dot{v}}{(1-K_1')v^2+(K_2'-1)v} + \frac{\dot{v}}{(1-K_1')v+(K_2'-1)} = \frac{\dot{y}}{y} + \frac{K_2'\dot{v}}{v(bv+a)} + \frac{\dot{v}}{(bv+a)}$$

$$b = (1-K_1') \qquad a = (K_2'-1)$$

$$\int_{y^o}^{y}\frac{\dot{y}}{y} + K_2'\int_{v^o}^{v}\frac{\dot{v}}{v(bv+a)} + \int_{v^o}^{v}\frac{\dot{v}}{(bv+a)} = 0$$

evaluating integrals (CRC Handbook 51, A162)

$$\int\frac{\dot{y}}{y} = \ln y$$

$$\int\frac{\dot{v}}{(bv+a)} = \frac{1}{b}\ln(-a-bv)$$

$$\int\frac{\dot{v}}{v(bv+a)} = -\frac{1}{a}\ln\left(\frac{-a-bv}{v}\right)$$

$a>0, \quad b>0$

$\frac{d\dot{u}}{u} = \ln -u \qquad u>0$

Thomas, "Calculus and Analytical Geometry" 3rd edition, page 304

$$\ln y\Big|_{y^o}^{y} + K_2'\left(-\frac{1}{a}\ln\left(\frac{-bv-a}{v}\right)\right) + \frac{1}{b}\ln(-bv-a)\Big|_{v^o}^{v} = 0$$

$$\ln y\Big|_{y^o}^{y} + \left(\frac{1}{b}-\frac{K_2'}{a}\right)\ln(-bv-a) + \frac{K_2'}{a}\ln v\Big|_{v^o}^{v} = 0$$

Applying integration limits

$$y = A_2 \qquad y^o = A_2^o \qquad v = (A_1/A_2) \qquad v^o = (A_1^o/A_2^o)$$

expressing constants in terms of Δ

$$\frac{K_2'}{a} = \frac{K_2'}{K_2'-1} = 1 - \frac{1}{\Delta_2}$$

Reproduced with permission of the copyright owner. Further reproduction prohibited without permission.

$$\left(\frac{1}{b}-\frac{K_2'}{a}\right) = \frac{1}{1-K_1'} - \left(1-\frac{1}{\Delta_2}\right) = \frac{1}{\Delta_1}+\frac{1}{\Delta_2} - 1$$

$$b = \Delta_1 \qquad a = -\Delta_2$$

Substituting

$$\ln A_2 - \ln A_2^\circ + \left(\frac{1}{\Delta_1}+\frac{1}{\Delta_2}-1\right)\left[\ln\left(-\Delta_1\frac{A_1}{A_2}+\Delta_2\right) - \ln\left(-\Delta_1\frac{A_1^\circ}{A_2^\circ}+\Delta_2\right)\right] + \left(1-\frac{1}{\Delta_2}\right)\left(\ln\frac{A_1}{A_2} - \ln\frac{A_1^\circ}{A_2^\circ}\right) = 0$$

$$\ln\left(-\Delta_1\frac{A_1}{A_2}+\Delta_2\right) = \ln\left(\frac{-\Delta_1A_1+\Delta_2A_2}{A_2}\right) = \ln\left(\Delta_2A_2-\Delta_1A_1\right) - \ln A_2$$

Collecting A_2 terms to the left side

$$\left[1-\left(\frac{1}{\Delta_1}+\frac{1}{\Delta_2}-1\right)-\left(1-\frac{1}{\Delta_2}\right)\right]\ln A_2 + \left(\frac{1}{\Delta_1}+\frac{1}{\Delta_2}-1\right)\ln\left(\Delta_2A_2-\Delta_1A_1\right) =$$

$$\left[1-\left(\frac{1}{\Delta_1}+\frac{1}{\Delta_2}-1\right)-\left(1-\frac{1}{\Delta_2}\right)\right]\ln A_2^\circ + \left(\frac{1}{\Delta_1}+\frac{1}{\Delta_2}-1\right)\ln\left(\Delta_2A_2^\circ-\Delta_1A_1^\circ\right)$$

$$+ \left(1-\frac{1}{\Delta_2}\right)\ln A_1^\circ - \left(1-\frac{1}{\Delta_2}\right)\ln A_1$$

$$\left[1-\frac{1}{\Delta_1}\right]\ln A_2 + \left(\frac{1}{\Delta_1}+\frac{1}{\Delta_2}-1\right)\ln\left(\Delta_2A_2-\Delta_1A_1\right) = \left[1-\frac{1}{\Delta_2}\right]\ln A_2^\circ + \left(\frac{1}{\Delta_1}+\frac{1}{\Delta_2}-1\right)\ln\left(\Delta_2A_2^\circ-\Delta_1A_1^\circ\right)$$

$$+ \left(1-\frac{1}{\Delta_2}\right)\ln A_1^\circ - \left(1-\frac{1}{\Delta_2}\right)\ln A_1$$

$$(10) \qquad A_2^\omega\left(\Delta_2A_2-\Delta_1A_1\right)^\sigma = A_2^{\circ\omega}\left(\Delta_2A_2^\circ-\Delta_1A_1^\circ\right)^\sigma A_1^{\circ\chi}A_1^{-\chi}$$

$$\omega = \left(1-\frac{1}{\Delta_1}\right), \quad \sigma = \left(\frac{1}{\Delta_1}+\frac{1}{\Delta_2}-1\right), \quad \chi = \left(1-\frac{1}{\Delta_2}\right)$$

Consideration of equation (10) shows that solution of it for A_2 and subsequent substitution into the expression for dA_1/dt is diffecult if not impossible. It is possible to go a little further if the special case $K_1'K_2'=1$ is considered. In this case $\sigma=0$ and

$$A_2 = A_2^\circ(A_1^\circ)^{\chi/\omega}(A_1)^{-\chi/\omega}$$

Substituting into dA_1/dt

$$-\frac{dA_1}{dt} = k_{11}K_1^2C^2A_1^2 + k_{12}K_1K_2C^2A_2^\circ(A_1^\circ)^{\chi/\omega}A_1^{1-\chi/\omega}$$

Substituting into $dA_1'A_1'$

$$dA'A' = k_{11}K_1^2C^2A_1^2A_1^\circ\left(\frac{1}{k_{11}K_1^2C^2A_1^2 + k_{12}K_1K_2C^2A_2^\circ(A_1^\circ)^{\chi/\omega}A_1^{1-\chi/\omega}}\right)dp_1$$

Reproduced with permission of the copyright owner. Further reproduction prohibited without permission.

$$dA'_1A'_1 = \frac{A_1^o dp_1}{1+K'_1A_2^oA_1^{\chi/\omega}A_1^{-(1+\chi/\omega)}} = \frac{A_1^o dp_1}{1+K'_1A_2^o(A_1^o)^{\Delta_2/\Delta_1}A_1^{-(\Delta_1+\Delta_2)/\Delta_1}}$$

$$A_1 = A_1^o(1-p_1)$$

$$dA'_1A'_1 = \frac{A_1^o dp_1}{1+K'_1(A_2^o/A_1^o)(1-p_1)^{-(\Delta_1+\Delta_2)/\Delta_1}}$$

The integration of such an equation is dependent on the value of the exponent of (1-p) and cannot be performed until a set of (K'_1,K'_2) values are given. Thus, to obtain a value for C_{11}, it would be necessary to know K'_1 and K'_2, iterate equation (10) for A_2 (if $K'_1K'_2 \neq 1$) and graphically integrate the differential equation for $A'_1A'_1$.

Similar procedure for C_{12} yields

$$dA'_1A'_2 = \frac{A_2^o(A_1^o)^{-(\Delta_1+2\Delta_2)/\Delta_1}}{K'_1(1-p_1)^{(\Delta_1+\Delta_2)/\Delta_1} + A_2^o(A_1^o)^{-2(\Delta_1+\Delta_2)/\Delta_1}} dp_1$$

For the same reason one may not proceed further without values for K'_1 and K'_2.

While the quantities of $A'_1A'_1$, $A'_1A'_2$ and $A'_2A'_2$ cannot easily be computed, those of A'_1 and A'_2 can. The relation between these two groups of quantities is

$$A'_1 = \tfrac{1}{2}A'_1A'_1 + A'_1A'_2$$

$$A'_2 = A'_1A'_2 + \tfrac{1}{2}A'_2A'_2$$

If the relative reactivities of the two monomers are substantially different $(K'_1 \gg K'_2)$, the following approximations can be made between the different linkages.

$$A'_1A'_1 \gg A'_1A'_2 \qquad A'_1A'_2 \gg A'_2A'_2$$

The first approximation should be good throught the whole extent of the reaction while the second will break down as the extent of reaction passes the stage shere cross-coupling is predominent.

With these approximations

$$\frac{C_2}{C_1} = \frac{A'_2}{A'_1} = \frac{A'_1A'_2 + 2A'_2A'_2}{2A'_1A'_1 + A'_1A'_2} \cong \frac{A'_1A'_2}{2A'_1A'_1} = \frac{1}{2}\frac{f_2^o}{f_1^o}\phi$$

Reproduced with permission of the copyright owner. Further reproduction prohibited without permission.

$$Q = \frac{A_1^{\prime}A_1^{\prime}}{2A_1^{o} + \phi A_2^{o}} = \frac{2A_1^{\prime}}{2A_1^{o} + 2(C_2/C_1)(f_1^{o}/f_2^{o})A_2^{o}}$$

$$Q = \frac{A_1^{\prime}}{A_1^{o} + A_2^{o}(C_2/C_1)(f_1^{o}/f_2^{o})}$$

The number average block length is then given by

$$\overline{X}_{b1} = \frac{1}{1 - Q}$$

The breaking down of the second approximation as the reaction passes the cross-coupling stage will result in a negative deviation in $\overline{X}_{b1}$. A plot of $\overline{X}_{b1}$ vs. p where the approximations are not made should yield a curve which rapidly converges to a constant value of $\overline{X}_{b1}$ while a similar plot where the approximations have been made should pass through an $\overline{X}_{b1}$ maxima as the second approximation breaks down.

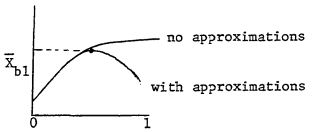

Copolymer block length vs. extent of reaction

By finding $\overline{X}_{b1}$ a reasonably good value of the block length should be obtained.

Just as $\overline{X}n$ for a homopolymerization may be obtained directly from its definition without going through Flory's statistical method, so too can $\overline{X}_{b1}$.

$$\overline{X}_{b1}^{\prime} = \frac{\text{number of } M_1 \text{ units}}{\text{number of } M_1 \text{ blocks}} = \frac{\text{initial concentration of } M_1}{\text{half concentration of } M_1 \text{ block ends}}$$

A block end on an M_1 oligomer must either be an unreacted A_1 group or a reacted A_2 group.

$$\overline{X}_{b1}^{\prime} = \frac{M_1^{o}}{\frac{1}{2}(A_1 + A_2^{\prime})} = \frac{\frac{1}{2}A_1^{o}}{\frac{1}{2}(A_1 + A_2^{\prime})} = \frac{A_1^{o}}{A_1 + A_2^{\prime}}$$

Inherent in this equation is that every $A_2^{\prime}$ functions as an M_1 block end, which is another way of stating the approximation

Reproduced with permission of the copyright owner. Further reproduction prohibited without permission.

$$A_1'A_2' \gg A_2'A_2'$$

Thus, this $\bar{X}_{b1}'$ will also go through a maxima with increasing extent of reaction. However, $\bar{X}_{b1\ max}'$ will be different from $\bar{X}_{b1\ max}'$ since the former does not involve the approximation $A_1'A_1' \gg A_1'A_2'$. This difference should make $\bar{X}_{b1\ max}$ slightly greater and occur at a slightly larger extent of reaction than $\bar{X}_{b1\ max}'$. $\bar{X}_{b1}$ and $\bar{X}_{b1}$ may be expressed in terms of extent of reaction if each component as follows.

$$Q = \frac{A_1'}{A_1^o + A_2^o(C_2/C_1)(A_1^o/A_2^o)} = \frac{P_1}{1 + (A_2^o/A_1^o)(C_2/C_1)(A_1^o/A_2^o)} = \frac{P_1}{1 + r_C}$$

$$(11)\quad \bar{X}_{b1} = \frac{1}{1 - Q} = \frac{1 + r_c}{1 + r_C - P_1}$$

$$(12)\quad \bar{X}_{b1}' = \frac{A_1^o}{A_1 + A_2'} = \frac{1 + r_C}{1 + (f_2^o/f_1^o)P_2 - P_1}$$

$$P_1 = \frac{A_1^o - A_1}{A_1^o} \qquad P_2 = \frac{A_2^o - A_2}{A_2^o} \qquad r_C = \frac{C_2}{C_1}$$

The weight average block length corresponding to $\bar{X}_{b1}$ would be

$$\bar{\bar{X}}_{wb1} = \frac{1 + Q}{1 - Q} = \frac{1 + r_C + P_1}{1 + r_C - P_1}$$

Azeotrope:

Analogous to chain copolymerization, an azeotrope should occur where the feed and copolymer compositions are equal over the entire extent of reaction. Since the feed composition does not drift as the reaction proceeds, it should enable exact calculation of $\bar{X}_{b1}$, as, under these conditions

$$\phi = \frac{f_1^o dA_2}{f_2^o dA_1}$$

Setting $f_1 = F_1$ and using equation (3)

$$f_1 = F_1 = \frac{f_1(K_1' - 1) + 1}{f_1(K_1' + K_2' - 2) + (K_2'/f_1) - 2K_2' + 2}$$

$$(K_1' + K_2' - 2)f_1^2 + (2 - 2K_2')f_1 + K_2' = (K_1' - 1)f_1 + 1$$

$$(a)f_1^2 + (b)f_1 + c = (d)f_1 + 1$$

$$af_1^2 + (b-d)f_1 + (c-1) = 0$$

Reproduced with permission of the copyright owner. Further reproduction prohibited without permission.

$$(b-d) = (2-2K_2')-(K_1'-1) = -2K_2' - K_1' + 3 = -K_2' + 1 - a = (\tfrac{1}{2}b - a)$$

$$(c-1) = (K_2' - 1) = (-\tfrac{1}{2}b)$$

$$af_1^2 + (\tfrac{1}{2}b - a)f_1 - \tfrac{1}{2}b = 0$$

$$f_1 = \frac{(a-\frac{1}{2}b) \pm ((\frac{1}{2}b - a)^2 - 4a(-\frac{1}{2}b))^{\frac{1}{2}}}{2a} = \frac{a - \frac{1}{2}b \pm (\frac{1}{2}b^2 - ab + a^2 + 2ab)^{\frac{1}{2}}}{2a}$$

$$f_1 = \frac{a - \frac{1}{2}b \pm ((\frac{1}{2}b + a)^2)^{\frac{1}{2}}}{2a} = \frac{a - \frac{1}{2}b \pm (a + \frac{1}{2}b)}{2a}$$

When the + option is used, $f_1=1$; acceptable only for homopolymerization. With the − option

$$f_1 = \frac{a - \frac{1}{2}b - a - \frac{1}{2}b}{2a} = -\frac{b}{2a} = \frac{-2K_2' + 2}{2(K_1' + K_2' - 2)}$$

$$(13) \quad f_1 = \frac{1 - K_2'}{(1-K_1') + (1-K_2')} = \frac{\Delta_2}{\Delta_1 + \Delta_2}$$

The same result may be obtained by setting $(dA_2/dA_1)=(A_2/A_1)$ and solving equation (1).

Since f_1 can neither be greater than one nor less than zero, the following must hold for the existance of an azeotrope.

$$f_1 = \frac{\Delta_2}{\Delta_1 + \Delta_2} > 0$$

$$\frac{2\Delta_2}{\Delta_1 + \Delta_2} > \frac{\Delta_2}{\Delta_1 + \Delta_2}$$

$$2\Delta_2\Delta_1 + 2\Delta_2^2 > \Delta_1\Delta_2 + \Delta_2^2$$

$$\Delta_1\Delta_2 > -\Delta_2^2$$

$$\Delta_1 > -\Delta_2$$

$$1 - K_1' > -(1-K_2')$$

$$-K_1' > K_2' - 2$$

$$K_1' < 2 - K_2'$$

$$K_1' + K_2' < 2$$

$$f_1 = \frac{\Delta_2}{\Delta_1 + \Delta_2} < 1$$

$$\frac{\Delta_1}{\frac{\Delta_1}{\Delta_2} + 1} < 1$$

$$1 < \frac{\Delta_1}{\Delta_2} + 1$$

$$\frac{\Delta_1}{\Delta_2} > 0$$

either $\{\Delta_1 > 0 \ldots\ldots K_1' < 1\}$ $\{\Delta_2 > 0 \ldots\ldots K_2' < 1\}$

or $\{\Delta_1 < 0 \ldots\ldots K_1' > 1\}$ $\{\Delta_2 < 0 \ldots\ldots K_2' > 1\}$

The requirement on the left rules out the case $(K_1'>1, K_2'>1)$. Since by definition K_1' and K_2' are positive, the requirement for the existance of an azeotrope is $(1>K_1'>0, 1>K_2'>0)$.

Reproduced with permission of the copyright owner. Further reproduction prohibited without permission.

Experimental:

To experimentally determine the number average block length, $\overline{X}_{bl}$, one of the monomers would be constructed so that it can quantitatively be cleaved (resulting in chain sission). The monomer and cleaving reaction are as follows (33).

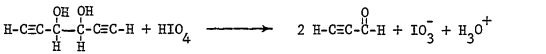

The reaction is usually quantitative and glycol content can be determined by titration with $AgNO_3$ or gravimetrically from the white $AgIO_3$ precipitate.

If for either reactivity of solubility reasons H-C≡C-CHOH-CHOH-C≡C-H is not suitable, variations may be made between the hydroxyl and alkynyl groups.

To demonstrate how number average block lengths will be experimentally determined, a copolymer molecule of $\overline{X}n$= 23 is illustrated below. M_2 is the monomer with the glycol structure. The vertical lines through M_2 represent HIO_4 cleavages. Quantities used in the determination of $\overline{X}_{bl}$ are as follows.

M' = number of monomer residues per polymer molecule

M_1' = number of units of monomer 1 per polymer molecule

M_2' = number of units of monomer 2 per polymer molecule

F = number of fragments of a polymer molecule after HIO_4 cleavage

F_1 = number of fragments which contain the M_1 blocks, also equal to the number of M_1 blocks (B_1)

F_2 = number of fragments which contain cleaved residues of M_2 and no M_1

B_2 = number of M_2 blocks in the copolymer

A_2 = an F_2 fragment from the chain end = H-C≡C-CHO

A_2A_2 = an F_2 fragment from the interior of the chain = OHC-C≡C-C≡C-CHO

The copolymer molecule of $\overline{X}n$= 23 and appropiate quantities are illustrated on the following page.

Reproduced with permission of the copyright owner. Further reproduction prohibited without permission.

	M_2-M_2-M_1-M_1-M_1-M_1-M_1-M_2-M_2-M_2-M_2-M_2-M_1-M_1-M_2-M_2-M_2-M_2-M_2-M_2-M_1-M_1-M_1-M_2																						
M'	1	2	3	4	5	6	7	8	9	10	11	12	13	14	15	16	17	18	19	20	21	22	23
M'_1			1	2	3	4	5					6	7							8	9	10	
M'_2	1	2						3	4	5	6			7	8	9	10	11	12				13
F	1	2			3			4	5	6		7		8	9	10	11	12			13		14
F_1					1							2									3		
F_2	1	2						3	4	5				6	7	8	9	10					11
B_2		1							2							3							4
A_2	1																						2
A_2A_2	1							2	3	4				5	6	7	8	9					

These quantities are summed from left to right for the copolymer molecule $\bar{X}n = 23$ above.

By inspection, it can be seen that

$$\bar{X}_{b1} = \frac{M'_1}{B_1} = \frac{M'_1}{F_1} = \frac{10}{3} = 3.33$$

$$\bar{X}_{b2} = \frac{M'_2}{B_2} = \frac{13}{4} = 3.25$$

To experimentally determine $\bar{X}_{b1}$ or $\bar{X}_{b2}$ it is necessary to measure M', M'_2, F, A_2A_2 and A_2. A_2 can be assumed to be 2 as it is highly probable the less reactive monomer will form the end groups. M' is obtained by measurement of $\bar{X}n$ of the polymer. M'_2 is obtained from the silver titration with IO_3^-. F would come from chemical of spectroscopic determination of aldehyde groups. A_2A_2 and A_2 can be determined by quantitative gas chromatographic measurements. M'_1 can be obtained from $M'_1 = M' - M'_2$ or by inclusion of a chromophore into M_1's structure. Of course, if the copolymerization is sufficently complete, M'_1 and M'_2 may be obtained from the initial comonomer concentrations. As easily seen from the above

$$F = F_1 + F_2 = B_1 + F_2 \quad \text{or} \quad B_1 = F - F_2$$

$$F_2 = A_2A_2 + A_2$$

$$B_1 = F - A_2A_2 - A_2 = 14 - 9 - 2 = 3$$

$$B_2 = B_1 + 1 = 3 + 1 = 4$$

$$\bar{X}_{b1} = M'_1/B_1 = 10/3 = 3.33 \qquad \bar{X}_{b2} = M'_2/B_2 = 13/4 = 3.25$$

Reproduced with permission of the copyright owner. Further reproduction prohibited without permission.

APPENDIX IV

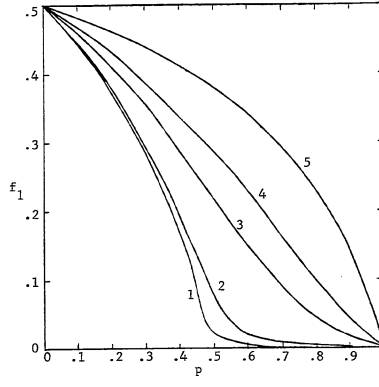

Figure 1. Dependence of feed mole fraction, f_1, on extent of reaction, p, where

$A_1^o = A_2^o = 1M$ $\quad K_2' = .5$

1. $K_1' = 1000$
2. $K_1' = 100$
3. $K_1' = 10$
4. $K_1' = 5$
5. $K_1' = 2$

Reproduced with permission of the copyright owner. Further reproduction prohibited without permission.

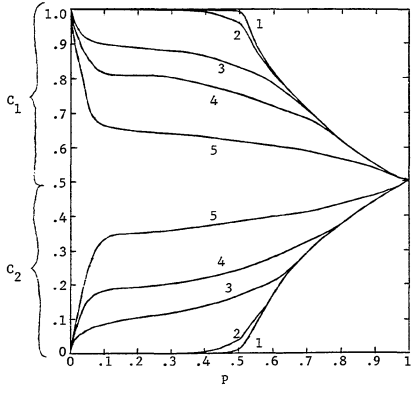

Figure 2. Dependence of accumulative copolymer mole fraction, C, on extent of reaction, p, where

$A_1^o = A_2^o = 1M$ $\quad K_1'K_2' = 1$

1. $K_1' = 1000$ $\quad K_2' = .001$
2. $K_1' = 100$ $\quad K_2' = .01$
3. $K_1' = 10$ $\quad K_2' = .1$
4. $K_1' = 5$ $\quad K_2' = .2$
5. $K_1' = 2$ $\quad K_2' = .5$

Reproduced with permission of the copyright owner. Further reproduction prohibited without permission.

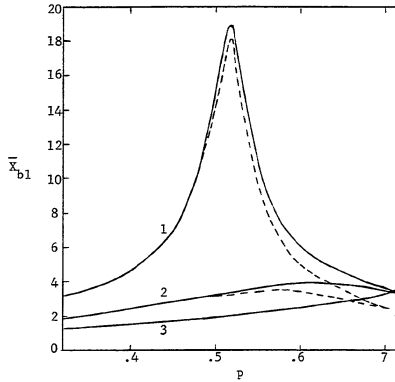

Figure 3. Dependence of monomer 1 block length, $\bar{X}_{bl}$, on extent of reaction, p. The solid line is for $\bar{X}_{bl}$, and the broken line is for $\bar{X}'_{bl}$.

$A_1^o = A_2^o = 1M$

1. $K'_1 = 100$ $K'_2 = .01$
   $\bar{X}_{bl\ max} = 18.9$ $p_{max} = .519$
   $\bar{X}'_{bl\ max} = 18.2$ $p'_{max} = .518$
2. $K'_1 = 10$ $K'_2 = .1$
   $\bar{X}_{bl\ max} = 3.95$ $p_{max} = .608$
   $\bar{X}'_{bl\ max} = 3.30$ $p'_{max} = .574$
3. $\bar{X}n$ of system

Reproduced with permission of the copyright owner. Further reproduction prohibited without permission.

TABLE I

Monomer 1 Block Lengths

$A_1^o = A_2^o = 1M$

K_1'	1000	100	10	5	2
K_2'	.001	.01	.1	.2	.5
$\bar{X}_{b1\ max}$	128	18.9	3.95	2.82	2.10
$\bar{X}'_{b1\ max}$	127	18.2	3.30	2.15	1.33
p_{max}	.503	.519	.608	.686	.890
p'_{max}	.503	.518	.574	.599	.625
$\bar{X}_{b1\ F_1=F_2}$	128	18.9	3.86	2.68	1.82
$\bar{X}'_{b1\ F_1=F_2}$	127	18.2	3.30	2.15	1.33

$A_1^o = A_2^o = 1M$

K_1'	1000	100	10	5	2
K_2'	.5	.5	.5	.5	.5
$\bar{X}_{b1\ max}$	21.6	7.00	2.84	2.39	2.10
$\bar{X}'_{b1\ max}$	21.3	6.63	2.30	1.77	1.33
p_{max}	.502	.518	.636	.732	.890
p'_{max}	.502	.511	.554	.580	.625
$\bar{X}_{b1\ F_1=F_2}$	21.6	6.97	2.72	2.22	1.82
$\bar{X}'_{b1\ F_1=F_2}$	21.3	6.63	2.30	1.77	1.33

$K_1'=100 \quad K_2'=.01$

A_1^o	.2	.4	.6	.8	1.0	1.2	1.4	1.6	1.8
A_2^o	1.8	1.6	1.4	1.2	1.0	.8	.6	.4	.2
$\bar{X}_{b1\ max}$	3.89	6.64	9.80	13.7	18.9	26.2	37.7	59.5	119
$\bar{X}'_{b1\ max}$	3.29	6.00	9.14	13.0	18.2	25.5	37.0	58.7	119
p_{max}	.120	.222	.322	.421	.519	.616	.713	.810	.906
p'_{max}	.113	.218	.319	.419	.518	.616	.713	.810	.906
$\bar{X}_{b1\ F_1=F_2}$	3.81	6.59	9.78	13.7	18.9	26.2	37.7	59.5	120
$\bar{X}'_{b1\ F_1=F_2}$	3.29	6.00	9.14	13.0	18.2	25.5	37.0	58.7	119

Reproduced with permission of the copyright owner. Further reproduction prohibited without permission.

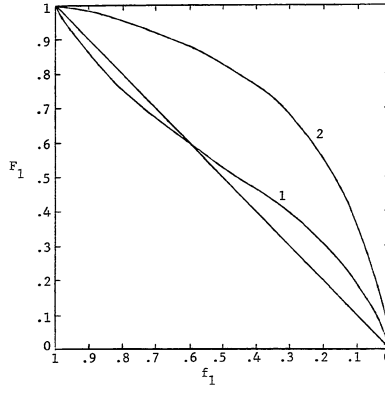

Figure 4. Dependence of instantaneous copolymer mole fraction, F_1, on feed mole fraction, f_1, where $A_1^o = A_2^o = 1M$.

1. $K_1' = .6$ $K_2' = .4$
   Azeotrope at $f_1 = F_1 = .6$

2. $K_1' = 5$ $K_2' = .2$
   No azeotrope

Reproduced with permission of the copyright owner. Further reproduction prohibited without permission.

REFERENCES

1. Hay, J. Poly. Sci., A-1, 7, 1625 (1969).
2. Tani, Murayama and Toda, Chem. Ind., (1962) 1980.
3. CA. 60:79536.
4. Hay, Bolon, Leimer and Clark, J. Poly. Sci., B, 8, 97 (1970).
5. CA. 56:7234.
6. CA. 59:5272.
7. Glasser, Chem. Ber., 422 (1869).
8. Hay, J. Org. Chem., 27, 3320 (1962).
9. Hay, J. Org. Chem., 25, 1275 (1960).
10. Hunt and Wilson, J. Chem. Phys., 34, 1301 (1961).
11. Linnet, Quart. Rev. (London), 1, 73 (1947).
12. Newkirk, Hay and MacDonald, J. Poly. Sci., A, 2, 2217 (1964).
13. Bohlman, Angew. Chem., 65, 385 (1953).
14. Bohlman and Inhoffen, Ber., 89, 1276 (1956).
15. Bu'Lock, Quart. Rev. (London), 10, 371 (1956).
16. Silverstein and Bassler, Spectrophotometric Identification of Organic Compounds, John Wiley & Sons, N.Y. (1967).
17. Hay, J. Org. Chem., 25, 637 (1960).
18. Flory, Principles of Polymer Chemistry, Cornell University Press, Ithaca, N.Y. (1953) p. 318-326; Flory, J. Am. Chem. Soc., 58, 1877 (1936).
19. Odian, Principles of Polymerization, McGraw Hill, N.Y. (1970) p. 99.
20. Bohlman, Schonowsky, Inhoffen, and Grau, Chem. Ber., 794 (1964).
21. Odian, ibid., p. 377; Meyer and Lwory, J. Poly. Sci., A3, 2843 (1965).
22. Eglinton and McCrae, Advances in Organic Chemistry, Methods and Results, Vol. 4, Interscience Publishers, N.Y. (1963).

Reproduced with permission of the copyright owner. Further reproduction prohibited without permission.

23. Clifford and Waters, J. Chem. Soc., 3056 (1963).

24. Tables of Interatomic Distances and Configuration in Molecules and Ions, The Chemical Society, London (1958).

25. McClellan, Tables of Experimental Dipole Monents, Freeman, San Francisco (1963).

26. Candlin, Taylor and Thompson, Reactions of Transition Metal Complexes, Elsevier Pub. Co., N.Y. (1968) p. 239.

27. Coates and Parker, J. Inorg. Nuclear Chem., 22, 59 (1961).

28. Bohlman, Angew. Chem., 69, 82 (1957).

29. Linnet, The Electronic Structure of Molecules. A New Approach, Methuen, London (1964).

30. Willet and Rundle, J. Chem. Phys., 40, 838 (1964).

31. Hogness and Johnson, Qualitative Analysis and Chemical Equilibrium, Holt, Reinhart and Winston, N.Y. (1966) p. 385.

32. Eglinton and McCrae, ibid. p. 252; Cotton and Wilkenson, Advanced Inorganic Chemistry, 2nd edition, Interscience, N.Y. (1966) p. 894-5.

33. March, Advanced Organic Chemistry; Reactions, Mechanisms and Structure, McGraw Hill Book Company, N.Y. (1968) p. 867-9; Morrison and Boyd, Organic Chemistry, 2nd edition, Allyn and Bacon, Inc., Boston (1967) p. 879; Odian, ibid., p. 169; Cotton and Wilkenson, ibid., p. 578.

Reproduced with permission of the copyright owner. Further reproduction prohibited without permission.